Characterizing the photosynthetic potential of the deep chlorophyll layer (DCL) in Lake Superior using **in situ** *fluorometry*

A THESIS
SUBMITTED TO THE FACULTY OF THE GRADUATE SCHOOL
OF THE UNIVERSITY OF MINNESOTA
BY

Geoffrey L. House

IN PARTIAL FULFILLMENT OF THE REQUIREMENTS
FOR THE DEGREE OF
MASTER OF SCIENCE

Stephanie J. Guildford, Robert E. Hecky

December 2011

Acknowledgements

I would like to thank my advisors Stephanie Guildford and Bob Hecky for their enthusiasm and support throughout this project, and for encouraging me to continue to expand its scope in interesting directions,

My committee members, Paul Bates and Donn Branstrator for their advice and suggestions to help continually clarify the project's overall objectives as I was working on it,

Greg Silsbe who generously provided data from Lake Erie for use in this project and was always happy to answer questions about the methods he introduced in his Ph.D. dissertation on Lake Erie,

Thomas Pevan for teaching me how to use all of the instruments and for his extensive help with data collection and analysis,

The other graduate students in the AEL lab group: Jessica Van Der Werff, Rozhan Zakaria, and Messias Macuiane for help with field data collection and laboratory sample analysis,

Jay Austin, Liz Minor, and Sergei Katsev at the LLO for letting our lab group join their sampling cruises spanning the summer of 2010, which allowed for the extended seasonal measurements that have been so fascinating,

Captain Mike King and the crew of the R/V Blue Heron for making these cruises possible and for their hospitality on the lake, and

Sea Grant Minnesota for project funding and the UMD Biology Department for providing support through a GTA.

Dedication

This thesis is dedicated to my mother, my father, and my brother.
I would not have been able to do this without you.

Abstract

The presence of a sub-surface deep chlorophyll layer (DCL) characterized by chlorophyll *a* concentrations exceeding those in the surface mixed layer is common in marine systems and in many lakes after thermal stratification is established during the summer. The formation and erosion of the DCL at four stations across Lake Superior was measured from late May to late September 2010 in response to strong seasonal temperature changes in the water column during that period. Shifts in phytoplankton pigment composition during the summer and with increasing depth were also observed.

In late July, the dissolved oxygen (DO) concentration of water immediately below the surface mixed layer was the highest measured in the water column, indicating the DCL may be a zone of active phytoplankton photosynthesis acting to increase the concentration of DO in the water. This hypothesis was supported by high depth resolution estimates of daily photosynthetic O_2 production calculated using pigment fluorescence-based water column profilers that showed areas of increased O_2 production within the DCL compared to the surface mixed layer. The mean fluorescence-based estimate of daily carbon assimilation within the DCL from 10-40 m in the western arm of the lake in early August (221 mg C m^{-2} d^{-1}) was comparable to the previously measured mean value of C assimilation using traditional ^{14}C incubations over the same depth range in early fall (209 mg C m^{-2} d^{-1}) (Sterner, 2010). However fluorescence-based daily production estimates made elsewhere in the lake and at different times of year were lower than estimates made using ^{14}C incubations. Diel variability in fluorescence-based photosynthesis estimates and the large influence of background water fluorescence on the estimates may make it difficult to determine a representative value for daily photosynthetic production. Nevertheless the improved depth resolution and speed of sampling provided by fluorescence profilers compared to ^{14}C incubations makes them an effective way to gain insight into the seasonal and depth variability of phytoplankton photosynthetic production across large lakes such as Lake Superior.

Table of Contents

Acknowledgements ..... **i**

Dedication ..... **ii**

Abstract ..... **iii**

List of Tables ..... **vi**

List of Figures ..... **vii**

List of Parameters ..... **x**

List of Abbreviations ..... **xi**

General Introduction **1**

Chapter 1: Changes in the photosynthetic characteristics of the DCL in Lake Superior through the summer

Introduction **12**

Methods **18**

Results **31**

Discussion **40**

Conclusions **51**

Chapter 2: Fluorescence-based oxygen production and carbon assimilation estimates

Introduction **53**

Methods **57**

Results **66**

Discussion **71**

Conclusions **83**

Overall Conclusions **85**

Figures (see list of figures) **87**

Tables (see list of tables) **112**

Literature Cited **116**

Appendix **121**

List of Tables

Table 1: Fraction of total extracted chl *a* represented by picoplankton above, below, and at the depth of the DCM 112

Table 2: Comparison of daily photosynthetic O_2 production and corresponding C assimilation integrated from 10-40 m for two consecutive days using two different *a*PSII estimation methods and O_2 method 1.....113

Table 3: Comparison of daily photosynthetic O_2 production and corresponding C assimilation integrated from 10-40 m for two consecutive days using single profiles taken at four different times during each day following O_2 method 2.....113

Table 4: Comparison of daily photosynthetic O_2 production and corresponding C assimilation integrated from 10-40 m for two consecutive days using profiles taken at four different times during each day and averaged through the day following O_2 method 3.....114

Table 5: Previously published values for daily C assimilation in Lake Superior (Sterner, 2010) from 10-40 m over three consecutive years calculated using the traditional ^{14}C incubation method.....114

Table 6: Comparison of daily photosynthetic O_2 production and corresponding C assimilation integrated from 10-40 m for three stations measured at four different times during the summer.....115

List of Figures

Figure 1: Diagram of a typical mid-summer water column temperature profile, deep chlorophyll layer, and deep chlorophyll maximum value in Lake Superior 87

Figure 2: Diagram of the electron transport chain and associated light absorption at photosystem I and photosystem II, as well as the general sites of O_2 production and C assimilation, ... 88

Figure 3: Diagram of fluorescence measurements used by the fast repetition rate fluorometer to determine the maximum quantum efficiencies of photosynthesis at PSII 88

Figure 4: Map of stations sampled on Lake Superior during 2010 89

Figure 5: Flowchart of PAS sample workflow to determine the absorption due to several different phytoplankton pigment types 90

Figure 6: Seasonal temperature profiles through the water column measured at four stations across the lake 91

Figure 7: Seasonal chlorophyll *a* fluorescence profiles through the water column measured at four stations across the lake 92

Figure 8: Seasonal profiles of dissolved oxygen through the water column (expressed as concentrations) measured at four stations across the lake 93

Figure 9: Seasonal profiles of dissolved oxygen through the water column (expressed as percent of saturation) measured at four stations across the lake 94

Figure 10: Seasonal variability in the percentage of surface light reaching the DCM and light extinction coefficient (k_d) values 95

Figure 11: Seasonal variability in the depth of the DCM and the water temperature at the DCM 95

Figure 12: Late June profiles of phytoplankton pigment groups through the water column at four stations as determined by pigment fluorescence using a spectrofluorometer 96

Figure 13: Late July profiles of phytoplankton pigment groups through the water column at four stations as determined by pigment fluorescence using a spectrofluorometer 97

Figure 14: Late August profiles of phytoplankton pigment groups through the water column at four stations as determined by pigment fluorescence using a spectrofluorometer 98

Figure 15: Changes in carotenoid and phycoerythrin pigment absorbance from 30-35 m at EM in early June, late July, and late August 99

Figure 16: Changes in carotenoid and phycoerythrin pigment absorbance from 10 m, 20 m, and 30 m at FWM in early August.....100

Figure 17: Ratio of photoprotectant carotenoids to photosynthetic carotenoids (PPC:PSC) for discrete depth samples through the water column.....101

Figure 18: Spectral correction factors for measurements of the effective absorption cross section of PSII (σ_{PSII}) measured with the FRRF.....101

Figure 19: Seasonal profiles of the maximum quantum efficiency of photosynthesis at PSII (F_v/F_m) through the water column 102

Figure 20: Seasonal profiles of the effective absorption cross section of PSII (σ_{PSII}) through the water column 103

Figure 21: Linear regression between log10-transformed *a*PS x 0.5 values and log 10-transformed mean FluoroProbe fluorescence used extensively in calculating *a*PSII values using *a*PSII method 3.....104

Figure 22: Comparison of chl *a* normalized *a*PSII values (*a*PSII*) calculated using three different *a*PSII estimation methods.....105

Figure 23: Comparison of *P*, the ratio of estimated *a*PSII to measured *a*PS for two different *a*PSII estimation methods.....105

Figure 24: Photosynthetic O_2 production calculated for PAS samples from discrete depths using three different *a*PSII estimation methods.....106

Figure 25: Daily photosynthetic O_2 production rates from 10-40 m calculated with O_2 method 1 for two consecutive days in early August using two different *a*PSII estimation methods 107

Figure 26: Four estimates of daily photosynthetic O_2 production rates from 10-40 m calculated using O_2 method 2 with single profiles collected at four different times through the day (day 1 of 2) 108

Figure 27: Four estimates of daily photosynthetic O_2 production rates from 10-40 m calculated using O_2 method 2 with single profiles collected at four different times through the day (day 2 of 2) 109

Figure 28: Estimates of daily photosynthetic O_2 production rates from 10-40 m using O_2 method 2 and profiles taken at three different times during the summer and at four stations.....110-111

Figure A1: Schematic diagram of the three methods used to calculate daily photosynthetic O_2 production in this study (O_2 methods 1, 2, and 3) and how each uses fluorometer profiles collected through the day differently in order to obtain whole-day O_2 production estimates.....121

List of parameters

Parameter Name	Description	Units	Derivation
*a*ACC(λ)	Absorption of photosynthetic accessory pigments (400-700 nm).	m^{-1}	
*a*chl*a*(λ)	Absorption of chlorophyll *a* (400-700 nm).	m^{-1}	
*a*NAP(λ)	Absorption of non-algal particles (400-700 nm).	Arbitrary Units	
*a*P(λ)	Absorption of phytoplankton in sample (400-700 nm).	Arbitrary Units	
*a*PH(λ)	Absorption of phytoplankton pigments (400-700 nm).	m^{-1}	Eqn. 3
*a*PHEO(λ)	Absorption of pheophytin (400-700 nm)	m^{-1}	
*a*PS(λ)	Absorption of photosynthetic pigments (400-700 nm).	m^{-1}	
*a*PSII(λ)	Absorption of pigments associated with PS II (400-700 nm).	m^{-1}	
*a*PSII method 1	aPSII from half of average aPS from 400-700 nm	m^{-1}	Eqn. 9
*a*PSII method 2	aPSII from σ_{PSII} and chl *a* measures and assumed n_{PSII} value	m^{-1}	Eqn. 10
*a*PSII method 3	aPSII from log10-transformed FluoroProbe fluorescence using regression with aPS x 0.5	m^{-1}	Eqn. 12
F’	Minimum Fluorescence Light-Adapted	Arbitrary Fluorescence Units (FSU)	
F_m	Maximum Fluorescence Dark Adapted	Arbitrary Fluorescence Units (FSU)	
F_m’	Maximum Fluorescence Light-Adapted	Arbitrary Fluorescence Units (FSU)	
F_o	Minimum Fluorescence Dark-Adapted	Arbitrary Fluorescence Units (FSU)	
F_q’	Variable Fluorescence Light-Adapted	Arbitrary Fluorescence Units (FSU)	F_m’-F’
F_q’/F_m’	Effective Quantum Efficiency (Light-Adapted)	Dimensionless	
F_v	Variable Fluorescence Dark-Adapted	Arbitrary Fluorescence Units (FSU)	F_m-F_o
F_v/F_m	Maximum Quantum Efficiency (Dark-Adapted)	Dimensionless	
P	Fraction of the total pigment absorption due to pigments associated with PSII	Unit less	(*a*PSII x *a*PS^{-1})
σ_{PSII}	Effective Absorption Cross Section of Photosystem II	$Å^2$ x $quanta^{-1}$	

List of abbreviations

Abbreviation	Description
chl *a*	Chlorophyll *a*
CTD	Conductivity, temperature, depth probe; also measures DO concentration
DCL	Deep chlorophyll layer; depth zone where chl *a* concentrations exceed those in the epilimnion
DCM	Deep chlorophyll maximum; depth of maximum chl *a* concentration located below the epilimnion
DO	Dissolved oxygen
ETC	Electron transport chain connecting photosystem II (PS II) to photosystem I (PS I) and the processes of O_2 production to C assimilation
ETR	Electron transport rate for electrons moving through the electron transport chain (ETC)
ETR_{PSII}	Electron transport rate for only photosystem II (PS II)
FRRF	Fast repetition rate fluorometer
PAR	Photosynthetically active radiation (400-700 nm)
PAS	Particle absorption spectrum (400-700 nm)
PC	Phycocyanin photosynthetic pigment absorbs light at 650 nm
PE	Phycoerythrin photosynthetic pigment absorbs light around 550 nm
PPC	Photoprotectant carotenoid pigment
PQ	Photosynthetic quotient for conversion of O_2 production rate to equivalent C assimilation rate
PS I	Photosystem I
PS II	Photosystem II; pigment fluorescence originates from PS II only
PSC	Photosynthetic carotenoid pigment
QFT	Quantitative filter technique used to determine the absorption spectra of different particle and phytoplankton pigments retained on a filter
SCF	Spectral correction factor used to normalize σ_{PSII} values measured with the blue excitation light of the FRRF to a spectrally flat (white) light field

General Introduction

Importance of photosynthesis in aquatic ecosystems

Photosynthesis in land plants and the carbon compounds it generates are critical to meet the energy demand of terrestrial ecosystems. In aquatic ecosystems photosynthesis can be even more important, since it not only provides much of the energy for the ecosystem, but it also produces dissolved oxygen (DO), which is essential for the survival of aquatic animals including fish and zooplankton. If a body of water is shallow, then photosynthesis by submerged aquatic plants may be able to provide substantial quantities of DO. However, in the pelagic zone of marine and lake ecosystems, most of the available DO is provided by small, free-floating photosynthetic phytoplankton.

Phytoplankton is a general term describing aquatic Eukaryotic and Prokaryotic photoautotrophic organisms that are suspended by turbulence and transported passively by water movements. In both oceans and lakes, different groups of phytoplankton are adapted to specific nutrient, light, and temperature conditions. Lakes typically have a more extreme and dynamic range of these critical factors than oceans, such as nutrient concentrations (Guildford & Hecky, 2000), and this leads to strong seasonal succession of phytoplankton communities as these ambient conditions change.

Either on land or in water, photosynthesis converts light energy into carbon compounds through a pathway that involves several distinct processes. The light-dependent reactions of photosynthesis require two different photosystems: Photosystem I (PS I) and Photosystem II (PS II) (Figure 2). Both photosystems have antenna pigment beds associated with them that include chlorophyll *a* (chl *a*) and other photosynthetic accessory pigments to absorb photons and transfer the resulting excited electron to the

photosystem where it can be used in photochemistry. The photosynthetic pathway begins with PS II using absorbed light energy to split water molecules, which yields free O_2 as well as four protons and four electrons for every two water molecules split. The O_2 is released to the ambient environment, the protons provide energy for the production of ATP, and the electrons enter the electron transport chain (ETC), where they eventually reduce CO_2 to organic carbon molecules (referred to as 'C assimilation' in this project).

Distribution of phytoplankton in aquatic systems

A deep chlorophyll layer (DCL) is a common feature in both stratified lakes and in oceans. The DCL is the depth band below the surface mixed layer where chl *a* concentrations exceed those in the surface mixed layer (often termed the epilimnion in lakes) (Figure 1). In lakes, the DCL is most often observed during the summer when thermal stratification has established a metalimnion, which represents a depth zone of rapidly decreasing temperatures, and therefore also rapidly increasing water densities, that overlies a deep colder zone of nearly constant temperature, the hypolimnion. The DCL is typically located below the thermocline, the plane of most rapid change in temperature and density) in the lower metalimnion to upper hypolimnion (Kiefer *et al*., 1972). Increased chl *a* concentrations in the DCL relative to the epilimnion are likely due to a combination of increased phytoplankton concentrations and increased chl *a* content per cell within these phytoplankton (Callieri, 2007, Fee, 1976).

There are currently two hypotheses to explain DCL formation. The first characterizes the DCL as a passive zone of accumulation for both viable and non-viable phytoplankton sinking from the epilimnion. This accumulation would mainly be due to decreases in phytoplankton settling rates that occur when nutrient limited cells reach the

relatively high nutrient concentrations immediately below the thermocline (Titman and Kilham, 1976), and to a lesser extent due to the presence of small-scale turbulence within the thermocline (Derenbach *et al.,* 1979). Alternatively, the DCL may result from viable phytoplankton with growth rates exceeding loss rates. In this case the DCL can be an important zone for photosynthesis and algal production in lakes. The location of the DCL below the thermocline may then be a population growth response to a favorable *in situ* light and nutrient environment where growth exceeds losses to sinking and grazing. In nature both the abiotic affects of phytoplankton sinking from the epilimnion and active *in situ* growth can contribute to the formation of a DCL, which may itself be directly modified by phytoplankton losses due to zooplankton grazing (Cullen, 1982). However because light and nutrient conditions at depth in the DCL will be quite different from conditions in the epilimnion, different algal groups will be favored and differences in the community composition of the DCL from the epilimnion would be expected if *in situ* growth were an important process. Because both abiotic and biotic processes can contribute to the DCL, determining the significance of the DCL to total lake productivity is often problematic if not controversial (Fahnenstiel and Glime, 1983, Sterner, 2010). In oligotrophic lakes of low productivity, sensitive *in situ* measurements of photosynthesis are required to determine the occurrence of significant algal growth within the DCL and to establish its importance to the productivity of the lake.

Techniques to measure aquatic photosynthesis

There are two major methods that can be used to measure the rate of photosynthesis in the DCL or at other depths in the water column. The conventional method measures ^{14}C assimilation during either *in situ* or artificial light incubations to

estimate rates of photosynthesis. This technique has been used successfully for several decades, and its estimates of primary production are widely accepted. Since it has been used so extensively, the results of this method allow for useful comparison of primary production estimates within and among lakes of different sizes, trophic states, and geographic distributions. The use of ^{14}C incubations has several limitations, however. Perhaps most importantly for estimating photosynthesis in the DCL, the ^{14}C method has limited depth resolution since it necessarily estimates water column photosynthesis from discrete sampling depths whereas chl *a* gradients are continuous and often very sharp. In the DCL, slight differences in the sample depth used for an incubation may therefore lead to very different results. In addition, bottle effects resulting from environmental changes during sampling and enclosing water in an incubation container relative to the open lake may alter ^{14}C uptake and apparent photosynthetic rates even when using *in situ* incubations to ensure exposure to natural light regimes. Since rates of photosynthesis are dependent on light quality, photosynthetic estimates derived from incubations using artificial light sources may not be representative of *in situ* photosynthesis as there are strong and wavelength selective gradients of light extinction that can lead to spectral affects not reproduced in the incubator. Finally, apparent ^{14}C assimilation rates and their corresponding estimates of photosynthesis may be altered by respiration from phytoplankton, bacteria, or zooplankton during the incubation, which can lead to recycling of ^{14}C and uncertainty as to whether the uptake of C is representative of gross or net production by the phytoplankton community (Peterson, 1980).

An alternate method to estimate phytoplankton photosynthesis uses photosynthetic pigment fluorescence to calculate estimates of photosynthetic O_2

production. Both PS II and PS I utilize non-photochemical quenching to dissipate absorbed light energy that is in excess of their photochemical capacity to use excited electrons. Unless the excess energy is efficiently quenched, it can cause damage to the photosystems through formation of reactive oxygen species. For pigments associated with PS I, excess light energy is mainly quenched through heat production. At PS II, antenna pigments also largely quench excess light energy by generating heat, but some of the excess light energy is transferred to a chl *a* molecule, which achieves additional energy quenching by emitting fluorescence.

Fluorometers take advantage of this fluorescent response by subjecting phytoplankton samples to flashes of light and then measuring the resulting pigment fluorescence. These measurements provide a commonly used, quick, non-invasive method to determine an estimate of chl *a* concentration in a sample. Analysis of the fluorescent response to variable excitation energies can also be used to measure several different photosynthetic characteristics of the phytoplankton sample. Recently commercial *in situ* spectral fluorometers have become available that not only measure the fluorescence of chl *a* but also of other photosynthetically important pigments which are diagnostic of different phytoplankton groups. In addition, since the fluorescence detected by these spectrofluorometers is mainly emitted from pigments associated with PS II, measurements of fluorescence by those pigments can therefore be used to estimate rates of photosynthetic O_2 production.

Measurement of photosynthetic parameters using Fast Repetition Rate Fluorometry

A Fast Repetition Rate Fluorometer (FRRF) uses multiple sub-saturating pulses of light in quick succession to chemically reduce and therefore progressively close all PS II reaction centers within a single turnover (ST). The FRRF first measures the minimum pigment fluorescence (F_o, see the list of parameters in the introductory material for explanation of all symbols used) before exposure to the pulses of light, and the maximum fluorescence (F_m in dark adapted samples or F_q' if measured under ambient light) after the PS II reaction centers have been closed. The resulting variable fluorescence (F_v/F_m in the dark or F_q'/F_m' under ambient light) provides a measure of how efficiently PS II reaction centers use absorbed light energy to drive photochemistry and produce O_2 (Figure 3). Larger F_v/F_m or F_q'/F_m' values indicate increased photosynthetic efficiency, and although both have a theoretical maximum value of 0.65 (Falkowski and Kolber, 1995), measurements of some phytoplankton have exceeded that value (Suggett *et al*., 2009b). In addition, the FRRF technique can characterize the rise in fluorescence resulting from the progressive closure of all PS II reaction centers. The slope of this fluorescence induction curve is the effective absorption cross section of PS II (σ_{PSII}), and is a measure of the size of the antenna pigment bed associated with PS II reaction centers (Kolber *et al*., 1998).

Estimating rates of photosynthesis using pigment fluorescence-based profilers has several advantages compared to ^{14}C incubations. The fluorescence measurements are taken *in situ*, which eliminates the environmental bottle effects present in the incubations. In addition, the fluorescence-based profilers inherently generate estimates of gross photosynthetic production and therefore avoid the ambiguity between gross and net production that is associated with estimates made using ^{14}C incubations (Peterson, 1980).

Finally, each profile can also be completed in several minutes and has extremely fine depth resolution compared to ^{14}C incubations, which allows for rapid measurement and accurate determination of photosynthetic changes over small depth intervals within the DCL.

Limitations of the FRRF technique

Like ^{14}C incubations, using FRRF profilers to estimate primary production also has potential limitations. Although FRRF profilers have been used fairly extensively to estimate phytoplankton photosynthesis in marine systems, there are relatively few studies using the FRRF to estimate photosynthetic rates in lakes. ^{14}C incubations are still the standard method to estimate primary production in freshwater systems. Because fluorescence-based measurements are derived from pigments associated with PS II, they directly estimate photosynthetic O_2 production, and not C assimilation. Although the two processes are related (Figure 2) by the photosynthetic quotient (PQ) conversion factor, estimates of photosynthetic C assimilation from fluorescence profilers using a PQ may introduce artificial variability for comparing estimates of O_2 production with estimates using ^{14}C assimilation. Finally, the FRRF profiler used in this project makes all of its fluorescence measurements using blue light with a peak wavelength of 470 nm. Blue light overlaps the Soret absorption band of chl *a* from roughly 400-475 nm (Falkowski and Raven, 2007), so the FRRF measurements are quite responsive to changes in the quantum efficiency of chl *a*, but cannot evaluate the fluorescent response of other photosynthetic pigments that do not absorb blue light. For this reason the measured σ_{PSII} values from FRRF, which are wavelength-dependent, need to be normalized to a

reference spectrum using a Spectral Correction Factor (SCF) before comparisons can be made across studies.

DCL location in Lake Superior and its ecological significance

After Lake Superior has stratified in the summer, the depth of the peak chl *a* concentration in the water column is the location of the deep chlorophyll maximum (DCM), which is usually found below the thermocline at depths ranging from 23-35 m (Barbiero and Tuchman, 2004). While the DCM represents the peak chl *a* concentration below the epilimnion, the DCL represents the depth range of increased chl *a* concentrations relative to the epilimnion, and includes the DCM (Figure 1). However, because Lake Superior is oligotrophic, the absolute chl *a* concentrations in the DCL are still low compared to more productive lakes. Although Lake Superior has extremely clear water with an average yearly light extinction coefficient (k_d) of roughly 0.17 m^{-1} (inferred from Figure 3 in Guildford *et al*., 2000), and a whole-lake summer average of roughly 0.16 m^{-1} (inferred from Figure 6 in Barbiero and Tuchmann, 2001b), phytoplankton growth within the mixed layer is light-limited for most of the year (Guildford *et al*., 2000) because of the large mixed layer depth during winter. Only when the lake becomes thermally stratified during the summer and the surface mixed layer becomes narrower are phytoplankton in this portion of the water column not light limited, but they become strongly nutrient limited instead (Guildford *et al*., 2000). During stratification, the increased chl *a* concentrations within the DCL may therefore be due to phytoplankton adaptations that allow more efficient light absorption for use in photosynthesis. The stability of the stratification within the metalimnion may allow for highly adapted organisms to maintain their position in the light and nutrient gradient that

develops during stratification. Measuring the concentration of chl *a* per phytoplankton cell, or the ratio of C to chl *a* can help determine whether increases in DCL chl *a* concentrations are mainly due to increased phytoplankton abundance or increased chl *a* concentration within each phytoplankton cell.

There are distinct changes in phytoplankton taxonomic groups in Lake Superior during the summer both in the epilimnion but also in the DCL. Early in the season cryptophytes and diatoms are the most common groups, although cyanobacteria and chrysophytes are also present in moderate numbers. By late summer chrysophytes reached higher densities in the epilimnion, with cryptophytes and diatoms also common (Barbiero and Tuchman, 2001a). Repeated measurements from a single station in 1979 showed that centric diatoms comprised the majority of chl *a* in the DCL (Fahnenstiel and Glime, 1983). However, single observations taken at multiple stations across the lake nearly 20 years later documented a decrease in centric diatom abundances as a proportion of total phytoplankton biovolume within the DCL compared to the epilimnion (Barbiero and Tuchman, 2004). In Lake Superior picoplankton less that 2 μm in diameter, mostly picocyanobacteria, are an ecologically important group, representing nearly 50% of total chl *a* concentrations in surface water and the DCL by early fall (Ivanikova *et al*., 2007).

In Lake Superior, the metalimnion and the DCL with its higher concentration of phytoplankton also represents an upward boundary for zooplankton diel vertical migration (DVM) from the hypolimnion (Bowers, 1988). The two dominant zooplankton species in Lake Superior by biomass are the calanoid copepod *Limnocalanus macrurus* and the crustacean *Mysis relicta*. Previous sampling on Lake Superior has shown that, unlike *Mysis*, *Limnocalanus* does not undergo DVM into DCL (Conway, 1977). At dusk

young *Mysis* especially move from the hypolimnion into the metalimnion and the depth range of the DCL, but they do not cross the thermocline into the warm epilimnion; before dawn they return to hypolimnion (Bowers, 1988). The nighttime ascent of the zooplankton into the DCL is likely in response to the DVM behavior of zooplanktivorous coregonine predators in the lake such as cisco (*Coregonus artedi*) and kiyi (*C. kiyi*), but the phytoplankton in the DCL likely also represent a major food resource for the migrating zooplankton.

The nutrients necessary to support the increased phytoplankton growth within the DCL may be provided in two distinct ways. Nutrients in the metalimnion may be supplied by the nutrient-rich water of the hypolimnion due to diffusion of each nutrient along its concentration gradient. Alternatively, zooplankton excretion, egestion, or sloppy feeding within the DCL can all increase concentrations of nutrients available to phytoplankton. Because the zooplankton only enter the DCL at night, their DVM serves to introduce nutrients into the DCL in nocturnal pulses. The availability of phosphorous, nitrogen and other nutrients in the water has been shown to affect both the photosynthetic efficiency (Berges *et al*., 1996) and growth rates (Healey, 1985, Sterner *et al*., 2004) of phytoplankton. In Lake Superior, phosphorus is the major limiting nutrient to phytoplankton growth, so it is possible the ability of *Mysis* to alter nutrient availability within the DCL could at least maintain the growth rate and photosynthetic capacity of phytoplankton within the DCL, and may in fact be sufficient to cause an increase in phytoplankton growth. If this is the case, it is likely that phytoplankton in the DCL are well-adapted to environments where the availability of nutrients is transient, and they could therefore efficiently use the nutrient pulses released by the zooplankton for growth

and photosynthesis. However if the nutrients supporting DCL growth mainly diffuse upward from the hypolimnion, then phytoplankton in the DCL may be adapted to conditions with more constant nutrient concentrations throughout the day.

Scope of this project

This research was driven by two major objectives. First we wanted to determine the duration and composition of the DCL in Lake Superior and its position in the water column across the lake during the summer of 2010. Here we sought to characterize changes in photosynthetic parameters of phytoplankton in the DCL through the season by using the fine resolution provided by fluorescence-based profilers and independent measurements of pigment absorbance at discrete depths. Second, we used our data to test the hypothesis that the DCL in Lake Superior is a zone of active photosynthesis and not simply a passive accumulation of phytoplankton settling from the epilimnion. Daily depth-integrated photosynthesis estimates below the mixed layer were calculated for consecutive days in mid-August and compared them to published ^{14}C incubation values for C assimilation in Lake Superior. Photosynthetic production estimates were also calculated using profiles collected at other times of year and other locations on the lake to begin to assess the spatial and seasonal variability of phytoplankton photosynthesis in Lake Superior. Finally the merits of using fluorescence profilers to better determine the spatial and depth variability of photosynthetic production in Lake Superior are discussed, including their potential utility in future community respiration studies.

Chapter 1

Changes in the photosynthetic characteristics of the DCL in Lake Superior through the summer

Introduction

Physical changes in the water column through the summer

Describing seasonal changes in physical parameters within a lake is critical to understanding the distribution of phytoplankton and their photosynthetic potential during the summer. The physical process of thermal stratification, which also determines the saturation concentration of DO in the water, is perhaps the most important factor affecting phytoplankton growth during the summer in temperate lakes that are deeper than a few meters. When a lake is thermally stratified, the sharp change in water temperature within the metalimnion splits the water column into epilimnion, comprising the warmer surface mixed layer, and cold hypolimnion, which usually contains higher concentrations of nutrients necessary for phytoplankton growth. Due to these thermal and nutrient gradients, phytoplankton communities within the epilimnion tend to be different from those deeper in the water column within the hypolimnion. Although there may be some degree of movement between the two communities through the settling of relatively heavy phytoplankton from the epilimnion (Titman and Kilham, 1976), or through phytoplankton moving using flagella or by adjusting their buoyancy, most phytoplankton are functionally non-motile over the scale of meters that separates portions of the water column in large lakes.

In addition to affecting phytoplankton distribution, the sharp temperature gradient within the metalimnion produces a water density gradient that strongly affects the capacity of the water to hold the DO produced by photosynthesis. Once the lake begins to stratify early in the summer, the warmer water in the epilimnion is not able to hold as much DO in solution as the colder water in the hypolimnion, resulting in decreased epilimnetic DO concentrations as the water equilibrates with the atmosphere. However the density gradient in the metalimnion prevents water in the metalimnion and hypolimnion from also equilibrating with the atmosphere, so DO concentrations may become supersaturated if more O_2 is being produced by phytoplankton photosynthesis than is being consumed by total organism respiration. In Lake Superior, both *Limnocalanus* (Conway, 1977) and *Mysis* (Bowers, 1988) typically remain in the hypolimnion where temperatures are cooler and DO concentrations are higher compared to the epilimnion. Phytoplankton populations in the epilimnion therefore face reduced grazing pressure by these zooplankton, but the water density gradient produced by the thermocline likely prevents any nutrient pulses released by the zooplankton from diffusing upward into the epilimnion.

Factors affecting the in situ light environment of phytoplankton

Over the course of one year, phytoplankton communities in either lakes and estuaries are exposed a wider range of ambient light intensities and changes in the spectral composition of photosynthetically active radiation (PAR = 400-700 nm) compared to phytoplankton living in the open ocean. Phytoplankton populations in both environments are exposed to the same general variations in PAR intensity on a diel and an annual basis due to changes in the sun angle. However in lakes and estuaries light

intensity through the water column may also vary due to seasonal changes in dissolved organic matter (DOM) present in the water or in response to changes in phytoplankton concentrations caused either by formation of the DCL or growth of phytoplankton blooms due to increased nutrient levels. All three of these phenomena increase the amount of surface light that is absorbed through the water column, which results in larger values of the light extinction coefficient, k_d.

As k_d increases, there is a decrease in the depth of the euphotic zone boundary, which represents the depth where ambient light in the water is 1% of surface PAR; this effectively compresses the depth range where light intensities are bright enough to sustain phytoplankton photosynthesis. In addition to limiting the portion of the water column where phytoplankton can survive, increases in k_d also cause the ambient light environment within the euphotic zone to be spectrally shifted towards longer wavelengths (Raateoja *et al*., 2004). In the open ocean where k_d remains fairly constant during the year and blue light penetrates deeply into the water column, phytoplankton mainly use chl *a* and a relatively small number of other photosynthetic pigments to effectively absorb this blue light. Like their marine counterparts, phytoplankton communities in lakes and estuaries contain chl *a*, but they also contain a wide range of other photosynthetic accessory pigments, allowing them to efficiently absorb the wide spectral range of PAR present in the environments where they live. Three of the most common accessory pigments found in freshwater phytoplankton are phycoerythrin (PE), which absorbs green light, phycocyanin (PC), which absorbs red light, and carotenoids, which absorb blue-green light.

Changes in phytoplankton community composition during the summer

Despite the low absolute pigment concentration in the DCL of Lake Superior, it is still possible to observe seasonal shifts in the phytoplankton community as determined by changes in pigment absorbance. Ivanikova *et al*. demonstrated that communities of *Synechococcus* picocyanobacteria (< 2 μm diameter) found in the lake changed from being PC-rich early in the summer to increasingly PE-rich once the DCL had formed (2007). Similar shifts between PC- and PE-rich *Synechococcus* strains have been observed in a variety of lakes and marine systems in response to changes in light extinction and mixed layer depth (Stomp *et al*., 2007) and were shown to be adaptations to changes in the in situ light spectrum. Although the pelagic zone of Lake Superior has consistently low turbidity, the light environment in the water column can change through the season due to changes in DOM content and increased phytoplankton concentrations in the water column that both effectively increase the light attenuation with depth while simultaneously causing spectral shifts.

Changes in phytoplankton photosynthetic parameters

In addition to changes in phytoplankton pigment composition through the summer, the measurements of photosynthetic potential in the water column made using the FRRF technique also have important ecological implications. As a measurement of the maximum quantum efficiency possible with all PS II reaction centers open (oxidized), the F_v/F_m value measured from dark-adapted cells also gives an indication of the relative number of PS II reaction centers present in a sample. A larger number of PS II reaction centers within each phytoplankton cell will allow it to effectively utilize a greater amount of light energy for use in photochemistry before all PS II reaction centers close and the cell reaches its maximal fluorescence (F_m). In contrast, under ambient light conditions

where phytoplankton are actively photosynthesizing and there are both open and closed (reduced) PS II reaction centers present, the variable fluorescence (F_q'/F_m') reflects how efficiently phytoplankton use absorbed light to drive photochemistry in situ.

As a measurement of the effective absorption cross section of PSII, σ_{PSII} varies with both the size and the orientation of the antenna pigment bed with respect to the ambient light field in the water column. When the angle between the antenna pigment bed and the incident light becomes increasingly perpendicular, then σ_{PSII} will also increase even if the physical size of the pigment bed remains constant (Falkowski and Raven, 2007). Measurements made on phytoplankton cultures representing all major phytoplankton taxonomic groups found that σ_{PSII} and F_v/F_m have an inverse relationship, likely related to trade-offs between the amount of light energy that can be absorbed and how efficiently that energy can be used for photochemistry (Suggett *et al*., 2009b).

Both the quantum efficiency (either F_v/F_m or F_q'/F_m') and σ_{PSII} respond to changes in water nutrient concentrations and also vary between different phytoplankton taxonomic groups. Nitrogen limitation preferentially decreases the function of PS II reaction centers instead of PS I reaction centers, and therefore substantially affects measured quantum efficiency values in both diatoms and cyanobacteria (Berges *et al*., 1996). Potentially even more important than affects of nutrient limitation are the intrinsic differences in quantum efficiency and σ_{PSII} values between various phytoplankton groups, especially between cyanobacteria and other phytoplankton (Suggett *et al*., 2009b). All FRRF profiles of in situ phytoplankton communities will therefore represent an amalgamation of the distinct photosynthetic parameters of each phytoplankton taxonomic group present in the water column.

Before stratification, we would expect fairly constant F_v/F_m and σ_{PSII} values through the water column because the phytoplankton are being mixed throughout the surface layer and cannot adapt to light conditions at a specific depth. After the water column has stratified, however, we hypothesize that σ_{PSII} will be variable with depth as the pigment content of the phytoplankton and their antenna pigment bed orientation with respect to the in situ light field both adapt to the ambient conditions at each depth. The quantum efficiency in turn depends both on the light absorption capacity as estimated by σ_{PSII} as well as the rate of electron transport in the photosynthetic pathway downstream of PS II. If the relatively low-light environment of the DCL represents a depth zone of active phytoplankton growth, we would expect the phytoplankton within the DCL to have relatively high values of F_v/F_m compared to the surface mixed layer, which would allow them to efficiently use any absorbed light energy to drive photosynthesis.

Objectives

Using various water column profilers, we first sought to describe the physical changes in the water column during the summer in Lake Superior, including temperature, light extinction, and DO concentrations. We then measured characteristics of the phytoplankton including the chl *a* concentration and pigment absorption spectra from discrete depth samples. Using pigment fluorescence profilers, we also measured the relative distribution of different pigment groups and both photosynthetic efficiency and effective absorption cross-section of PSII through the water column during the summer. Finally the abiotic and the biotic data were analyzed together to look for linkages and feedback between the two, especially within the DCL.

Methods

Chlorophyll *a* fluorescence, water temperature, and DO concentration data were measured using an extended-capability conductivity, temperature, and depth (CTD) instrument package (SeaBird Electronics Bellevue, WA) on nine cruises aboard the R/V Blue Heron from late May to late September 2010 and pigment fluorescence profilers were used on seven cruises from early June to early September 2010. Samples from each of six mooring locations distributed across the lake were taken at least twice during the season, and several other stations were sampled once during the summer, giving broad temporal and spatial coverage (Figure 4). Stations CM, EM, FWM, and WM were sampled the most frequently during the summer, and only the data from these stations are reported here.

Water samples for chl *a* analysis and for measuring the particle absorption spectrum (PAS) of suspended material in the water, including phytoplankton, were collected using a Niskin sampling rosette and were kept cool and dark after collection. As soon as possible the water was filtered through GF/F filters (Whatman). Triplicate filters for chl *a* were each prepared using 1-2 L of water that was pre-screened using 210 μm nitex mesh. Size-fractioned phytoplankton samples for determination of picoplankton (< 2 μm) chl *a* content were also taken by passing at least 1 L of pre-screened water through a 2 μm polycarbonate membrane filter (Millipore) and collecting the filtrate, which was then filtered through a GF/F filter. Samples for use in PAS measurement were prepared by filtering as much pre-screened water as possible through a GF/F filter, but no less than 1.5 L. All GF/F sample filters were frozen immediately after sample collection, and kept frozen until analysis. Background water fluorescence offsets for the FRRF and spectral

fluorometer were prepared at the same time as the chl *a* and PAS samples by filtering water through a 0.2 μm polycarbonate membrane filter (Millipore) to remove all phytoplankton. The filtered water was then stored in the refrigerator until the offset measurements were taken.

Phytoplankton community and size-fractioned picoplankton samples filtered onto GF/F filters for chl *a* determination were extracted with 10 mL of 90% acetone overnight and fluorescence was then measured using a 10-AU fluorometer (Turner Designs, Sunnyvale, CA) before and after acidification with several drops of 6N HCl. The fluorometer was calibrated using chl *a* extracted from *Anacystis nidulans* (Sigma). Concentrations of chl *a* and pheophytin *a* were calculated from the fluorescence values.

The SeaBird CTD-fluorescence-O_2 instrument package was attached to the water-sampling rosette and was used to collect temperature, total chl *a* fluorescence, and DO concentration data through the water column at each sampling location. Profiles of absolute DO concentrations were also converted into equivalent percentages of DO saturation through the water column. The concentration of DO necessary to reach saturation varies based on water temperature and lake altitude (183 m used for Lake Superior), and all calculations followed the methods described by Benson and Krause, particularly using Eqns. 18, 22, and 28 (1980).

FRRF measurements

For all FRRF profiles the instrument (FastTrackaII Chelsea Instruments, UK) was programmed to deliver 100 single-turnover flashlets 1 μs apart with an intensity of 0.0336 photons x [nm x flashlet]$^{-1}$ and to collect the fluorescence response for 25 of these sequences per acquisition. The relative LED intensity was set to 48 and the

photomultiplier tube voltage was set to 550 V for all profiles. The peak excitation wavelength of the FRRF is 470 nm, with a half bandwidth of 20 nm, which overlaps the Soret absorption band of chl *a*. An attached PAR sensor and depth sensor allowed for simultaneous F_v/F_m and σ_{PSII} acquisitions together with PAR measurements that could later be matched to data from other profilers at the same depth. Prior to each profile, the FRRF was lowered into the surface water and held stationary for roughly one minute to equilibrate with the water temperature. The profile was then taken by lowering the FRRF through the water column at about 0.5 m x s^{-1} to a depth up to 80 m and well below the DCL. Whenever possible, at each sampling station profiles were taken using both the dark and the light chamber of the FRRF, which are interchangeable chambers attached to the same measuring sensors. Both chambers allow water to flow past the measuring sensors while the FRRF is being lowered, but the dark chamber allows for transient dark-adaptation of phytoplankton to give measurements of F_v/F_m, while the light chamber measures the phytoplankton under ambient light conditions to give measurements of F_q'/F_m'.

Offsets to correct raw fluorescence measurements for the effect of background water fluorescence not due to phytoplankton were measured using filtrate samples from 0.2 μm membrane filters, which were prepared as described above. Offsets values were determined by measuring the fluorescence of the filtrate in the dark chamber of the FRRF using the same acquisition protocol and settings as for the water column profiles. At least 25 fluorescence data acquisitions were averaged to give mean F_o and F_m values for each offset. Overall, average offset values showed no apparent trends with station location, sample depth, or time of year (n=78; data not shown). Fifteen offset measurements had

considerably higher F_o and F_m values than all other offsets, however, which is likely a result of cell rupture or filter leakage related to size fractionation procedures and not due to inherent water properties in the lake. These offsets were therefore disregarded, and the mean F_o and F_m values from all other offsets combined (n = 63) were applied as a standardized correction to all FRRF profiles. Offsets were applied by subtracting the mean F_o and F_m offset values from the raw F_o and F_m values for each profile and then calculating updated F_v/F_m or F_q'/F_m' values for that profile after the mean F_o and F_m offsets were applied.

The presence of pheophytin *a* in the water in high concentrations can cause measured F_v/F_m and F_q'/F_m' values to be underestimated. This was corrected by using a rearrangement of Equation 13 in Fuchs *et al*. (2002):

$$(1) \quad \Phi_{\text{chl}a} = \Phi_{\text{mix}} \times \left[\left(0.9 \times (1 - R) + 0.1 \right) \times (1 - R)^{-1} \right]$$

Where R is the molar ratio of the pheophytin *a* concentration to the combined pheophytin *a* and chl *a* concentration (R = [pheophytin *a*] x ([chl *a*] + [pheophytin *a*])$^{-1}$), using pigment concentrations measured with the acetone extraction technique described above, Φ_{mix} is the measured quantum efficiency (F_v/F_m or F_q'/F_m') from a FRRF profile, and $\Phi_{\text{chl}a}$ is the calculated quantum efficiency due only to photosynthetically active chl *a*.

FluoroProbe measurements

To complement the PAS measurements, a spectral fluorometer (FluoroProbe, bbe Moldaenke, Kiel, Germany) was used to measure chl *a* fluorescence in response to five excitation wavelengths (470 nm, 525 nm, 570 nm, 590 nm, and 610 nm) that have been chosen to best distinguish different phytoplankton taxonomic groups containing chl *a* and

other photosynthetic accessory pigments (Beutler *et al*., 2002). The FluoroProbe was used to profile the water column immediately before or after the FRRF was deployed, and provided data with the same depth resolution as the FRRF. Because fluorescence is predominantly emitted by PS II, the FluoroProbe software (FluoroProbe) can apply spectral algorithms to the collected data to determine the relative photosynthetic pigment composition associated only with PS II, as first introduced in Beutler *et al*. (2002). This was done using factory-defined fluorescence spectra characteristic of phytoplankton in each measured pigment group (greens, blue greens (PC-rich), browns (phytoplankton containing brown pigments including carotenoids), and cryptophytes (PE-rich)). Each of these reference spectra is derived from measurements of several different cultured phytoplankton strains belonging to each pigment group. Critically, all of these reference spectra must be linearly independent, must remain relatively unchanged for each algal group regardless of the number of cells measured or the specific growth conditions for the phytoplankton, and must have enough accuracy in the measurements to confidently separate the reference spectra from each pigment group (Beutler *et al*., 2002). If these conditions are met then the total chl *a* fluorescence of a phytoplankton community sample measured at the five excitation wavelengths of the FluoroProbe can be separated into the chl *a* fluorescence due to phytoplankton in each pigment group. This is accomplished through a regression of each of the four reference spectra against the measured total fluorescence at all five excitation wavelengths to give a weighting factor for each reference spectrum. However because the reference spectrum for each of the pigment groups will have different accuracy, and the accuracy of each spectrum can also vary across the excitation wavelengths, this is incorporated into the residual sum of

squares equation that is minimized in order to yield the final regression values for the reference spectrum weights (Beutler *et al*., 2002).

To ensure accurate pigment group determination, fluorescence data collected from the FluoroProbe needs to be corrected for background fluorescence using offsets prepared in the same way as for the FRRF. FluoroProbe measurements of background fluorescence were made by placing a quartz cuvette filled with 0.2 μm filtered water into the measuring chamber of the FluoroProbe and then taking measurements following the same acquisition protocol as for the profiles. After measurements for all offset samples (n = 59) had been taken, however, it was evident that the presence of the cuvette had artificially increased the recorded fluorescence values for the offsets. For some samples the influence of the cuvette made the fluorescence measurements of the phytoplankton-free offsets larger than those recorded during the in situ profile. We determined a 'cuvette correction factor' by making three replicate measurements of a Milli-Q filtered water blank in the cuvette, which represented the combined effects of instrument noise and the cuvette itself on our measurements. In addition, two different FluoroProbes were used to collect profiles during the summer of 2010, each with its own instrument noise and cuvette offset value derived from the Milli-Q filtered water blanks. To ensure the final, offset-corrected profile measurements were not overestimates of the actual in situ phytoplankton fluorescence, the 'cuvette correction factor' value at each of the five excitation wavelengths from the FluoroProbe with the smaller mean 'cuvette correction factor' was used as the universal correction factor. Furthermore, from visual inspection of the raw fluorescence measured in response to each of the five excitation wavelengths for all offset samples, the values for each wavelength were similar for samples collected

during the same cruise but were different from samples collected on other sampling cruises. The mean offset value at each wavelength and for each cruise was therefore applied only to profiles taken during that cruise, resulting in seven different offset values being applied to the 2010 data. The final offset corrected profile measurement for each of the five different excitation wavelengths was calculated by first finding the difference between the measured filtered water sample value and the 'cuvette correction factor'; this value was then subtracted from the raw profile measurement to give the final offset corrected measurement.

Depth measurements for the FluoroProbe and FRRF profiles at each station were calibrated to each other by first setting their depth values relative to the water surface, and then averaging all data into 1 m depth bins. Only the downcast portion of these depth-binned values was used in all subsequent calculations and analyses.

Light extinction through the water column

Light extinction coefficients (k_d) were calculated using irradiance data collected from both the CTD and the FRRF PAR sensors. The natural log-transformed irradiance data were plotted as a function of depth and any obvious anomalies from a straight line were removed before a linear regression was fit. These deviations normally occurred near the top or bottom of the profile, and there were no large changes in light extinction through the DCL, which is consistent with the low chl *a* values in Lake Superior and their generally small effect on light extinction. The absolute value of the slope of the fitted regression line provided the k_d value. Where measurements from both the FRRF and CTD were available, k_d values were linearly correlated (R^2=0.88, n=10, $P < 0.001$) with values calculated from the FRRF being on average 76% of the CTD – derived value.

This difference is likely due to the PAR sensor geometry. The FRRF PAR sensor is a plane, but the CTD PAR sensor is spherical, allowing it to measure ambient light that has travelled a longer path length through the water column and reaches the CTD PAR sensor from angles that the FRRF PAR sensor is not able to measure. Therefore the k_d value derived from the CTD for a given ambient light field would be larger than the k_d value derived from the FRRF PAR sensor in the same light environment. This project mainly used the k_d values derived from the FRRF PAR sensor because they were measured simultaneously with the F_q'/F_m' and σ_{PSII} values used to calculate photosynthetic production estimates. The k_d values from the CTD were only used to track seasonal trends in k_d values because they spanned a longer portion of the summer than the FRRF-based values.

Spectral Correction Factors (SCFs)

Measured values of σ_{PSII} are dependent on the excitation spectrum of the FRRF, which is centered at 470 nm to overlap the Soret absorption band of chl *a*. Correcting for this spectral bias is necessary to account for accessory pigment absorption other than chl *a* and aids comparability of σ_{PSII} values between studies with different light environments or measurement protocols. This is done by dividing all raw σ_{PSII} values by a PAS-derived spectral correction factor (SCF) to normalize σ_{PSII} to a spectrally flat (white) spectrum with a constant irradiance value at all wavelengths between 400-700 nm (Markager and Vincent, 2001, Suggett *et al*., 2001). In addition, the σ_{PSII} values measured by the FRRF are converted from the raw output in nm^2 x $quanta^{-1}$ to $Å^2$ x $quanta^{-1}$ by multiplying each value by 100 to be consistent with most measurements in the scientific literature. The SCF value from 400-700 nm at each discrete sampling depth

is then calculated as:

$$(2) \qquad SCF = \left[\sum_{\lambda=400}^{\lambda=700} [aPS(\lambda) \times E(\lambda)] \times \left[\sum_{\lambda=400}^{\lambda=700} E(\lambda) \right]^{-1} \right] \times \left[\sum_{\lambda=400}^{\lambda=700} [aPS(\lambda) \times W(\lambda)] \times \left[\sum_{\lambda=400}^{\lambda=700} W(\lambda) \right]^{-1} \right]^{-1}$$

Where aPS(λ) is the absorption of photosynthetic pigments in the PAS sample at each wavelength, which is described further in the following section, E(λ) is the photon flux density of the excitation spectrum of the FRRF (μmol quanta x $[m^2 \text{ x sec}]^{-1}$), and W(λ) is the photon flux density of the spectrally flat correction spectrum (1 μmol quanta x $[m^2 \text{ x sec}]^{-1}$ at all wavelengths). The σ_{PSII} value from each PAS sampling depth is then divided by its corresponding SCF to give the SCF-corrected σ_{PSII} value. It is only possible to calculate SCFs at discrete depths where PAS measurements were available, so σ_{PSII} profiles were spectrally corrected by linearly interpolating whole summer mean SCF values at 10 m, 20 m, and 30 m through the water column. These sample depths were the ones where the greatest numbers of PAS samples were collected during 2010 (10 m mean=1.96, s.d.=0.081, n=17; 20 m mean=1.93, s.d.=0.080, n=11; 30 m mean=2.02, s.d.=0.11, n=11).

Measuring PAS from water samples

After sampling, GF/F filters for determination of PAS were frozen at -20°C until analysis using the quantitative filter technique (QFT) (Tassan and Ferrari, 1995). Each filter was then thawed by passing about 5 mL of Milli-Q filtered water through it using a gentle vacuum. Two reference blank GF/F filters were prepared in the same way and their baseline absorbance was measured using a scanning spectrophotometer (UV-1800 Shimadzu, Kyoto Japan) from 350-750 nm in 0.5 nm increments. The collection

software subtracted this baseline measurement from all subsequent sample absorbance spectra. Another baseline measurement was taken after each set of sample measurements was completed to confirm the measurement stability of the spectrophotometer.

Immediately before measuring each sample absorbance spectrum, both the sample filter and the blank reference filter were moistened by passing a small amount of Milli-Q water through them using a vacuum and were then kept in covered Petri dishes with a drop of water under the filter until measurement. This ensured consistent moisture levels in each sample filter because GF/F filters display strong changes in absorbance depending on their water content (Mitchell *et al*., 2003).

The QFT separates the total particle absorbance of each filter sample into several different absorption fractions due to non-organic particles, inactive phytoplankton pigments, and phytoplankton photosynthetic pigments (Figure 5). Each sample was measured initially to give the absorption spectrum of all particulate matter (*a*P). The photosynthetic pigments were then removed from the filter by bleaching it using a 1:4 dilution of a commercial bleach solution (Chlorox, 5.2% sodium hypochlorite) in Milli-Q water to yield the approximately 1% active chlorine concentration used in previous studies (Tassan and Ferrari, 1995). Roughly 15 drops of this diluted bleach solution was applied evenly across the filter. After two minutes the filter was thoroughly rinsed by filtering approximately 10 mL of Milli-Q water through it using a gentle vacuum. The absorbance of the sample filter was then measured again to give the absorption spectrum of non-algal particles (*a*NAP). Between samples, the spectrophotometer absorbance was set to zero using the same GF/F filters as for the initial baseline correction. To account for the inherent light scattering produced by GF/F filters, the mean absorbance for each

sample between 746-750 nm was subtracted from both *a*P and *a*NAP spectra at each measured wavelength (Silsbe, 2010). Both spectra were then trimmed to only retain absorbance measurements between 400-700 nm, corresponding to the wavelengths of PAR, which is denoted by lambda (λ) in this project and yields *a*P(λ) and *a*NAP(λ).

To find *a*PH(λ), the absorbance spectrum of phytoplankton pigments in each sample, first *a*NAP(λ) was subtracted from *a*P(λ) at each wavelength. This quantity (termed A_s) is used to calculate a dimensionless path length amplification factor at each wavelength (*a*SUS(λ)) following the empirical relationship described in equation 17 of Tassan and Ferrari (1995). Alternative path length amplification factors including the constant β=2 as derived by Roesler (1998), have also been used with success (Binding *et al*., 2008). *a*PH(λ) in m^{-1} was then calculated using equation 14 from Tassan and Ferrari (1995) omitting the particle concentration:

$$(3) \quad aPH(\lambda) = 2.303 \times aSUS(\lambda) \times \left[V \times A^{-1}\right]^{-1}$$

Where 2.303 is the natural log of 10 and is a constant, *a*SUS(λ) is as described above, V is the volume of water filtered for the sample (m^3), and A is the effective clearance area of the filter (m^2), which will vary with different filtration equipment.

To separate *a*PH(λ) into the absorbance due to different pigments, a standard absorption spectrum of chl *a* (Sigma) dissolved in 90% acetone was taken together with an absorption spectrum of pheophytin *a* following chl *a* acidification with 6N HCl. To reconstruct the portion of *a*PH(λ) due to absorbance from pheophytin *a* (*a*PHEO(λ)), the reference pheophytin *a* absorbance spectrum was first normalized to its value at 676 nm (*a*PHEO(676)). The normalized reference spectrum was then multiplied by the estimated

value of *a*PHEO(676) for each sample calculated from Equation 1 in Culver and Perry (1999) using the previously measured extracted chl *a* and pheophytin *a* concentrations (mg x m^{-3}) for that sample.

The absorbance from photosynthetic pigments is defined as:

(4) $$aPS(\lambda) = aPH(\lambda) - \left(aPHEO(\lambda) + aPP(\lambda)\right)$$

Where *a*PP(λ) is the absorbance of photoprotective pigments. This project did not directly measure the concentrations of photoprotective pigments. However *a*PP(λ) would not be expected to contribute a large amount of pigment absorbance because most of the samples (57 of 61) were collected at or below 10 m where PAR intensities are low and the need for photoprotective pigments is minimal. Phytoplankton at these depths would likely not be subject to intense light that would cause an accumulation of photoprotectant pigments. The value of *a*PP(λ) was therefore assumed to equal zero, and *a*PS(λ) was estimated as the difference between *a*PH(λ) and *a*PHEO(λ).

One of the major groups of photoprotectant pigments is photoprotectant carotenoids (PPC). Carotenoids are a diverse group of pigments, and photosynthetic (PSC) carotenoids are also important in phytoplankton cells. To understand if the assumption that *a*PP(λ) equalled zero for PAS samples was reasonable, the ratio of PPC to PSC pigments was estimated to provide a relative indicator of phytoplankton light adaptation and the fraction of total carotenoid pigments used in photosynthesis. This was done using the empirical relationship presented by Eisner *et al*. (2003) Figure 3, panel b:

(5) $$PPC : PSC = \left(\Delta aPH + 0.0056\right) \times \left(-0.0126\right)^{-1}$$

Where Δ*a*PH is the slope of *a*PH from 488-532 nm normalized to *a*PH(676):

(6) $$\Delta aPH = \left[aPH(488) - aPH(532)\right] \times \left[aPH(676) \times \left(488 - 532\,\text{nm}\right)\right]^{-1}$$

The fraction of *a*PS due to chl *a* absorbance (*a*chl*a*(λ)) was estimated in a similar way to *a*PHEO(λ) assuming all photosynthetic pigment absorption at 676 nm (*a*PS(676)) was due only to chl *a*. The measured chl *a* absorbance peaks from the reference spectrum in 90% acetone were offset roughly 11 nm towards shorter wavelengths than the observed in vivo chl *a* peaks in the *a*PS(λ) spectra due to the presence of solvent (Culver and Perry, 1999) and the lack of pigment and protein interactions found in vivo. The wavelengths of the reference spectrum were horizontally translated to better match the *a*PS(λ) absorbance peaks. Next the absorbance values of the reference spectrum at all wavelengths were normalized to the absorbance of the chl *a* standard at 676 nm. This spectrum was then multiplied by the measured sample *a*PS value at 676 nm (*a*PS(676)) to derive the *a*chl*a*(λ) spectrum for each sample. Finally the absorption of all photosynthetic accessory pigments other than chl *a* (*a*ACC(λ)) was calculated as the difference between *a*PS(λ) and *a*chl*a*(λ). Three of the most common accessory pigments are PC, PE, and members of the PSC family. The blue-green PC pigment absorbs orange to red light around 650 nm and is common in cyanobacteria. PE pigments appear pink, absorb green light near 550 nm, and are found in both cyanobacteria and motile cryptophytes. Finally PSC pigments such as fucoxanthin, which give diatoms and chrysophytes their characteristic golden color, absorb blue-green light near 490 nm and also partially overlap the absorption wavelengths of chl *a* (Falkowski and Raven, 2007). A wide range of other phytoplankton taxonomic groups also use fucoxanthin and other PSC pigments, although in lesser concentrations than diatoms.

Once all absorption spectra had been calculated for a sample, they were binned into

3 nm bins, for a total of six measurements per bin. Examination of the data showed this bin size to smooth the variability in the spectral absorbance measurements without losing resolution for the absorbance peaks, especially the chl *a* peak absorbance around 676 nm.

Results

Seasonal trends in water column temperature, chlorophyll a *and dissolved oxygen concentrations*

During 2010 thermal stratification began to form at FWM and EM by early June and late June respectively, and was well-established at all four stations by late July (Figure 6). Slightly elevated chl *a* concentrations below the surface were present at all stations except WM in early June (Figure 7). DO concentrations were a constant 13 mg L^{-1} through the water column for CM, EM, and WM from late May through late June (Figure 8), and they remained at or slightly above fully saturated levels through the entire water column (Figure 9). At FWM in late June the DO concentrations from the surface to approximately 15 m were lower than at other stations during this time, but because the surface water was warmer than any other station, the water was slightly super-saturated with DO. By late July the chl *a* fluorescence within the DCM at FWM was the highest measured during the summer at any of the four stations. Beginning in late July there was a distinct surface reduction in DO concentrations accompanied by a deeper sub-surface DO concentration peak at all four stations (Figure 8). In late July this peak spanned more than 30 m of the water column at WM with maximum DO concentrations reaching roughly 14 mg L^{-1}. These increases in DO concentrations below the surface in late July are retained in the DO saturation profiles, with peak saturation values located at the depth of the thermocline where they reached 120% of saturation at FWM and approached 115%

of saturation at the other stations. In August all stations except WM had surface water DO concentrations lower than those in late July, which is also the case for the DO saturation profiles. The sub-surface peak in DO was still present at all stations with maximum concentrations similar to those in late July, but due to the continuing warming of the water, the maximum saturation values were much higher than in July, from above 115% of saturation at CM to nearly 125% of saturation at FWM. In August however, the peaks in both DO concentration and DO saturation profiles at all stations except WM had more distinct boundaries, bounded from above by a sharp oxycline located at the same depth as the thermocline (Figure 6), and not continuing below 40 m at any station. The surface waters began to cool by early September, which was accompanied by a deepening of the surface mixed layer as the thermocline weakened and moved lower in the water column. By late September there was still a DCL present at all stations except EM, but its depth range was wider and the chl *a* concentration at the DCM was substantially lower than the late July maximum. At all stations measured in early September, the DO concentrations of surface water were greater than those in late August and remained similar from early to late September between 10.5-11.5 mg L^{-1}. During September DO concentrations similar to those at the surface moved further into the water column as the thermocline deepened, reaching 10 m at FWM and between 30-40 m at CM, EM, and WM. The progressive deepening of the surface mixed layer allowed warm water that had DO concentrations in equilibrium with the atmosphere to reach deeper into the water column, resulting in DO saturation profiles fairly similar to those measured in late May before the lake had thermally stratified. .

DCM depth in relation to ambient light and water temperature

The monthly mean values of the light extinction coefficient k_d measured with the CTD at all stations across the lake nearly doubled during the summer, increasing from 0.11 m^{-1} in June to 0.19 m^{-1} in early August, and then decreasing again by September to 0.14 m^{-1}, but still remaining larger than the June value (Figure 10). When the DCL was forming in June and eroding in September, the DCM was located above the boundary of the euphotic zone as defined by 1% of surface PAR. Once thermal stratification was well established during July and August, the DCM received a smaller fraction of surface light compared to June, and in August the DCM was located slightly below the euphotic zone boundary. It is important to note, however, that all data from August were collected during multiple days only at FWM station and therefore may not represent conditions across the rest of the lake.

Through the summer the DCM at all stations was usually located either at the base of the metalimnion where water temperature was close to 4°C and therefore the water was near its maximum density, or the DCM was located near 15 m regardless of water temperature (Figure 11). For CM and WM, the DCM formed deep in the water column and moved upward during the summer, exposing it to higher temperatures. For EM and FWM there was no straightforward seasonal progression of DCM depth, although the overall relationship between depth of the DCM and water temperature followed the same trend as for CM and WM, making it a relatively consistent relationship across the lake.

Phytoplankton pigment groups as determined by the FluoroProbe

Water column profiles from CM, EM, FWM, and WM measured using the FluoroProbe display seasonal shifts in phytoplankton pigment groups between late June and late August. Phytoplankton containing brown pigments and PE-rich phytoplankton

represented nearly all the estimated chl *a* at all depths and seasons; chlorophytes did not appear in any of these profiles and the only occurrence of PC-rich phytoplankton was below 50 m at FWM in early August.

In late June when the water column was becoming thermally stratified, all stations except WM showed the highest brown phytoplankton concentrations located well below the surface (Figure 12). The brown phytoplankton concentrations generally decreased below 30 m at all stations, while the concentration of PE-rich phytoplankton increased at these depths. At FWM, the only station displaying thermal stratification at this time, a well-defined DCM comprised of brown phytoplankton had formed slightly above 20 m, coinciding with a decrease in the concentration of PE-rich phytoplankton.

By late July a DCL was present at all stations and the entire phytoplankton community through the water column as determined by the FluoroProbe was comprised of brown-pigmented phytoplankton (Figure 13). With the exception of FWM, the estimated chl *a* concentration at the DCM was greater than the maximum concentration in late June and exceeded 2 $\mu g\ L^{-1}$. The depth of the DCM varied widely between stations, from 20 m at FWM to nearly 45 m at CM.

In late August, PE-rich phytoplankton were again present through the entire water column at all stations (Figure 14). Like in late July, an increased concentration of phytoplankton containing brown pigments was mainly responsible for the presence of the DCL. In contrast, PE-rich phytoplankton concentrations remained relatively constant through the water column with the exception of slight increases within the DCL at EM and FWM, and a steady increase in concentration from the surface to roughly 40 m at WM. Below the DCM beginning at approximately 50 m for CM and 40 m for the other

three stations, the concentration of brown phytoplankton decreased sharply, and PE-rich phytoplankton comprised nearly all of the chl *a* concentration. At FWM PC-rich phytoplankton were present at increasing concentrations with depth starting at 50 m. This was the only instance of the FluoroProbe measuring PC-rich phytoplankton at any of the four stations during the summer of 2010.

Changes in measured pigment absorption spectra

The shape of pigment absorption spectra from PAS sample filters also displayed changes through the summer and with depth. Two of the most pronounced trends occurred at EM between 30-35 m from early June to late August, and at FWM from 10 m to 30 m during one day in early August. While the changes in pigment absorption due to carotenoids and PE both at EM (Figure 15) and at FWM (Figure 16) are visible to an extent in the three *a**PSII spectra from each station, the relative absorbance of each pigment was also quantified. Values of *a**PSII were numerically integrated from 470-510 nm for carotenoid absorbance and from 525-560 nm for PE absorbance (Falkowski and Raven, 2007). For each absorption spectrum, both of these integrated *a**PSII values were then expressed as a ratio to their respective integrated *a*chl*a* values over the same wavelength ranges; these ratios are noted on the graphs. Pigment absorbance due to both carotenoids and PE relative to chl *a* increased at EM between 30-35 m as the season progressed. Relative carotenoid absorbance at the end of the season in late August was more than 45% larger than at the start of the season in early June, and relative PE absorbance increased by more than 150% during the summer (Figure 15). At FWM the pigment absorbance changes with depth in early August were less pronounced though still quantifiable. The relative absorbance of PE relative to chl *a* increased slightly

though consistently with depth from the epilimnion to the DCM at 30 m, while the relative absorbance of carotenoids decreased with depth (Figure 16).

Increasing PE absorbance during the summer at EM and with depth at FWM agrees fairly well with trends from FluoroProbe profiles taken concurrently with PAS samples. The FluoroProbe profile at FWM in early August showed an increase in the concentration of PE-rich phytoplankton from 10 m to 20 m, consistent with PE absorbance measurements from PAS samples, but concentrations then remained unchanged or decreased slightly from 20 m to 30 m (Figure 14). For EM, the concentration of PE-rich phytoplankton increased at 30-35 m between late June and late August (Figures 12 and 14). The largest disagreement between measured pigment absorbance from PAS samples and the FluoroProbe profiles was during late July at EM, where PAS samples indicated an increase in PE pigment absorbance compared to late June (Figure 15), but PE-rich phytoplankton were absent throughout the water column in the FluoroProbe profiles (Figure 13).

Carotenoid pigments are prevalent in diatoms and chrysophytes, but changes in carotenoid absorbance from PAS samples at both EM and FWM did not always agree with trends in the 'browns' group as determined by the FluoroProbe, which was calibrated using diatom and dinoflagellate cultures, but not chrysophyte cultures (Beutler *et al*., 2002). At EM, both carotenoid absorbance and the 'browns' group increased from June to July at 30-35 m, but the 'browns' group decreased from July to August whereas the carotenoid absorbance increased. At FWM in early August the two methods were in sharp disagreement, as the 'browns' group increased sharply with depth from 10-30 m (Figure 14), but relative carotenoid absorbance from PAS samples decreased with depth

(Figure 16).

Distribution of autotrophic picoplankton through the water column

The extracted picoplankton chl *a* concentration for each sample was expressed as a percentage of the total extracted chl *a* measured at each station and depth. Picoplankton chl *a* measurements through the water column were then separated into three groups: above the DCM, at the DCM, and below the DCM by using the CTD chl *a* fluorescence profiles for each sampling date. Finally the percentages of total chl *a* contained in picoplankton for all samples through the summer at each depth group were averaged to give an overall seasonal contribution of picoplankton to total phytoplankton chl *a* (Table 1). Picoplankton represented more than one third of the overall chl *a* concentration in the water at each of the depth ranges. The mean ranks of picoplankton chl *a* percentages between the three depth groups were significantly different (Kruskal-Wallis test, $P = 0.023$). Picoplankton found below the DCM represented a significantly greater portion of the total chl *a* at those depths than did picoplankton found above the DCM, but there was no significant difference between the percentage of chl *a* contributed by picoplankton found within the DCM and that contributed by picoplankton either above or below the DCM (Tukey range test).

Trends in PPC:PSC and SCFs

The ratio of PPC:PSC for all PAS measurements, and especially the occurrence of high ratios, decreased with increasing depth (Figure 17). Whereas the portion of aPS(λ) due to the absorption of photoprotectant pigments (aPP(λ)) was not measured in this project, the estimated values of PPC:PSC give an indication that the relative concentration of photoprotectant pigments in the samples steadily decreased with depth

as the ambient light intensity became lower. In contrast, SCF values for correcting the FRRF σ_{PSII} measurements to the in situ pigment absorption spectrum increased fairly consistently with depth although the trend became less clear below 30 m (Figure 18).

Trends in F_v/F_m and σ_{PSII} through the summer

Profiles of the maximum quantum efficiency of PS II (F_v/F_m) from the major stations CM, EM, FWM, and WM generally showed increased quantum efficiencies below the epilimnion at depths that roughly correspond to the DCL regardless of the time of year (Figure 19). The major exceptions to this trend occurred late in the summer after the DCL was well established where there are distinct drops in the measured quantum efficiency that occurred within the DCL. F_v/F_m reached a minimum around 35 m for EM in late July, there was a sharp 'notch' in the early August FWM profile from 20-30 m, and a less pronounced drop in F_v/F_m at WM was present below 30 m in late July. Upon examination of the fluorescence induction for acquisitions within these depth ranges, it was evident that the phytoplankton fluorescence exceeded the measuring range of F_m values for the FRRF, while F_o values remained within the measurable range. This resulted in an artificial decrease in measured F_v/F_m values solely as a result of instrument settings, and therefore did not represent an actual decrease in quantum efficiency of phytoplankton within the DCL. By late August and early September when the thermal stratification was deepening and the DCL was eroding, both F_o and F_m values were again within the measurable range of the FRRF, and the measured quantum efficiencies at CM, EM, and WM once again either increased or remained relatively unchanged with depth. Correcting F_v/F_m profiles for pheophytin *a* fluorescence caused a slight increase in measured F_v/F_m values, but did not cause overall changes in the shape of the F_v/F_m

profiles or have large differential effects on the F_v/F_m profiles as a function of depth.

Profiles of SCF-corrected σ_{PSII} values did not show seasonal or depth trends between stations that were as consistent as the F_v/F_m profiles (Figure 20). There was a large amount of variability in σ_{PSII} values for CM in late June to a depth of 30 m. In general at CM σ_{PSII} values tended to be slightly lower above 30 m compared to below 30 m in late June and late July, with the opposite trend during the late August. EM profiles displayed a distinct seasonal trend in σ_{PSII} values above 40 m, where they became progressively lower through the season from early June to late August and then increased again by early September to levels comparable to those in late July. With the exception of the early June sampling, σ_{PSII} values at EM below 40 m remained relatively unchanged through the summer and displayed no trend with increasing depth. At FWM σ_{PSII} values measured during the early June and late July profiles both increased slightly with depth. The early August profile however showed a sharp 'notch' similar to the one present in the F_v/F_m profile, and was located at the same depth within the DCL. σ_{PSII} values immediately above this 'notch' from 5-20 m were lower than the values measured at the surface, and portion of the water column corresponded to the depths of increased quantum efficiencies from the F_v/F_m profile. At WM in contrast to EM, profiles of σ_{PSII} displayed strong consistency in both their absolute values and their trends with depth throughout the summer. Surface σ_{PSII} values were almost 50% larger than σ_{PSII} values below 60 m, showing a strong depth effect regardless of thermal stratification or DCL formation.

Discussion

Summary

The summer of 2010 was ideal for measurements of the DCL due to the unusually strong thermal stratification and the extended stratified season as a result of warm air temperatures during the spring and summer. Large changes in DO concentrations through the water column took place during mid summer, including the formation of a depth band of water that was super-saturated with DO located immediately below the thermocline. The presence of water super-saturated with DO supports the hypothesis of net photosynthetic O_2 production occurring within the DCL. We also recorded distinct seasonal and depth changes in phytoplankton pigment composition using the FluoroProbe that are generally comparable to those reported in previous studies. Finally, the phytoplankton communities across the lake showed seasonal and depth variability in measured F_v/F_m and σ_{PSII} values that likely indicate differing phytoplankton community adaptations to in situ light and nutrient conditions in the lake.

Thermal structure in the lake during 2010

The FWM station displayed earlier establishment of thermal stratification and DCL formation than any of the other stations, which could be due in part to its slightly more sheltered position at the western end of the lake and shallower water compared to the other three stations. On our first sampling at FWM in early June, the water column already displayed a temperature gradient, with surface water nearly twice as warm as the deeper isothermal water. Two weeks later in late June, increasing surface water temperatures at the three other stations were evident, with thermal stratification well established across the lake by late July (Figure 6). The establishment of lake-wide

thermal stratification during 2010 was not substantially earlier than the average date of stratification measured from whole lake surveys of Lake Superior during the late 1960s and early 1970s (Bennett, 1978). However, perhaps due to the trend of increasing water temperatures in Lake Superior throughout the 20th century, with especially notable temperature increases within the last 30 years (Austin and Coleman, 2008), the average maximum surface water temperature from the four stations measured for this study (18.3 °C) occurred slightly earlier in the year and was roughly 15% larger than the highest temperature recorded (16 °C) roughly forty years ago (Bennett, 1978). In late August the water column temperature at WM was lower than at the other stations, likely a result of an extreme wind-induced mixing event in the western arm of Lake Superior that occurred in mid-August. Profiles of DO concentrations will be discussed at the end of this section since they link photosynthetic parameters measured in this chapter to O_2 production rates estimated in chapter 2.

There was a clear lake-wide relationship between DCM depth and water temperature during the summer (Figure 11). At all stations the DCM initially formed in fairly deep water that was nearly 4°C. As the summer progressed, the DCM moved upward in the water column at all stations except EM, where it was generally exposed to progressively warmer ambient water as the thermocline deepened in late summer. Water temperatures throughout the water column during the summer of 2010 were usually warmer than 4°C, and the DCM was not located closer to the surface than 15 m at any station, making these values appear as a vertical and a horizontal asymptote respectively for the DCM depth and temperature relationship (Figure 11).

Implications of varying light extinction and light intensity at the DCM during the

summer

The percentage of surface light reaching the DCM and values of k_d were inversely related during the summer, with the largest percentage of surface PAR reaching the depth of the DCM in June and September (Figure 10). If the portion of surface light reaching the DCM is held constant through the summer, the ambient PAR intensity through the water column in September will nevertheless be less than the intensity in June because decreasing solar elevation with respect to the horizon after the summer solstice lowers surface PAR intensity. The average portion of surface light reaching the DCM for the whole summer measured in this project (3.8% of surface PAR), was near the lowest value of mean light intensity at the DCM measured in Lake Superior (3.3 to 7.1% of surface PAR) from 1996 to 2001 (Barbiero and Tuchman, 2004), which would expose phytoplankton in the DCM in 2010 to a slightly lower portion of surface PAR than normal. When Lake Superior is thermally stratified, phytoplankton growth above the thermocline in the epilimnion is not light-limited (Guildford *et al*., 2000), but low light conditions below the thermocline must eventually limit phytoplankton growth in the DCL. During August the DCM was located at the lower limit of the euphotic zone, representing severe light limitation for photosynthesis, but the upper DCL was located above the euphotic zone boundary. Although all August measurements were taken at FWM and therefore their comparability with other stations across the lake cannot be assessed, the location of the DCM at the euphotic zone boundary suggests that its depth is not determined solely by light availability, given the variation in the percentage of surface light reaching the DCM through the summer. In addition, although the depth of the DCM appears to vary somewhat predictably through the season in response to both

changes in k_d values as well as temperature, the combination of the two variables together did not yield a statistically significant regression for the prediction of actual DCM depth ($P = 0.24$).

Changes in phytoplankton pigment groups during the summer identified by FluoroProbe profiles

The apparent lack of chlorophytes lacking many accessory pigments and the minimal concentrations of PC-rich phytoplankton through the summer as determined by the FluoroProbe profiles is supported by a previous microscopy-based study that found abundances of chlorophytes and cyanophytes (presumably PC-rich) were consistently low across the lake regardless of season (Munawar and Munawar, 1978). The apparent lack of PC-rich phytoplankton in late June may indicate that the shift in *Synechococcus* communities from PC-rich during the spring to PE-rich during late summer (Ivanikova *et al*., 2007) had already taken place by that time, although this would need to be confirmed by further examination of samples either with an epifluorescence microscope or using flow cytometry. The relative abundance of PE-rich phytoplankton through the water column at all stations in late June agrees well with previous observations that cryptophytes and other flagellates dominated the phytoplankton community during isothermal conditions in the spring (Fahnenstiel and Glime, 1983). At FWM, the only station showing a pronounced thermal gradient through the water column during this time, the prevalence of diatoms in the DCL is accompanied by a decrease in PE-rich phytoplankton. This suggests that the growth of brown pigment-containing phytoplankton, such as diatoms and chrysophytes was largely responsible for the formation of the DCL early in the stratified season. Both above and below the DCL,

however, nearly all of the chl *a* is still comprised of PE-rich phytoplankton.

The dominance of phytoplankton containing brown pigments and the absence of PE-rich phytoplankton in the water column at all stations after thermal stratification was well established in late July was unexpected. At this time of year, the deep-water phytoplankton communities in Lake Superior are dominated by groups containing brown pigments, whether centric diatoms within the DCL (Fahnenstiel and Glime, 1983), or chrysophytes, pinnate diatoms, and centric diatoms at the DCM (Barbiero and Tuchman, 2004, Munawar and Munawar, 1978). However in all of these surveys PE-rich cryptophytes persisted in the DCL during the stratified season, and PE absorbance peaks were present in many of the PAS samples taken for this study during late July (see the middle panel of figure 15 as an example). Therefore the large abundance of browns and the lack of greens and blue-greens in the fluorescence-based FluoroProbe profiles may be a fairly realistic determination of those phytoplankton pigment groups in the lake, but the apparent lack of PE-rich phytoplankton in the FluoroProbe profiles likely does not represent the actual abundance of PE-rich phytoplankton during late July.

In late August, the FluoroProbe profiles again showed PE-rich phytoplankton comprising a large portion of the total chl *a*. The presence of a DCL largely composed of brown phytoplankton, and the replacement of these brown phytoplankton with PE-rich phytoplankton below the DCM measured at all stations in this study has previously been observed in the western arm of Lake Superior during early August (Munawar and Munawar, 1978). Microscopic examination of concentrated water samples collected in 2010 from the epilimnion and DCL at FWM qualitatively supported the phytoplankton pigment group composition determined by the FluoroProbe. Samples showed a relative

lack of green phytoplankton, but also moderately high abundances of PE-rich phytoplankton in both the epilimnion and the DCL including *Oscillatoria sp.*, *Synechococcus sp.,* and *Cryptomonas sp.* as well as other flagellates; pennate and centric diatoms were also common. However, in a previous study the phytoplankton community at an open water station in early September was almost entirely comprised of cryptophytes (Munawar and Munawar, 1978), which sharply contrasts with the current FluoroProbe profiles showing elevated abundances of browns at open-lake stations WM, CM, and EM.

Picoplankton distribution in the water column

The quantification of extracted chl *a* from picoplankton by using size fractioning allowed an assessment of summer phytoplankton distribution through the water column based on size. During 2010 picoplankton represented more than 40% of total chl *a* within the DCM, and a slightly lower percentage above the DCM (Table 1). Both of these values compare favorably with previous measurements from the western section of the lake, although picoplankton above the DCM represented slightly more of the total chl *a* than was measured in the current study (Ivanikova *et al*., 2008). The majority of picoplankton in Lake Superior during late summer, especially in the DCM, are PE-rich (Fahnenstiel *et al*., 1986, Ivanikova *et al*., 2007), and it seems that in the current study the FluoroProbe was unable to effectively measure these picoplankton at any station during late July, because a PE absorbance peak was present in many PAS samples collected during that time. This may partly be due to continuing problems measuring or applying representative filtered water offsets to fluorescence profiles, which has been shown to cause large changes in the apparent phytoplankton community composition for

FluoroProbe profiles taken in Lake Ontario (Twiss, 2011). The identification of PE-rich phytoplankton appears not to be primarily a problem related to using fluorescence reference spectra from phytoplankton strains not endemic to Lake Superior to determine pigment groups in the lake, because PE-rich phytoplankton did comprise much of the phytoplankton in the late June and late August profiles at all stations. However, because both cryptophytes and PE-rich picocyanobacteria contain PE, the ability of the FluoroProbe to accurately distinguish between those two groups may require the use of reference spectra derived from strains of cryptophytes and PE-rich picocyanobacteria native to Lake Superior.

Changes in phytoplankton pigment absorption spectra during the summer compared to FluoroProbe profiles

Phytoplankton in the DCL need to adapt to changing light conditions through the summer. Using the FluoroProbe, the relative abundance of both brown and PE-rich phytoplankton in late June suggests that the spectral distribution of light and the nutrient availability in the water column favors the co-existence of the two phytoplankton pigment groups. Later in the summer brown phytoplankton became the dominant pigment group in the DCL based on the FluoroProbe profiles, but the accompanying peak in carotenoid pigment absorption that would be expected for diatoms at FWM was not seen in PAS samples except in the epilimnion where the ratio of PPC to PSC was greatest. Carotenoids are a family of pigments, each with its own slightly different absorption spectrum. It is possible that the PSCs contained in the brown phytoplankton had absorption spectra that overlapped with the absorption of chl *a* (Falkowski and Raven, 2007), therefore masking the PSC absorption peak in the PAS samples. An

epilimnetic carotenoid absorption peak was still apparent from PAS samples, likely in response to increased light intensities near the surface, and probably representing PPCs with a peak absorbance at slightly longer wavelengths than the PSCs.

The increased PE absorbance measured from PAS samples between 30-35 m at EM through the summer were not represented in the FluoroProbe profile that showed solely 'brown' phytoplankton at these depths in July and August. However the increased PE pigment absorbance with depth measured at FWM in early August were largely present in the FluoroProbe profile except from 20-30 m where the PE-rich phytoplankton concentration either remained unchanged or decreased slightly.

These changes in absorbance by carotenoid and PE pigments likely represented phytoplankton photo adaptation to changes in the spectral composition and intensity of PAR within the DCL compared to the epilimnion during the summer. The comparatively high k_d values measured using the CTD during late summer (Figure 10), have been shown to cause a disproportionate loss of blue light (approximately 400-470 nm) compared to other wavelengths of PAR through the water column in Lake Superior (Jerome *et al*., 1983). Also, after the summer solstice the angle of the sun with respect to the horizon decreases. This effectively increases the path length of PAR from the water surface to the DCL compared to June, with corresponding increases in the magnitude of spectral shifts caused by changes in the CTD-derived k_d values. This shift towards increasingly green light at depth later in the season was represented by the early September PAS sample from EM, which showed the strongest chl *a*-normalized PE absorption peak of any sample collected during the summer of 2010.

Potential limitations to interpretation of PAS and FluoroProbe results

As defined in this project, the spectral correction of σ_{PSII} was accomplished by dividing the raw FRRF σ_{PSII} value by the appropriate SCF. PAS samples that showed strong pigment absorption at wavelengths overlapping with the FRRF excitation spectrum will have the largest SCF values. SCF-corrected σ_{PSII} values using these samples will therefore be proportionately lower than comparable σ_{PSII} values that are spectrally corrected using PAS samples that show less blue light absorption. SCF values for PAS samples increased with depth through the water column, which suggests increased blue light absorption deeper in the water column. This does not seem to be due to the increased chl *a* concentration in the DCL, because SCF values and extracted chl *a* concentrations show a statistically significant but extremely weak linear relationship ($n = 61$; $P = 0.049$; $R^2 = 0.064$). It is possible that other photosynthetic pigments that have absorption spectra partially overlapping that of the FRRF's blue excitation spectrum, such as PSCs or chlorophyll *b*, are responsible for the increased SCF values at depth. Both PSCs and chlorophyll *b* are common in diatoms (Falkowski and Raven, 2007) and other phytoplankton recognized as 'browns' by the FluoroProbe, although the increased concentrations of brown phytoplankton in the DCL during the summer measured with the FluoroProbe were not accompanied by increased carotenoid absorbance in PAS samples.

Changes in maximum quantum efficiencies during the summer

Maximum quantum efficiency (F_v/F_m) profiles showed distinct trends through the season and with increasing depth that likely reflect the dynamic nutrient and light environments in the lake during the summer. The generally higher F_v/F_m values through the DCL compared to the epilimnion soon after thermal stratification was established support the hypothesis that phytoplankton in the DCL are capable of efficiently using

absorbed light energy for photosynthesis. This may partly be a result of increased phosphorus availability for phytoplankton in the DCL of Lake Superior compared to surface mixed layer, where phytoplankton are severely P deficient (Barbiero and Tuchman 2001b).

Later in the year, however, chl *a* concentrations in the DCL were high enough to give maximum fluorescence values (F_m) that exceeded the measuring range of the FRRF under the measurement settings used. It is possible to modify the measuring sensitivity of the FRRF by changing the voltage across its photomultiplier tube, but since these anomalous F_m values were not identified while the profiles were being taken, the measurement sensitivity of the FRRF was not modified to reflect the in situ conditions. This resulted in a decrease in measured F_v/F_m values as F_o values increased due to higher chl *a* concentrations near the DCM and became closer to the artificially low F_m values. Unfortunately there is no way to correct the measured F_v/F_m profiles for this effect after the profile has been taken, and it results in a lack of resolution for F_v/F_m values in the DCM. Apparent "recovery" of F_v/F_m values at depths below the DCM in late July and early August, and throughout the water column in late August and early September, represent conditions where F_m values were once again within the measurement range of the FRRF.

Changes in effective absorption cross section of PSII (σ_{PSII}) during the summer

The most pronounced seasonal trend in σ_{PSII} values was measured at EM and, like F_v/F_m, appears to represent phytoplankton adapting to changing environmental condition in the lake as the summer progressed. When the ambient light levels in the water column began to decrease after the summer solstice, paradoxically the measured σ_{PSII} values also

decreased, indicating phytoplankton were unable to maintain a fairly consistent level of light absorption during the summer. However σ_{PSII} values increased again in September after thermal stratification began eroding, suggesting they were responding to increased nutrient availability due to water mixing. The smaller σ_{PSII} variation through the summer at both CM and WM suggests phytoplankton at these stations may be primarily responding to shifts in ambient conditions during the season in ways other than changing their effective PSII absorption cross sections. At FWM in early August the measured σ_{PSII} values showed distinct declines at depths corresponding to the 'notch' in the F_v/F_m profile. This is likely also an artifact of the in situ F_m values being above the measurement range of the FRRF for the settings used, and therefore is unlikely to represent actual changes in the ability of phytoplankton near the DCM to absorb ambient light.

Implications of increased dissolved oxygen concentrations through the water column during the summer

In dimictic lakes such as Lake Superior, the entire water column is typically saturated with DO during late spring when the deep mixing associated with isothermal conditions allows for rapid translocation of oxygen-rich water from the surface throughout the water column. During the early summer the measured DO concentration was approximately 13 mg L^{-1} through the entire water column at all stations (Figure 8), and was consistently near full saturation as expected (Figure 9). Later in the summer as water temperatures rose and stratification prevented equilibration of the metalimnion and the hypolimnion with the atmosphere, DO concentrations reached 14 mg L^{-1} at all four stations immediately below the thermocline (Figures 6 and 8), resulting in super

saturation (Figure 9). Part of this increase in DO saturation may be driven by the increase in water temperature compared to earlier in the year, which acts to decrease the concentration of DO needed to reach saturation. Changes in water temperature cannot increase the absolute DO concentration in the water, however. The increased DO concentrations measured below the thermocline also cannot be attributed to physical processes such as translocation of deeper hypolimnetic water because the DO concentrations found below the thermocline were the highest measured anywhere in the water column. This measured increase in absolute DO concentrations at all stations during late summer would therefore require in situ photosynthetic O_2 production, and provides strong evidence that in Lake Superior O_2 production exceeds O_2 consumption due to organism respiration below the epilimnion and within the depth range of the DCL. The next chapter further tests this hypothesis that the net increase in DO concentrations below the thermocline is mainly a result of increased gross O_2 production within the DCL by estimating photosynthetic O_2 production rates in the DCL.

Conclusions

Having data from several sampling cruises between late May and late September 2010 gave detailed information about the seasonal trends in temperature, chl *a* fluorescence, and DO concentrations across the lake, which were especially prominent due to the presence of strong thermal stratification during that summer. The phytoplankton community displayed similarly strong seasonal and depth trends at all stations across the lake. Phytoplankton containing brown pigments represented most of the chl *a* within the DCL, and PE-rich phytoplankton were relatively common throughout the water column in late June and late August. Profiles of F_v/F_m and σ_{PSII} also displayed

changes with depth and through the season, but these were not as consistent between stations as the shifts in the phytoplankton community. This implies that the photosynthetic parameters varied in response to light, nutrients, and other environmental conditions unique to each station in addition to varying with changes in phytoplankton community composition. The presence of a depth band of water with supersaturated DO concentrations located immediately below the thermocline in late July and late August strongly suggests that phytoplankton within the DCL were actively photosynthesizing and provided a net increase in DO concentrations at these depths.

Chapter 2

Fluorescence-based oxygen production and carbon assimilation estimates

Introduction

Establishment of fluorescence-based photosynthetic production estimates

Photosynthetic production estimates derived from fluorescence profilers provide a powerful means to estimate the instantaneous phytoplankton photosynthesis in situ through the entire water column, and at any time during the course of the day. The use of variable fluorescence to estimate photosynthetic rates in phytoplankton was first proposed more than two decades ago (Genty *et al*., 1989), and variations of the same method are still used extensively to generate estimates of photosynthetic rates from fluorescence measurements, although the measuring instrumentation has changed. The FRRF technique was introduced as a way to make profiles of phytoplankton variable fluorescence with high depth resolutions relatively quickly (Kolber and Falkowski, 1992, Kolber *et al*., 1998). The technique has since has found wide use in marine systems to systematically measure changes in F_v/F_m or F_q'/F_m' and σ_{PSII} values with depth and across broad spatial scales (e.g. Falkowski and Kolber, 1995, Suggett *et al*., 2009b). When combined with concurrent measurements of PAR, the F_q'/F_m' and σ_{PSII} values from the FRRF have been used to calculate estimates of photosynthetic production in the open ocean that are largely comparable to estimates made using conventional ^{14}C incubations (Corno *et al*., 2006, Pemberton *et al.,* 2006). In contrast, there have been relatively few

studies using the FRRF to calculate photosynthetic production in lakes (e.g. Kaiblinger and Dokulil, 2006, Kromkamp *et al*., 2008) and two studies to date in the Laurentian Great Lakes (Pemberton *et al.*, 2007, Silsbe 2010). This project extends fluorescence-based estimates of photosynthetic production to Lake Superior.

Ways to express phytoplankton photosynthetic production

The photosynthetic rate in phytoplankton and most other photosynthetic organisms can be expressed as the rate of formation for any of three related photosynthetic products. In its simplest form, the photosynthetic rate is the electron transport rate (ETR). The ETR is a measure of how quickly the electrons split from water at PS II move through the electron transport chain (ETC), which creates the reducing potential and ATP necessary for carbon assimilation downstream of PSI (Figure 2). The ETR for PS II only (ETR_{PSII}) can be estimated using the FRRF, FluoroProbe, and measurements of ambient PAR intensity. Because O_2 is produced only at PS II, the value of ETR_{PSII} can itself be used to estimate the rate of photosynthetic O_2 production. Finally, because the ETC links O_2 production with C assimilation through electron movement, the rate of O_2 production can be used to calculate an equivalent C assimilation rate if conversion efficiencies are either known or are assumed.

The conversion between ETR_{PSII} and O_2 production is generally made by assuming that four photons must be absorbed by PS II to generate one O_2 molecule, and a further four photons need to be absorbed by PS I for the eventual assimilation of one CO_2 molecule. Cyanobacteria, however, exhibit greater flexibility in their ETC compared to other phytoplankton groups because photosynthesis and respiration both use the same pathways, which effectively reduces the efficiency with which cyanobacteria convert

electrons to assimilated carbon. These reductions in photosynthetic efficiency are especially common in surface waters where strong PAR intensities and UV light can overload photosynthetic systems, resulting in decreased quantum efficiencies and transient damage to PSII reaction centers (Vassiliev *et al*., 1994), and can drive phenomena such as state transitions that are common in cyanobacteria (Campbell *et al*., 1998).

The Photosynthetic Quotient (PQ) is used as the conversion factor between the number of moles of O_2 produced for each mole of CO_2 reduced to organic C. The value of PQ is usually greater than one due to a variety of factors that can partially de-couple O_2 production from C assimilation. Large increases in PQ values can occur during the afternoon when ATP generated by the ETC may be diverted from C assimilation and used instead to repair PSII reaction centers damaged by high light conditions (Behrenfeld *et al*., 2004). Values for the PQ will also vary depending on the nitrogen source in the water. If nitrate is prevalent, the phytoplankton need to expend photosynthetic reductant to make it biologically available, and the PQ will increase compared to conditions where ammonia concentrations are high (Suggett *et al*., 2010).

Parameters necessary to estimate photosynthetic production using pigment fluorescence

The amount of temporal, spatial, and depth resolution possible with fluorescence-based production estimates is unmatched by traditional ^{14}C incubations. Like ^{14}C incubations, production estimates made using fluorescence profiles require measurements of ambient PAR taken concurrently with the FRRF profile. However, the high resolution of production estimates made using pigment fluorescence requires the measurement of

two additional parameters related to light absorption and photosynthetic efficiency in the phytoplankton. First, the absorption spectrum of pigments associated with PS II (*a*PSII) needs to be quantified in order to determine how much light energy will be available at PS II within each phytoplankton cell to drive photosynthesis and O_2 production. The spectral composition of ambient light and how closely it matches *a*PSII will therefore affect the amount of light energy available for photosynthesis at PS II. Next a measurement of the quantum efficiency with which PS II in the phytoplankton cell uses this absorbed light energy to drive photosynthesis (*fPSII*) is required. *fPSII* is usually represented by F_q'/F_m', the quantum efficiency measured by the FRRF under ambient light conditions where photosynthesis is actively occurring. F_q'/F_m' values usually vary through the course of one day in response to light exposure. For example, under increased intensities of ambient light at noon on a cloudless day, phytoplankton will dissipate more absorbed light energy through fluorescence because the ETC is overloaded and cannot provide sufficient energy quenching through photochemistry alone. This increases the baseline fluorescence of the phytoplankton, F', compared to the morning or evening of the same day or when surface irradiance is low because of cloud cover. Under conditions of higher irradiance the accompanying increase in F' will therefore cause F_q'/F_m' values to decrease.

Objectives

This study first sought to compare estimates of photosynthetic production for the DCL of Lake Superior calculated using two different *a*PSII calculation techniques. The commonly used estimation technique for *a*PSII in marine systems has been shown to underestimate photosynthetic production in Lake Erie compared to values from ^{14}C

incubations (Silsbe, 2010). An alternative method to estimate *a*PSII in freshwater systems was therefore introduced and shown to give estimates of photosynthetic production comparable to ^{14}C incubations in Lake Erie (Silsbe, 2010). The photosynthetic production estimates generated from the two *a*PSII estimation techniques are compared here for Lake Superior. These production estimates made using pigment fluorescence are then compared to previously published C assimilation estimates for Lake Superior made using ^{14}C incubations. The spatial, seasonal, and diel variability of the calculated photosynthetic production rates is also explored. From these production estimates, we then sought to better understand whether the DCL in Lake Superior is likely a zone of active phytoplankton growth and therefore whether the increased DO concentrations below the thermocline measured with the CTD in the chapter 1 could be an indication of photosynthetic activity within the DCL.

Methods

Calculating the ETR and O_2 production rate for PS II

The initial estimate of photosynthetic production using pigment fluorescence is the ETR for PSII only (ETR_{PSII}), calculated using:

(7) $$ETR_{PSII} = E \times fPSII \times aPSII$$

Where E is the photon flux of PAR from 400-700 nm (μmol quanta x $[m^2 \times s]^{-1}$), *fPSII* is the quantum efficiency of PS II (dimensionless), and *a*PSII is the absorption of PAR by pigments associated with PS II (m^{-1}). ETR_{PSII} is equivalent to the rate of photon conversion to electrons by PS II, so can be used to find the resulting rate of O_2 production (P_{O2}) using equation 8 assuming the maximum quantum yield of O_2 production for PS II only ($\Phi_{O2\ PS\ II}$) is one mole of O_2 produced per four moles of photons absorbed

(Falkowski and Raven, 2007, Suggett *et al*., 2009a):

(8) $P_{O_2} = ETR_{PSII} \times 16.2$

Where the constant 16.2 converts rates of photon absorption by PS II to rates of O_2 production using $\Phi_{O2\ PS\ II}$ and unit conversion factors ([10^{-6} mol quanta x μmol quanta^{-1}] x [1 mol O_2 x 4 mol quanta^{-1}] x [16000 mg x mol^{-1} O_2).

Estimating aPSII

Three different methods to calculate *a*PSII were used in this project, with two of the three used to calculate phytoplankton photosynthetic production. The first method (*a*PSII method 1) is the most straightforward and assumes that for large sample sizes exactly half of the average pigment absorbance from 400-700 nm is associated with both PS II and PS I:

(9) $$aPSII = \left[(700 - 400\ \text{nm})^{-1} \times \sum_{\lambda=400}^{\lambda=700} aPS(\lambda) \right] \times 0.5$$

In the absence of more detailed information about the distribution of pigments between PS II and PS I, this method can provide a rough estimate for *a*PSII.

It is important to note that this value of *a*PSII was not wavelength dependent for the data analysis in this project. Instead it represents half of the average *a*PS for a given sample from 400-700 nm, corresponding to the wavelengths of PAR. While this lack of wavelength dependence results in a lack of resolution for absorbance measurements, O_2 production is calculated as a function of total PAR, so estimating *a*PSII in this way should not greatly affect estimates of O_2 production.

*a*PSII method 2 has been used successfully in marine environments and is calculated from the product of the SCF-corrected PSII effective absorption cross-section

from the FRRF (σ_{PSII}, $Å^2$ x quanta^{-1}), a linearly interpolated value of the chl *a* concentration at each sample depth (mg m^{-3}) in the water measured using the acetone extracted chl *a* technique described in the methods section of chapter 1, and the number of moles of PS II reaction centers per mole of chl *a* (n_{PSII}; mol PSII x mol chl a^{-1}) (Equation 10). The value of n_{PSII} is commonly assumed to be 1:500 or 0.002, which corresponds fairly well with experimentally measured values for dense cultures representing a range of phytoplankton functional groups (Suggett *et al*., 2009b). However n_{PSII} is variable, and another study estimating O_2 production from FRRF profiles successfully used a n_{PSII} value of 1:300, or 0.003 (Corno *et al*., 2006).

(10) $$aPSII = \sigma_{PSII} \times n_{PSII} \times \text{chl}a \times 0.00675$$

Where 0.00675 is a unit conversion factor ([10^{-20} m^2 x $Å^{-2}$] x [6.02 x 10^{23} quanta x mol^{-1}] x [mol chl *a* x 89200 mg^{-1}]).

Like *a*PSII method 1, *a*PSII method 3 also assumes that on average half of photosynthetic pigments are associated with PS II. This method uses the background fluorescence-corrected FluoroProbe data obtained in chapter 1 to find the average fluorescence value at each profile depth measured over the five visible excitation wavelengths of the FluoroProbe (470 nm, 525 nm, 570 nm, 590 nm, 610 nm). However, since this uses the fluorescence measured at each LED channel instead of the phytoplankton pigment group determinations used in chapter 1, it gives an estimate of all the light absorption due to pigments linked to PS II. This was then compared to the estimated pigment absorption of *a*PSII for each sample calculated using a modified version of equation 9 where the five discrete FluoroProbe excitation wavelength peaks were substituted for the continuous PAR range from 400-700 nm. This *a*PSII estimation

technique will be referred to as five-wavelength average *a*PS x 0.5 for the remainder of this section because its value is not the same as the *a*PSII value resulting from *a*PSII method 1.

After plotting the average FluoroProbe fluorescence value from the five excitation peak wavelengths against the five-wavelength average *a*PS x 0.5 value for each sample in this dataset (n=61), two problems were evident. First, while a linear trend was apparent, there was a large amount of scatter in the points. The measured values from Lake Superior also did not represent a wide enough range of measured sample values to be confident in the predictive capacity of a linear regression. Second, the standardized residual plot of the fitted linear model showed increasing variance with increasing five-wavelength average *a*PS x 0.5 values.

To make our dataset larger (expanded to n=141), Greg Silsbe provided average FluoroProbe fluorescence and five-wavelength average *a*PS x 0.5 values measured on Lake Erie (Silsbe, 2010). The Lake Superior values were lower than most of the Lake Erie values as expected from the lower phytoplankton biomass in Lake Superior, but considerable overlap and a smooth transition between the two data sets gave the combined data a strong linear trend (Figure 21). Unequal variance was successfully addressed by a log10-transformation of the FluoroProbe and five-wavelength average *a*PS x 0.5 values as confirmed by the standardized residual plot of the linear regression fit to the log10-transformed data. Applying a log10-transformation to the data also ensured estimates of *a*PSII calculated using the regression line could not be negative, which would have no physical meaning. Two points representing surface water collections from Sandusky Bay in Lake Erie during a cyanobacterial bloom had abnormally high

FluoroProbe florescence and five-wavelength average *a*PS x 0.5 values compared to all other samples (Figure 21, circled upper right). These points were excluded from the final regression used in all subsequent data processing because they were atypical of the open-lake values measured in Lake Superior. Additionally, three points from Lake Superior representing mainly near-surface samples from 5 to 10 m during one cruise in late July had average FluoroProbe fluorescence values less than one (Figure 21, circled lower left), and a further two points from the same cruise do not appear on the graph because they had negative average FluoroProbe fluorescence values. These five points were also excluded from the linear regression because the low mean fluorescence likely did not represent a phytoplankton pigment fluorescence signal above the level of background instrument noise.

The equation of the resulting linear regression was:

$$\log 10(F) = 0.6316 \times \log 10(aPSII) + 1.9418;\ R^2 = 0.5689 \quad (11)$$

This relationship allows *a*PSII values to be predicted from the FluoroProbe fluorescence:

$$aPSII = 10^{\left[(\log 10(F) - 1.9418) \times [0.6316]^{-1}\right]} \quad (12)$$

This in turn enables estimates of *a*PSII to be calculated continuously through the water column using FluoroProbe profiles.

Conceptually, if the fluorescence measurement for a phytoplankton sample falls above the regression line then it has a higher level of fluorescence than would be predicted from the five-wavelength average *a*PS x 0.5 value alone, and therefore more than half of its pigments are associated with PS II. If *P* is defined as the ratio of estimated *a*PSII to measured *a*PS, then these samples have $P > 0.5$ (Suggett *et al*., 2004).

Samples with fluorescence measurements below the regression line will have $P < 0.5$, and fluorescence measurements falling on the regression line imply that pigments are evenly shared between PS I and PS II ($P = 0.5$). For the Lake Superior PAS samples represented in the linear regression (n = 56) where the actual value of *a*PS was known, some *a*PSII estimates from the FluoroProbe fluorescence (n = 15) were greater than the total *a*PS, giving $P > 1$. This is not possible since *a*PS is defined to always be larger than *a*PSII, so *P* was set to one for these samples.

Calculating O_2 production for PAS samples

*a*PSII values corresponding to each PAS sample depth were used to isolate the effects of the three different *a*PSII estimation techniques on calculated O_2 production rates using equations 7 and 8 with standardized light intensity values. For this analysis the surface PAR intensity was 1275 μmol quanta x $[m^2 \text{ x sec}]^{-1}$, measured at CM on the summer solstice (20 June 2010) with the FRRF, and light intensity at each depth through the water column was calculated using the summer mean k_d value from the FRRF PAR sensor ($k_d = 0.1511 \text{ x } m^{-1}$, n=32). *fPSII* values used in these calculations were F_q'/F_m' values from the FRRF light chamber profile at the same depth as the water sample taken for PAS analysis. For nighttime PAS sample collections, F_v/F_m values from the FRRF dark chamber were used for *fPSII*. All O_2 production rates from the same *a*PSII calculation technique were then plotted as a function of depth. Because all O_2 production rates were calculated using identical PAR intensities, this allowed for identification of changes in the distribution of O_2 production through the water column caused solely by the different *a*PSII calculation methods.

Calculating daily O_2 production using fluorometer profiles

Separately, instantaneous O_2 production rates in the DCL were calculated for 1 m depth intervals from 10-40 m using FRRF and FluoroProbe profiles taken at FWM on two consecutive days in early August using *a*PSII values calculated using *a*PSII methods 2 and 3. This depth range was chosen to span the upper portion of the DCL. In the high light intensity environment above 10 m, mechanisms that decouple processes in the ETC, such as cyclic electron flow around PSI, are often active and we had no way to quantify their effects; below 40 m there was effectively no available PAR for photosynthesis. Water column O_2 production rates from 10-40 m were calculated at equal time intervals throughout the day; these values were then integrated through the day to obtain an estimate for daily gross O_2 production within this depth range of the DCL. First, surface PAR was calculated at ten-minute increments throughout the day based on the latitude (47° N) and day of year using the equations presented in Kirk (1994). The calculated PAR intensity at solar noon was then scaled to the actual PAR measured before a FRRF profile taken at midday (E = 1185 μmol quanta x $[m^2 \text{ x sec}]^{-1}$). PAR through the water column at each time increment was calculated using the average k_d value from the FRRF PAR sensor for this cruise ($k_d = 0.1726 \text{ x } m^{-1}$, n=10).

FRRF and FluoroProbe profiles were taken sequentially during each day at early morning (07:00 h), mid-morning (11:00 h), mid-afternoon (15:00 h), and evening (20:00 h). The profile values of σ_{PSII} were corrected using mean SCF values for this cruise calculated from PAS samples taken at 10 m, 20 m, and 30 m (n = 5 for each depth) and linearly interpolated through depth. Daily O_2 production values integrated from 10-40 m were obtained by assigning the four measured profiles to portions of the day in three different ways. Method 1 (O_2 method 1; see Appendix for a diagram showing differences

in the three O_2 methods) used FRRF and FluoroProbe profiles from mid-morning to estimate O_2 production from sunrise until 11:00 h, and the mid-afternoon profiles to estimate O_2 production for the remainder of the day. There was no interpolation applied across the intersection between the estimates, and this method was designed to give a lower limit for calculated O_2 production values. This was the only method that used both *a*PSII method 2 and *a*PSII method 3 to calculate O_2 production; the other two methods only used *a*PSII method 3. The second O_2 calculation technique (O_2 method 2) investigated how decreases in F_q'/F_m' values caused by light loading during the day affected whole-day O_2 production estimates. Values from FRRF and FluoroProbe profiles taken at one of the four measurement times were applied to the whole day and then daily O_2 production was calculated. The third method (O_2 method 3) was meant to give smoother transitions between profiles measured at different times when they were linearly interpolated through a day. The day was divided into three major sections: from morning to mid-morning, from mid-morning to mid-afternoon, and from mid-afternoon to evening. For each section the FRRF and FluoroProbe profiles used in O_2 production calculations were the average of the two profiles collected at the start and the end of that section. For the time intervals between sunrise and the morning profile and between the evening profile and sunset, the morning and evening profiles were used, respectively.

For each ten-minute time increment through the day, the rate of O_2 production at each depth was calculated using ambient PAR for that depth and time, the appropriate F_q'/F_m' value from the light chamber of the FRRF normalized to 0.65, and the appropriate *a*PSII value derived either from *a*PSII method 2 or 3. O_2 production rates (mg O_2 x $[m^3$ x $h]^{-1}$) calculated for each ten-minute interval were then numerically

integrated from 10-40 m and divided by six to obtain the total O_2 production during that ten-minute interval (mg O_2 x [m^2 x 10 min]$^{-1}$). These 'time slices' of O_2 production from 10-40 m were then added together to give a daily integrated O_2 production rate (mg O_2 x [m^2 x d]$^{-1}$) from 10-40 m.

To investigate the seasonal and spatial differences in photosynthetic production, daily O_2 production estimates were calculated for stations sampled during the summer of 2010 where both FluoroProbe and FRRF light chamber profiles had been taken during the mid afternoon (between 14:00 h and 16:00 h, n = 5). Mid afternoon profiles were chosen because they gave the lowest daily production rates using O_2 method 2, and therefore would err toward underestimating the true daily photosynthetic production. These profiles represented four cruises: early June (FWM), late June (CM), late July (CM and FWM), and late August (EM). Estimates of O_2 production for these profiles were calculated in the same way as the estimates for FWM in early August described above, but using a different PAR profile through the water column. For each of the four cruises, the PAR profile used to calculate O_2 production was defined using a representative surface light value measured during that cruise, and the mean k_d value for that cruise calculated using the FRRF PAR sensor.

Converting O_2 production to C assimilation

Converting calculated O_2 production rates into C assimilation rates requires the use of a photosynthetic quotient (PQ), defined as the molar ratio of O_2 produced per C assimilated. A PQ value of 1.29 (Depew *et al*., 2006) measured in the oligotrophic east basin of Lake Erie was used in this project because, like Lake Superior, it is part of the Laurentian Great Lakes system, and also has both low chl *a* concentrations and

phosphorus limitation similar to Lake Superior. All of the photosynthetic production estimates for the DCL made in this study were calculated at least 10 m below the water surface. The ambient light intensity at these depths was therefore assumed to be low enough to minimize cyclic electron flow and its alteration of PQ values.

Results

Comparison of aPSII estimation methods

There were distinct differences between mean *a*PSII values calculated using the three *a*PSII estimation methods after normalization to their respective extracted chl *a* concentration (*a**PSII) (Figure 22). Values calculated using *a*PSII method 3 had the highest median value and also the greatest variability of the three *a*PSII calculation methods. The ratio of *a*PSII to *a*PS was also greater than 0.5 (median $P = 0.66$, n = 56) for *a*PSII method 3 with *P* values capped at one, signifying increased pigment allocation to PSII compared to PSI (Figure 23). *a**PSII values calculated using *a*PSII method 2 showed little variability across samples and were significantly less than *a**PSII values calculated using either *a*PSII method 1 or *a*PSII method 3 (One-way ANOVA; $F = 64.27$; $P < 0.001$). This was also reflected in low median *P* value of 0.10, which was significantly lower than 0.5 (One sample t-test; $P < 0.001$) and predicts that only about 10% of photosynthetic pigments are associated with PSII. The median value for *a**PSII calculated using *a*PSII method 1 ($P = 0.5$ because *a*PSII is always assumed to be half of *a*PS for this method) as well as the variability in the calculated *a**PSII values using *a*PSII method 1 fall between those calculated using *a*PSII method 2 and those calculated using *a*PSII method 3.

O_2 production rates for PAS samples

By using a standard PAR profile through depth, I was able to evaluate differences in O_2 production rates caused by the *a*PSII estimation technique alone. When using either *a*PSII method 1 or *a*PSII method 2, the relative depth distribution of O_2 production closely followed the PAR profile (Figure 24), although using *a*PSII method 1 gave O_2 production values that were roughly four times greater than those using *a*PSII method 2. Both methods estimated the maximum O_2 production would occur at 5 m where PAR was greatest, and production would effectively stop below 35 m due to lack of light. In contrast O_2 calculated using *a*PSII method 3 did not follow the same depth trend. Although the maximum production rates were still located at 5 m, there was a prominent increase in production rates from 15-20 m compared to the other two *a*PSII estimation methods despite the decreasing PAR. Like the other two *a*PSII estimation techniques, there was no calculated O_2 production below 35 m.

Comparing O_2 production rates through the water column using two different aPSII estimation methods

The distribution and magnitude of O_2 production rates during two consecutive days and calculated using *a*PSII methods 2 and 3 together with O_2 method 1 are markedly different (Figure 25). O_2 production rates calculated using *a*PSII method 3 are larger than rates using *a*PSII method 2 at all time intervals and depths. Using *a*PSII method 3 results in maximum O_2 production rates in the DCL being located from 17-22 m, which is slightly above the DCM (Figure 7) but well below the depths of maximum irradiance. The disjunction in the contour lines around ten hours after midnight, which is more evident on August 11th, is the connection point between estimates using mid-morning

profile values and those using mid-afternoon profile values. On both days, however, the mid-morning and mid-afternoon profiles closely align below 22 m, indicating that O_2 was produced at a fairly constant rate throughout the day at these depths.

In contrast, rates of O_2 production calculated using *a*PSII method 2 generally followed the changes in PAR intensity throughout the day and were greatest at 10 m where the PAR was highest. The O_2 production rates then declined consistently with depth and did not show any production below 22 m.

Daily O_2 production and C assimilation integrated from 10-40 m

Estimates of daily O_2 production from 10-40 m calculated using O_2 method 1 with both *a*PSII methods 2 and 3 gave fairly consistent values between the two days (Table 2). The daily production calculated using *a*PSII method 3 was nearly five times larger than estimates made using *a*PSII method 2, and averaged 613 mg O_2 x $[m^2 \times d]^{-1}$ over the two days. Using the PQ value measured in Lake Erie (Depew *et al*., 2006) this production is equivalent to an average of 179 mg C x $[m^2 \times d]^{-1}$.

Diel variations in photosynthetic potential through the water column

Using O_2 method 2 with profiles of *fPSII* and *a*PSII method 3 measured at different times of day had a large impact on the distribution of O_2 production through the water column over the two consecutive days (Figures 26 and 27). The estimates of daily O_2 production and C assimilation integrated from 10-40 m was also strongly dependent on the time of day the profiles were taken (Table 3). During both days, estimates calculated using profiles measured during the morning and the evening both showed the zone of greatest photosynthetic rates located at 10 m near solar noon, with the rate of photosynthesis decreasing fairly evenly with depth (Figures 26 and 27). There was no O_2

production in excess of 1 mg O_2 $[m^3 \times hr]^{-1}$ below roughly 30 m regardless of the time of day each profile was taken. This indicates that most O_2 production in the DCL occurs within the portion closest to the thermocline, with a minimal amount of photosynthesis occurring below the DCM due to essentially no PAR reaching those depths. The lowest daily integrated O_2 production value for both days occurred using the mid-afternoon profiles. The mid-afternoon profile gave estimated daily O_2 production that was roughly 60% lower than the production calculated using the morning profile on August 11th, and was nearly 40% lower than production calculated from the morning profile on August 12th. On both days, using mid-afternoon profiles gave maximum O_2 production rates within the DCL from 17-22 m, and corresponding to depths above the DCM. O_2 production around 10 m was sharply lower compared to estimates using either morning or evening profiles. Daily estimates of production using mid-morning profiles display O_2 production distributions (Figures 26 and 27) and depth-integrated daily production values (Table 3) that are intermediate between estimates using morning and mid-afternoon profiles.

After observing the greatly increased O_2 production potential near sunrise and sunset compared to both mid-morning and mid-afternoon profiles, O_2 method 3 was used with *a*PSII method 3 to give a more detailed estimate of daily O_2 production that included measured values from the morning and evening. Daily O_2 production values using this method (Table 4) were on average 24% larger than those using O_2 method 1 (Table 2), which reflects the increased O_2 production potential during the morning and evening. The values from O_2 method 3 were also roughly comparable to whole day values calculated from O_2 method 2 using solely mid morning profiles (Table 3).

Spatial variability in Lake Superior O_2 production estimates

The magnitudes of calculated daily O_2 production through the water column and at different times of year for stations across the lake vary widely, but they all display maximum O_2 production rates within DCL (Figure 28). At FWM in early June, when thermal stratification was becoming established and a DCL was evident, the maximum O_2 production was centered around 20 m, slightly above the DCM at 30 m (Figure 7), though relatively high O_2 production rates above 2 mg O_2 x $[m^3$ x $h]^{-1}$ were present from 10 m to near the DCM. This sampling of FWM during early June also yielded the highest daily O_2 production integrated from 10-40 m for any of the stations or dates in this comparison of spatial variability in O_2 production (Table 6). By late July at FWM the maximum O_2 production rate through the day was larger than in early June (Figure 28), and was again located directly above the DCM (Figure 7), but its depth interval was extremely narrow. The portion of the water column showing photosynthetic production was also much more limited than in early June, with all production occurring from roughly 11-25 m and the depth integrated daily O_2 production was less than half of the early June value (Table 6). In contrast, the photosynthetic O_2 production at both CM and EM was consistently lower than at FWM (Figure 28).

At CM on the summer solstice the light conditions were unique because the combination of increased PAR due to the high angle of the sun and the lowest k_d value measured with the FRRF PAR sensor at any station during the summer provided exceptionally high levels of PAR through the water column. O_2 was produced at all depths from 10-40 m (the three isolated O_2 production zones from 10-20 m visible in the graph are due to a lack of FRRF-measured F_q'/F_m' values at four depths and do not

represent actual zones of reduced phytoplankton photosynthesis), with the zone of maximum production spanning nearly 10 m from 24-34 m (Figure 28). This corresponds to depths of increased chl *a* concentrations relative to surface waters, although a well-defined DCM had not yet formed at CM during this sampling (Figure 7). Later in the summer, the daily O_2 production at CM in late July integrated from 10-40 m was less than 20% of the daily production estimated in late June (Table 6). This discrepancy is mainly due to a lack of calculated O_2 production above roughly 23 m in late July and low O_2 production below that depth (Figure 28). The apparent lack of photosynthetic production above 23 m is due to a lack of useable *a*PSII values calculated using the FluoroProbe and *a*PSII method 3. At these depths mean FluoroProbe fluorescence values were negative, which resulted in *a*PSII estimates of zero. This will be discussed further in the following section.

During late August at EM, the absolute amount of daily O_2 production was also lower than estimates for other stations earlier in the year (Table 6), although O_2 production took place at low rates through the entire portion of the water column from 10-40 m (Figure 28). Like for the late June CM sampling, the disjunctions in O_2 production at roughly 13 m and 22 m are caused by lack of F_q'/F_m' values at those depths, and not an inherent lack of photosynthetic production. For EM the zone of maximum O_2 production rates occurs in the DCL starting at 25 m and ending at the DCM located at 34 m (Figure 7) making it fairly wide, similar to CM during late June.

Discussion

Summary

As in Lake Erie, the *a*PSII estimation method (*a*PSII method 2) successfully used in

marine systems gives unrealistically low estimates of photosynthetic production when used in Lake Superior. Using an alternate *a*PSII estimation method (*a*PSII method 3) gives estimates of photosynthetic production in the DCL over two consecutive days that are comparable to those measured in a previous study using ^{14}C incubations (Sterner, 2010). Other estimates of daily O_2 production show a large amount of daily, spatial, and seasonal variability, which may make calculating estimates of O_2 production that accurately represent "typical" daily photosynthetic production in the lake difficult. However the pigment fluorescence-based technique with its high depth resolution shows that O_2 production is in fact highest within the DCL between 17 and 22 m, and therefore the water supersaturated with DO below the thermocline as measured with the CTD in chapter 1 can be the result of net photosynthetic production within the DCL.

Evaluating aPSII from different estimation methods

The linear regression of the combined, log10-transformed Lake Erie and Lake Superior data showed good overlap and continuity between the two datasets. Slightly more than half of the samples from Lake Superior lie above the regression line (Figure 21), however, which suggests that more than half of the total photosynthetic pigment absorbance is associated with PS II. This is reflected by the median *P* value for Lake Superior samples being greater than 0.5, even after the *P* value for 15 samples was capped at the maximum value of one. In contrast, *a*PSII method 2 gave extremely low estimates of PSII absorbance, which would suggest most of the photosynthetic pigment absorbance is directed toward PS I. The comparatively low estimate of PSII pigment absorbance calculated using *a*PSII method 2 was also demonstrated in Lake Erie (Silsbe, 2010), and is not likely a realistic representation of pigment distribution between PS I and

PS II.

O_2 production rates from PAS samples

Given the low *a*PSII values calculated using *a*PSII method 2, it is not surprising that O_2 production rates for PAS samples using these *a*PSII values were roughly four times less than those using *a*PSII method 1 (Figure 24). Interestingly, compared to O_2 production calculated using *a*PSII method 1, using values from *a*PSII method 3 for PAS samples increased the calculated O_2 production for depths from 15-30 m, corresponding with the DCL at many stations. This is in contrast to measurements near the bottom of the epilimnion at 10 m where *a*PSII method 1 gave increased values for O_2 production. Although O_2 production rates using *a*PSII method 3 at 5 m appear much lower than those using *a*PSII method 1, this may be due to high near-surface irradiance preventing the fluorometer from accurately measuring the comparatively dim fluorescence response of the pigments, and not due to actual changes in phytoplankton pigment absorption. Because fluorescence is only emitted from PS II, it is reasonable to assume that *a*PSII method 3 values calculated using the fluorometer data will give a more precise estimate of PS II pigment absorption compared to *a*PSII method 1 values calculated using the measured sample absorption spectrum. Together this suggests that *a*PSII values calculated using *a*PSII method 3 may give more accurate estimates of O_2 production rates through the water column with the exception of near-surface waters. Therefore while measurement of *a*PS from PAS sample filters is necessary to derive the relationship between total pigment absorbance and FluoroProbe fluorescence, *a*PSII values using *a*PSII method 1 alone may not be sufficient to give a representative estimate of O_2 production in the DCL in Lake Superior.

Comparison of production estimates between fluorescence-based methods and ^{14}C incubations

The average daily estimate of C assimilation from 10-40 m for FWM in early August and using O_2 method 1 with *a*PSII method 3 values (179 mg C x $[m^2 \times d]^{-1}$, Table 2) is slightly lower by 15% compared to the previously reported average daily ^{14}C incubation estimate from 10-40 m during late July or early August in three consecutive years (209 mg C x $[m^2 \times d]^{-1}$, Table 5) (Sterner, 2010). These ^{14}C incubation estimates are directly comparable to fluorescence-based estimates because they do not need spectral corrections, having been incubated in situ, and the incubation depths were evenly spaced throughout the euphotic zone. The portion of the water column from 10-40 m provided roughly 60% of the total primary production through depth as calculated using the same ^{14}C incubation estimates (Sterner, 2010). This portion of the DCL is therefore important to photosynthetic C assimilation and O_2 production in the lake. Even though the production estimates integrated over depth appear comparable between fluorescence and ^{14}C incubation techniques, the fluorescence profilers with their high depth resolution show that production is not in fact highest at 10 m as the ^{14}C incubation results indicate (Sterner, 2010), but is instead highest between 17 and 22 m. Daily C assimilation values using O_2 method 2 with morning or evening profiles (Table 3) are substantially larger than daily estimates from ^{14}C incubations (Table 5) (Sterner, 2010). Although the ambient PAR intensity in the water column is relatively low at these times of day, phytoplankton are capable of efficiently using this light for photosynthesis and subsequent C assimilation. Incorporating these increased morning and evening photosynthetic efficiencies into whole day production estimates using O_2 method 3

yielded an average daily C assimilation value (221 mg C x $[m^2 \times d]^{-1}$, Table 4) that was within 6% of the mean ^{14}C incubation-based C assimilation value for the same depth range (Table 5) (Sterner, 2010).

Light loading and its effects on daily O_2 production

Phytoplankton in the DCL showed marked diel variability in calculated O_2 production, likely in response to changes in the ambient light environment through the day. Although the PAR profile through the water column was kept constant for all O_2 production estimates made using O_2 method 2, there were still pronounced diel changes in the calculated potential O_2 production using *a*PSII method 3 and *fPSII* values from profiles at different times of day. From visual inspection, the profiles of *a*PSII from the FluoroProbe closely matched the shape of chl *a* fluorescence through the water column and did not appear to undergo substantial changes through the day. The low O_2 production potential from 10-17 m using the mid-afternoon profiles was primarily caused by decreases in F_q'/F_m' values driven by increases in the minimum fluorescence F'. This was likely due to the effect of cumulative light loading as the day progressed or perhaps a transient drawdown of an essential nutrient, although in either case phytoplankton were likely also P limited (Guildford *et al*., 2000). This implies that the apparent zone of maximum O_2 production deeper in the water column during the afternoon is not due to increased production by phytoplankton at that depth during the course of one day, but rather is due to decreased photosynthetic inhibition compared to phytoplankton located closer to the water surface. Although the mid-morning and mid-afternoon profiles were each taken roughly two hours from solar noon (13:00 h) and therefore were exposed to similar in situ light intensities when the profiles were taken, estimates of potential daily

O_2 production using the mid-morning profile are substantially higher than using the mid-afternoon profile.

This further supports the hypothesis that when using profiles from different times of day, measured values of F_q'/F_m' are lower than either their morning or evening maximum value in response to high and cumulative light loading of the phytoplankton through the day, and not due to the instantaneous intensity of PAR in the water column. However the potential for these diel variations in photosynthetic potential to be partly in response to fluctuations in essential nutrient concentrations, possibly mediated by zooplankton DVM into the DCL, cannot be ruled out. Estimated rates of O_2 production or C assimilation from a station will therefore be extremely sensitive to the time of day when measurements are made and will also depend on the prior light history of water column, especially the amount of cloud cover through the day. Estimates of daily O_2 production made with O_2 method 3, which used four profiles from morning until evening, were most similar to values resulting from applying mid-morning profile values to an entire day using O_2 method 2. This suggests that if only a single profile can be taken at each station due to sampling time constraints imposed by expensive ship time, FRRF and FluoroProbe profiles taken at mid-morning would provide the most representative estimate of whole-day O_2 production. Where it is not feasible to collect profiles during mid-morning, profiles from other times of day still give valuable information about O_2 production, but they need to be interpreted in the context of cumulative light loading through the water column between sunrise and the time the profiles were taken. In addition to this diel and depth variability in photosynthetic production, the data in chapter 1 showed that phytoplankton quantum efficiency and photosynthetic pigment composition also varied

over the immense area of Lake Superior, resulting in calculated photosynthetic rates that showed substantial spatial variability as well.

Seasonal and spatial variability in calculated O_2 production

All profiles used to compare the spatial and seasonal variability of O_2 production through the water column were taken during mid-afternoon in an effort to control as much as possible the diel variability in these estimates caused by light loading. However seasonal differences in light levels due to changes in day length and the incident angle of sunlight on the water surface will still create differences in the in situ light environment for profiles taken during the same time of day but at different dates during the summer. In addition, when calculating the O_2 production estimates, the PAR profile used for each cruise date was determined using a representative surface light intensity and mean k_d value from the FRRF PAR sensor for that cruise. Therefore the spatial and seasonal O_2 production estimates calculated in this study were meant to estimate the potential in-lake production during each cruise date as much as possible, instead of providing a standardized seasonal comparison of O_2 production.

The complete lack of calculated O_2 production above 24 m at CM in late July (Figure 28) is the result of extremely low *a*PSII estimates using *a*PSII method 3, and was therefore caused by the FluoroProbe profile values and not the FRRF profile values. The mean filtered water offset value for the FluoroProbe during the late July cruise was the largest measured for any cruise during 2010. For the profile from CM, applying this mean cruise offset to profile depths above 24 m where the raw measured fluorescence was already relatively low resulted in a negative value for the mean FluoroProbe fluorescence at the five excitation wavelengths. When the mean fluorescence value is

negative, *a*PSII cannot be calculated because the required log-10 transformation cannot be performed. Because the value of the filtered water offset applied to the profile can effectively drive the calculated O_2 production to zero, it appears that the phytoplankton chl *a* concentrations in Lake Superior may be at the limit of measurement sensitivity for the FluoroProbe. The reduction in calculated *a*PSII values caused by the filtered water offset appears to also be partly responsible for the extremely low daily C assimilation value from late August in this study (Table 6), which is less than 25% of that measured previously at EM in early August using ^{14}C incubations (Table 5) (Sterner, 2010).

At slightly greater chl *a* concentrations in Lake Superior like those at FWM in early August, *a*PSII profiles derived from the FluoroProbe using *a*PSII method 3 were highly consistent between two consecutive days and allowed the calculation of C assimilation estimates in good agreement with previously published values from ^{14}C incubations. This suggests that the FluoroProbe can give effective measurements in the low chl *a* environment of Lake Superior, but extreme care needs to be taken in selecting the proper filtered water offset to apply to each profile because this can strongly influence the calculated O_2 production value.

Implications for lake wide primary production in the DCL

At FWM during August 2010 the presence of increased photosynthetic O_2 production in the DCL from 17-22 m was calculated using the FRRF and FluoroProbe, and CTD profiles taken at the same time show supersaturated DO concentrations from 10-30 m. This strongly suggests that the increased DO concentration measured in the DCL is the result of gross photosynthetic O_2 production rates in excess of organism respiration rates at those depths, and is not solely due to other phenomena such as a

combination of decreased respiration and increased temperatures.

The portion of the DCL in the upper metalimnion therefore appears to be net autotrophic during the stratified season at this station. This amount of photosynthesis in the DCL is likely made possible by a combination of the thermal stratification that allows the phytoplankton to adapt to the relatively constant spectral quality and intensity of light below the thermocline, and also the relatively higher concentrations of N and P at those depths compared to the epilimnion. Because the horizontal extent of O_2 production within the DCL in lake during the summer is so extensive (Figure 28), any photosynthesis taking place in the DCL will give rise to a large absolute amount of whole-lake photosynthetic production. It is therefore possible that photosynthesis in the DCL contributes a substantial amount of the yearly lake primary production, even though the DCL measured in this study is only established from mid to late summer. It is also possible that a DCL is present in Lake Superior during the winter, particularly in relatively stable conditions under ice although that was not evaluated in the current study. Increased photosynthetic production within the DCL identified using fluorescence-based profilers would imply that the contribution of in situ production to the formation and persistence of the DCL through the summer may be larger than has been assumed using ^{14}C incubations, which display a consistent decrease in C assimilation rates with depth from 10 to 40 m (Sterner, 2010). The presence of high photosynthetic rates within the DCL suggests that continual phytoplankton growth may offset grazing losses due to zooplankton and other grazers, and therefore the daily increase in gross phytoplankton biomass due to growth may be higher than has previously been identified. The combination of net autotrophy that occurs seasonally in the DCL and the enhanced

energy availability that increased biomass in the DCL represents for grazers displaying DVM behavior such as *Mysis* may therefore have important implications for the lake C budget, which currently is understood to be net heterotrophic with respiration at least four times larger than total production (Cotner *et al*., 2004, Urban *et al*., 2005).

Effects of cyanobacterial pigment composition and ETC uncoupling on community photosynthesis estimates

Picocyanobacteria represent a large proportion of the phytoplankton present in Lake Superior, and their contribution to *a*PSII can measured using the FluoroProbe because its multiple excitation wavelengths allow it to quantify fluorescence from accessory pigments in addition to chl *a*. However, *fPSII* values measured with the blue excitation spectrum of the FRRF instrument used in this study do not fully represent the quantum efficiency of cyanobacterial PC and PE pigments because those pigments do not absorb blue light efficiently. Furthermore, the flexibility of the photosynthetic pathway in cyanobacteria with respect to absorbed energy utilization can uncouple the normal ETC connection between O_2 production and C assimilation in both high and low light environments. At high in situ light intensities a variety of mechanisms such as cyclic electron flow (Campbell *et al*., 1998), can cause O_2 production rates to overestimate actual C assimilation. It is also possible for O_2 production and C assimilation to become decoupled through electron slippage at very low light levels (<0.5% of surface PAR) resulting in the decay of unstable energy transport intermediates in the electron transport chain (Quigg *et al*., 2006). However since most photosynthetic production takes place at light levels greater than this, and since phytoplankton adapted to these low light conditions have mechanisms to limit electron slippage (Quigg *et al*., 2006), decoupling of

O_2 production from C assimilation was considered to be most likely under high light conditions in this study. Limiting O_2 calculations to depths greater than 10 m was assumed to prevent substantial uncoupling between O_2 production and C assimilation due to high PAR intensities and therefore a single PQ value was used to represent the entire phytoplankton community, including cyanobacteria. Therefore the relative lack of spectral overlap between the FRRF excitation spectrum and the cyanobacteria pigment absorption spectra likely resulted in the largest source of error in accurately measuring the cyanobacterial contribution to the quantum efficiency of the phytoplankton community, which in turn would affect the estimates of photosynthetic rates in the lake. Because picocyanobacteria comprised roughly 40% of the total phytoplankton chl *a* in Lake Superior during 2010 (Table 1), the photosynthetic production estimates in this study are probably not fully representative of the phytoplankton production in the lake. This excitation wavelength limitation could be addressed in future studies to give more comprehensive estimates of photosynthetic production representative of the whole phytoplankton community in the lake.

Limitations of FRRF σ_{PSII}-based production estimates in freshwater systems

Fluorescence-based C assimilation estimates using *a*PSII values from σ_{PSII}-based *a*PSII method 2 were on average less than 20% of the ^{14}C-based estimates, and appear not to give accurate estimates of primary production in Lake Superior. It seems that there are severe limitations to using this *a*PSII estimation technique derived only from σ_{PSII} measurements made using the blue excitation light of this FRRF to accurately estimate photosynthetic O_2 production of the diverse phytoplankton in the lake, even when SCFs are applied. Studies of primary production in marine systems demonstrate that the σ_{PSII}-

based estimates of C assimilation are generally comparable to those from ^{14}C incubations (Corno *et al*., 2006, Pemberton *et al*., 2006). The two methods were also found to give remarkably comparable C assimilation estimates for the relatively shallow Lake Mondsee during the spring, fall, and winter when diatoms dominated the phytoplankton assemblage, but not during the summer when PE-rich cyanobacteria were common (Kaiblinger and Dokulil, 2006). In other freshwater systems including Lake Erie, σ_{PSII}-based estimates of C assimilation underestimate ^{14}C incubation values mainly because they did not provide a satisfactory measurement of the light absorption by phytoplankton communities (Silsbe, 2010). In the open ocean blue wavelengths of light penetrate deepest into the water column. Consequently marine phytoplankton need a relatively limited range of accessory pigments beyond chl *a* with its Soret absorption band to effectively absorb ambient light. Phytoplankton in freshwater live in a more dynamic and variable light environment, however, and use accessory pigments with peak absorptions at longer wavelengths than blue light in order to adapt to their ambient light conditions, as demonstrated by the PAS and FluoroProbe results from chapter 1. Similar to the measurements of quantum efficiency, using only the blue light of this FRRF instrument to measure σ_{PSII} values of these phytoplankton therefore can represent a substantial underestimation of the true absorption spectrum of pigments associated with PSII. SCFs serve to standardize σ_{PSII} values between studies for comparability, but they cannot correct for the effects of accessory pigments whose absorption is not measured by the FRRF's blue excitation spectrum. The use of Fluoroprobe mean fluorescence to estimate light absorption by PSII accessory pigments can at least address the underestimation of *a*PSII, but the FRRF still may not provide sufficient characterization of the quantum

efficiency of cyanobacteria.

Conclusions

The method of calculating photosynthetic rates using the FluoroProbe together with the FRRF was first introduced and used successfully on Lake Erie together with limited measurements on Lake Superior (Silsbe, 2010). This project demonstrates that the same method also provides estimates of photosynthetic production comparable to previously published ^{14}C-based estimates (Sterner, 2010) for FWM when using a larger combined Lake Erie and Lake Superior dataset to estimate *a*PSII using *a*PSII method 3.

For the stations CM and EM however, the fluorescence-based estimates of C assimilation were substantially lower than the photosynthetic production measured with ^{14}C incubations. This discrepancy in production estimates was primarily caused by profile measurements with low overall fluorescence measured with the FluoroProbe at CM and EM and relatively high filtered water offset values. Together this combination resulted in *a*PSII values estimated using *a*PSII method 3 that were either zero or were extremely low compared to *a*PSII values estimated using the same method at FWM. The low photosynthetic production estimates for CM and EM were therefore probably not due to the profiles being taken during mid afternoon, because measurements of *a*PSII remained fairly constant through the course of one day in early August at FWM, and only *fPSII* showed stong diel variations. The use of filtered water offset values that correspond closely to the in situ conditions at the time each profile was taken therefore becomes crucial. Examination of all filtered water offset values taken during 2010 at each of the five excitation wavelengths revealed no considerable differences between sample depths, but there was a large amount of seasonal variability, which has also been

observed in Lakes Erie and Huron (Twiss, 2011), and variability in offset values measured repeatedly at FWM over three days in early August (data not shown). To ensure the greatest possible accuracy in offset measurements, it may prove best to measure them as soon as possible after the profile they are meant to correct so the water is fresh and any instrument noise present in the offsets would likely be similar in magnitude to instrument noise present in the profile.

With these limitations in mind, use of the fluorescence profilers to estimate photosynthetic production on a body of water as large as Lake Superior can represent a large improvement over existing estimation methods because of the dramatically enhanced depth resolution and decreased time necessary for measurement of each profile compared to traditional ^{14}C incubations. In addition, because they necessarily calculate O_2 production rates before calculating C assimilation rates by applying a PQ, the measurements from fluorescence-based profilers can also be useful in biological respiration studies. These calculated photosynthetic rates establish the magnitude of gross O_2 production in the water column and therefore allow comparisons with previously published O_2 consumption rates, such as studies measuring respiration rates in Lake Superior (McManus *et al*., 2003, Urban *et al*., 2004). Understanding the balance between photosynthetic O_2 production and organism respiration is essential to determining whether the water column is autotrophic with net O_2 production, or heterotrophic with net O_2 consumption. Although ^{14}C incubations can also estimate O_2 production knowing the rate of C assimilation, there is unavoidable uncertainty about whether the radiocarbon method measures net or gross photosynthesis (Peterson, 1980). Consequently it would be preferable to measure O_2 production directly. The sensitivity

of fluorescence-based measurements makes this possible even in extremely oligotrophic environments where direct measurement of changes in DO concentrations from incubations within reasonable time intervals is not possible. Overall, the short amount of time needed to take each profile combined with their extremely high depth resolution make these pigment fluorescence profilers powerful tools in addressing questions related to both primary productivity and community respiration.

Overall conclusions

During the summer of 2010, the water column in Lake Superior became thermally stratified early in the season and reached surface temperatures that surpassed the decadal average temperature of the lake observed forty and fifty years ago. With these conditions the DCL began forming in late June, and was well established across the lake through late August. The DCL represented a dynamic phytoplankton community exhibiting seasonal changes in pigment composition, photosynthetic quantum efficiency and functional absorption cross-section of PS II. Notable areas of DO super saturation below the thermocline measured with the CTD corresponded closely to depths of increased phytoplankton photosynthesis within the DCL identified using fluorescence profilers.

The comparability between previously published ^{14}C incubation-based C assimilation estimates for Lake Superior and those made with the fluorescence profilers at FWM using a method first introduced on Lake Erie demonstrated that the two methods can give comparable measurements of photosynthetic production in oligotrophic Lake Superior. Estimates of photosynthetic production across the lake at different times of year suggest a high amount of spatial and seasonal variability exists in estimated daily photosynthetic production values as well as in the depth distribution of photosynthesis

through the water column. In all cases, however, areas of increased photosynthetic production within the DCL were evident.

The filtered water offsets applied to the FluoroProbe profiles were found to have a large influence on both the apparent phytoplankton pigment composition with depth from chapter 1 as well as the estimated *a*PSII values used for O_2 production estimates in chapter 2. Therefore, more than any other methodological aspect of this project, the selection of appropriate FluoroProbe offsets is critical in order to obtain results that are representative of the in situ environment in the Lake Superior when the profiles were taken.

The improved depth resolution of fluorescence-based photosynthetic estimates, however does support the hypothesis that the portion of the DCL in the upper metalimnion is an area of in situ production, and is not mainly due to non-viable phytoplankton settling from the epilimnion. In contrast, relatively little photosynthesis appears to occur within the DCM and lower DCL due to low light intensities at those depths. Further expanding the use of fluorescence-based profilers to systematically estimate photosynthetic production across the lake and through the year would give dramatically increased resolution in photosynthetic estimates for Lake Superior. As long as the results from fluorescence profilers are interpreted in accordance with their potential measurement limitations, especially with regard to filtered water offsets, then they will likely improve understanding of energy flow and nutrient cycling within the DCL and may therefore help to address the measured imbalance between respiration and photosynthesis in Lake Superior.

Figure 1: Diagram of a typical water column temperature and chl *a* fluorescence profile in Lake Superior showing the extent of the DCL and the location of the deep chlorophyll maximum (DCM) after thermal stratification has been established in late summer. The gray shading denotes the depth range of the DCL, where chl *a* concentrations are greater than those at the surface, and the arrow indicates the DCM where the chl *a* concentration is the highest in the water column. The approximate depth intervals of the surface mixed layer, the metalimnion (the depth interval having the greatest temperature gradient), and the hypolimnion as determined from the temperature profile are also noted.

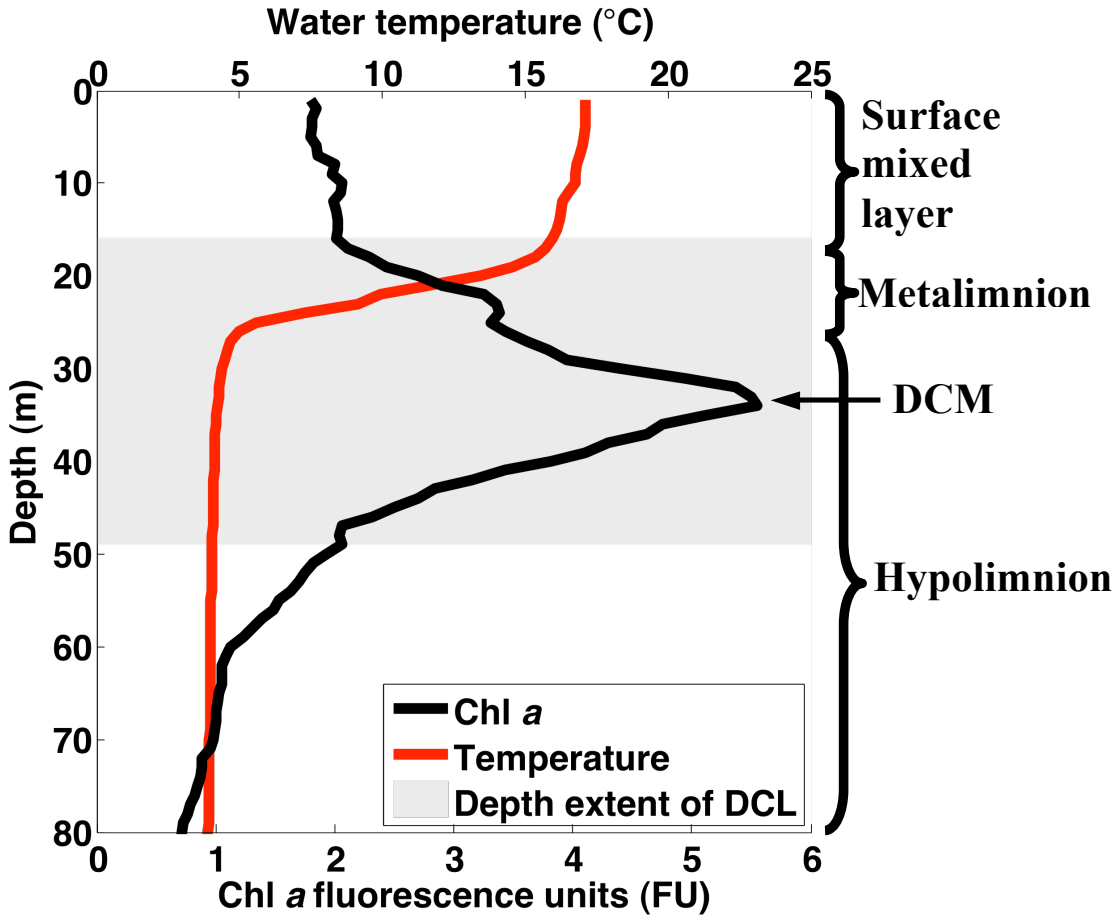

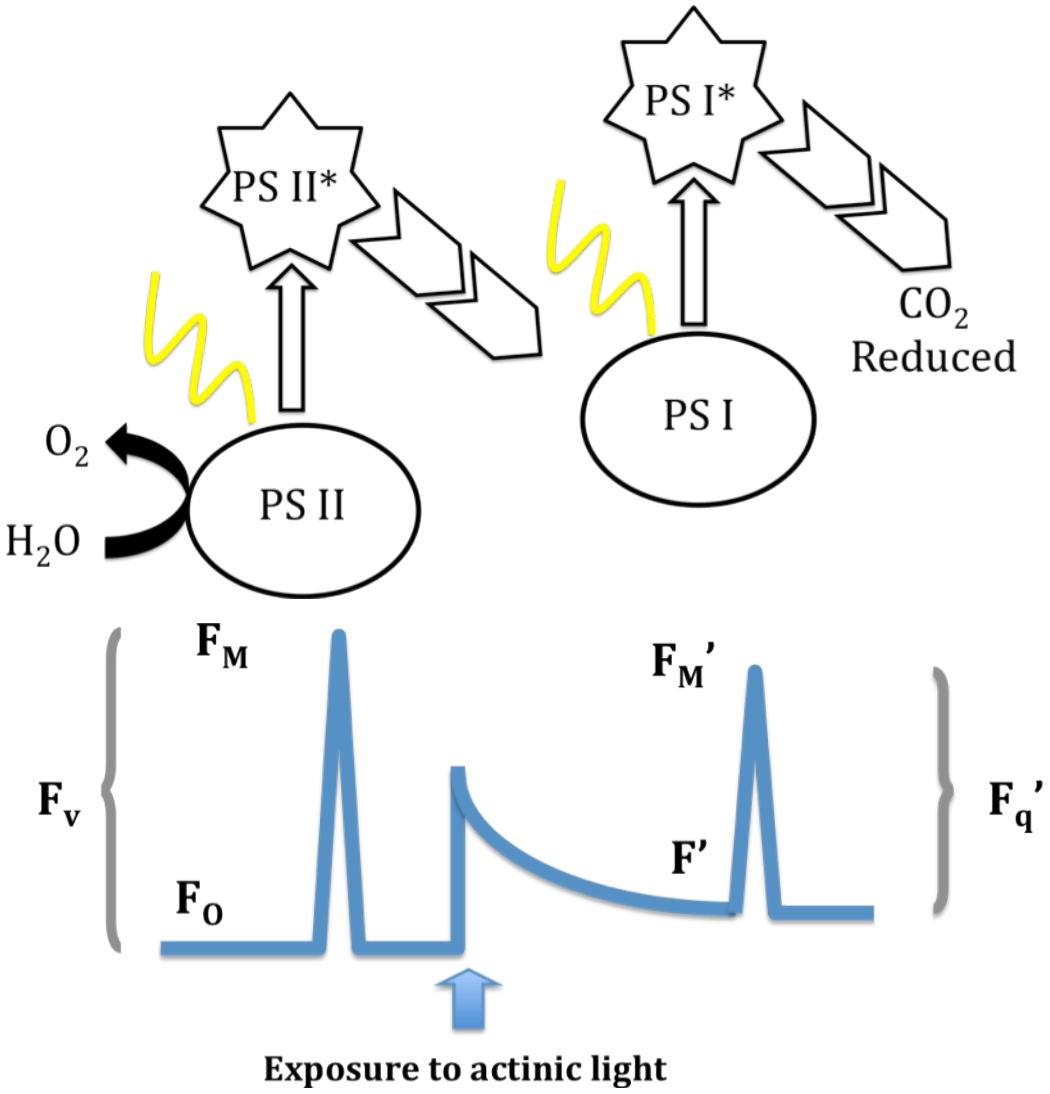

Figure 2: Diagram of photosynthetic light absorption and sites of O_2 production and C assimilation. O_2 is produced when water is split at Photosystem II (PS II). PS II absorbs light (yellow line) and moves to a higher energy state (PS II*). Chevrons denote the electron transport chain (ETC) connecting PS II to Photosystem I (PS I), which absorbs light energy like PS II to become PS I*. Electrons continue moving through the ETC downstream of PS I and eventually are used to reduce CO_2 in the Calvin cycle, assimilating C into organic molecules.

Figure 3: Diagram of fluorescence measurements used in this study modified from Maxwell and Johnson (2000). F_o represents the minimal fluorescence measured in a dark-adapted sample. After exposure to a saturating flash of light, fluorescence increases to a maximum value, F_m. Photosynthesis is then activated after exposure to actinic light. The lowest level of fluorescence under these conditions is F'. A second saturating flash is used to determine the maximum level of fluorescence in the light F_m'. Variable fluorescence in the dark (F_v) is F_m-F_o, and variable fluorescence under actinic light (F_q') is F_m'-F'.

Figure 4: Map of stations sampled on Lake Superior during the summer of 2010. Letters next to each marker denote the station name, and numbers in parentheses denote the number of times that station was sampled during the summer.

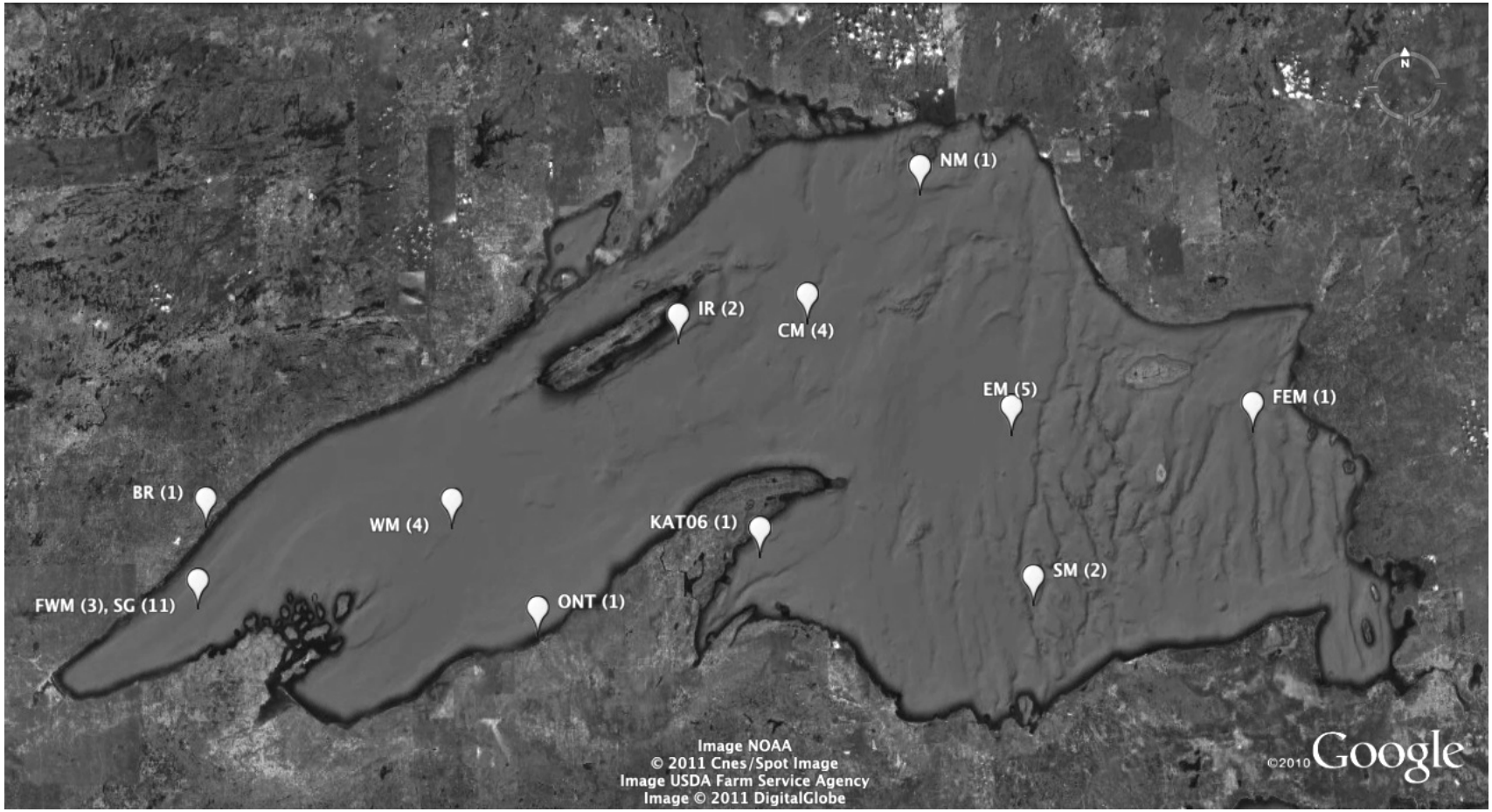

Figure 5: Flowchart of steps required for determination of various absorbance spectra from sample filters adapted from Culver and Perry (1999) and Silsbe (2010). Absorption spectra for each sample filter are taken before (*a*P(λ)) and after (*a*NAP(λ)) bleaching with sodium hypochlorite to give the absorption of all filter-retained particles and absorption of non-algal particles, respectively. Subtracting *a*NAP(λ) from *a*P(λ) and accounting for the volume of filtered water and filter area for each sample gives the absorbance of phytoplankton (*a*PH(λ)). The absorption of photosynthetic pigments (*a*PS(λ)) is obtained once the absorption due to pheophytin *a* (*a*PHEO(λ)) is subtracted from *a*PH(λ). *a*PS(λ) can further be split into absorbance from photoprotectant pigments (*a*PP(λ)), absorbance from chl *a* (achl*a*(λ)), and absorbance from accessory pigments (*a*ACC(λ)). The gray arrow and dashed line denote the extent of parameters used in chapter 1. *a*PS(λ) can also be divided into absorbance from pigments associated with PS I (*a*PSI(λ)) and PS II (*a*PSII(λ)). *a*PSII(λ) will be used in chapter 2.

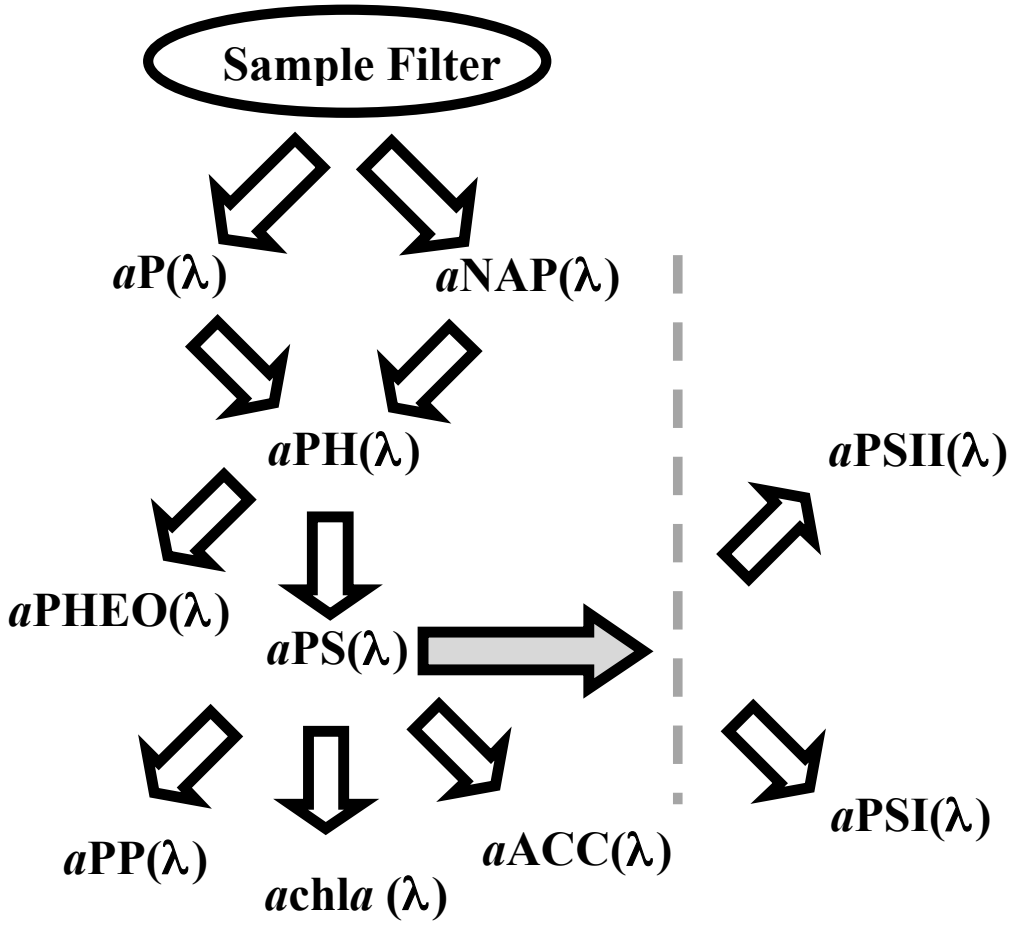

Figure 6: Water temperature profiles at four stations from west to east across the lake (clockwise from upper left: FWM, WM, CM, EM) through the summer of 2010. Note the different August sampling date for FWM compared to the other three stations. All profiles collected using the R/V Blue Heron CTD.

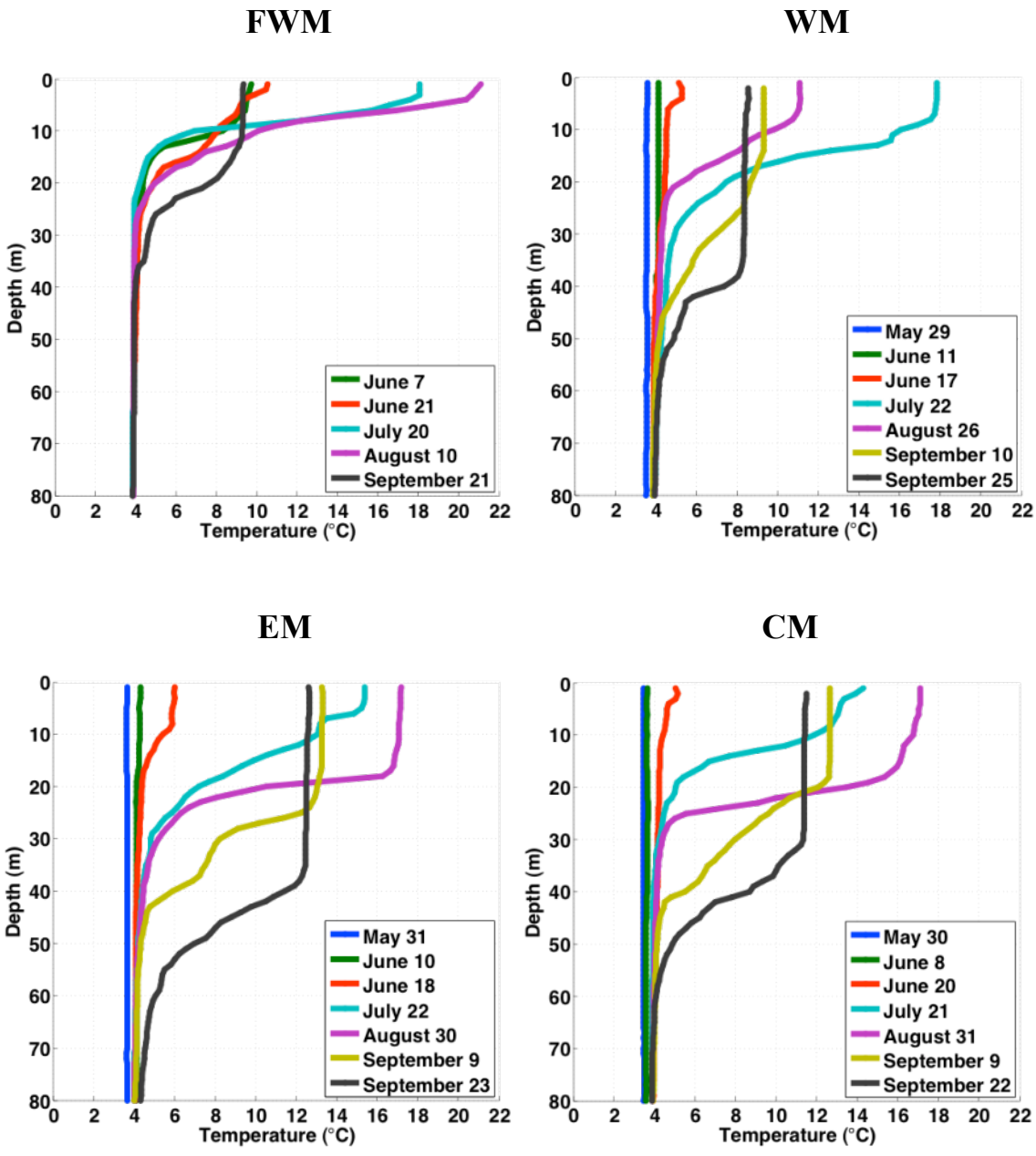

Figure 7: Chlorophyll *a* fluorescence profiles from west to east across the lake (clockwise from upper left: FWM, WM, CM, EM) through the summer of 2010. Note the different August sampling date for FWM compared to the other three stations. All profiles collected using the Blue Heron CTD fluorometer and measured in fluorescence units (FU), which do not correspond to absolute chl *a* concentrations.

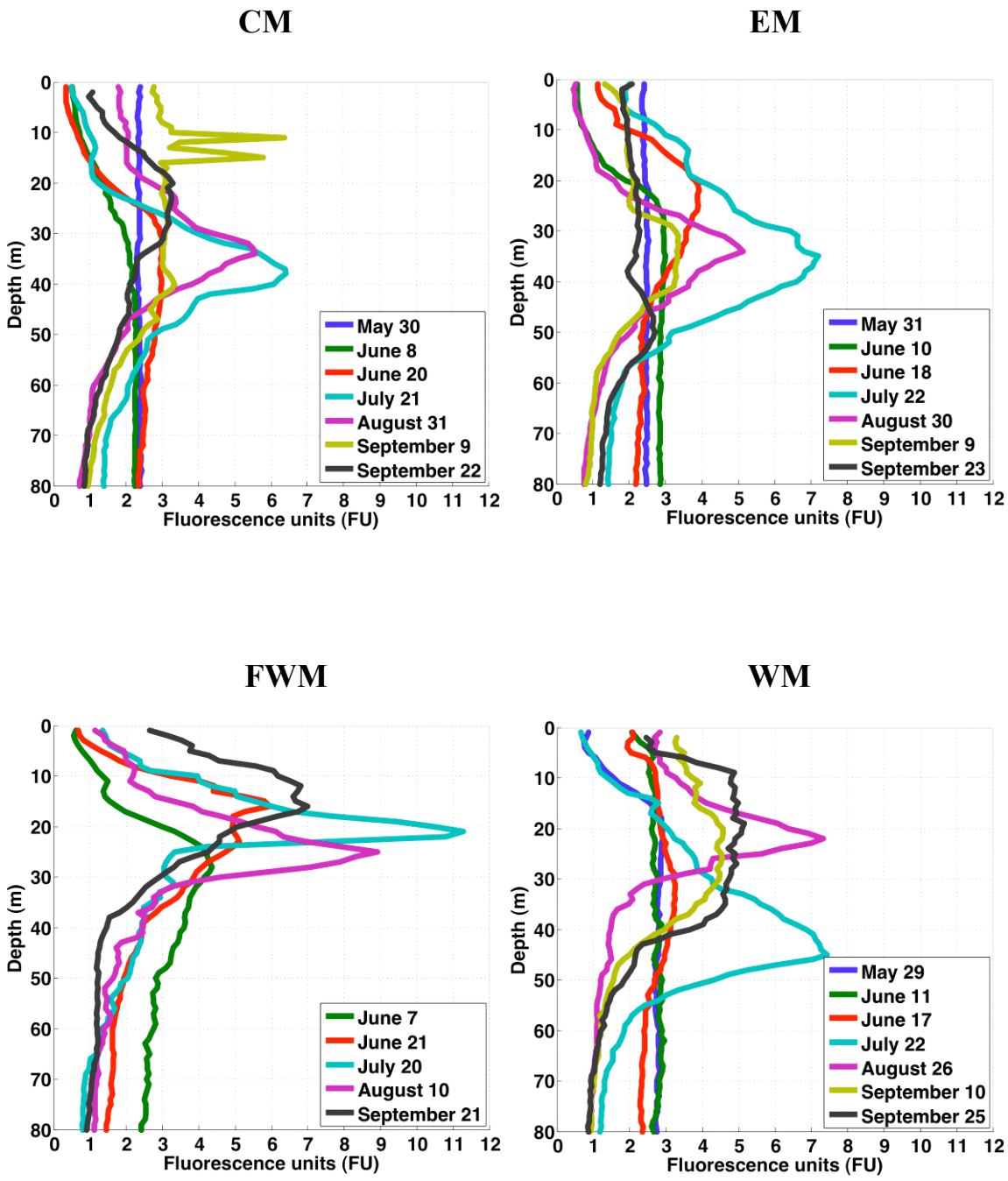

Figure 8: Profiles of dissolved oxygen concentrations from west to east across the lake (clockwise from upper left: FWM, WM, CM, EM) through the summer of 2010. Note the different August sampling date for FWM compared to the other three stations. All profiles collected using the Blue Heron CTD.

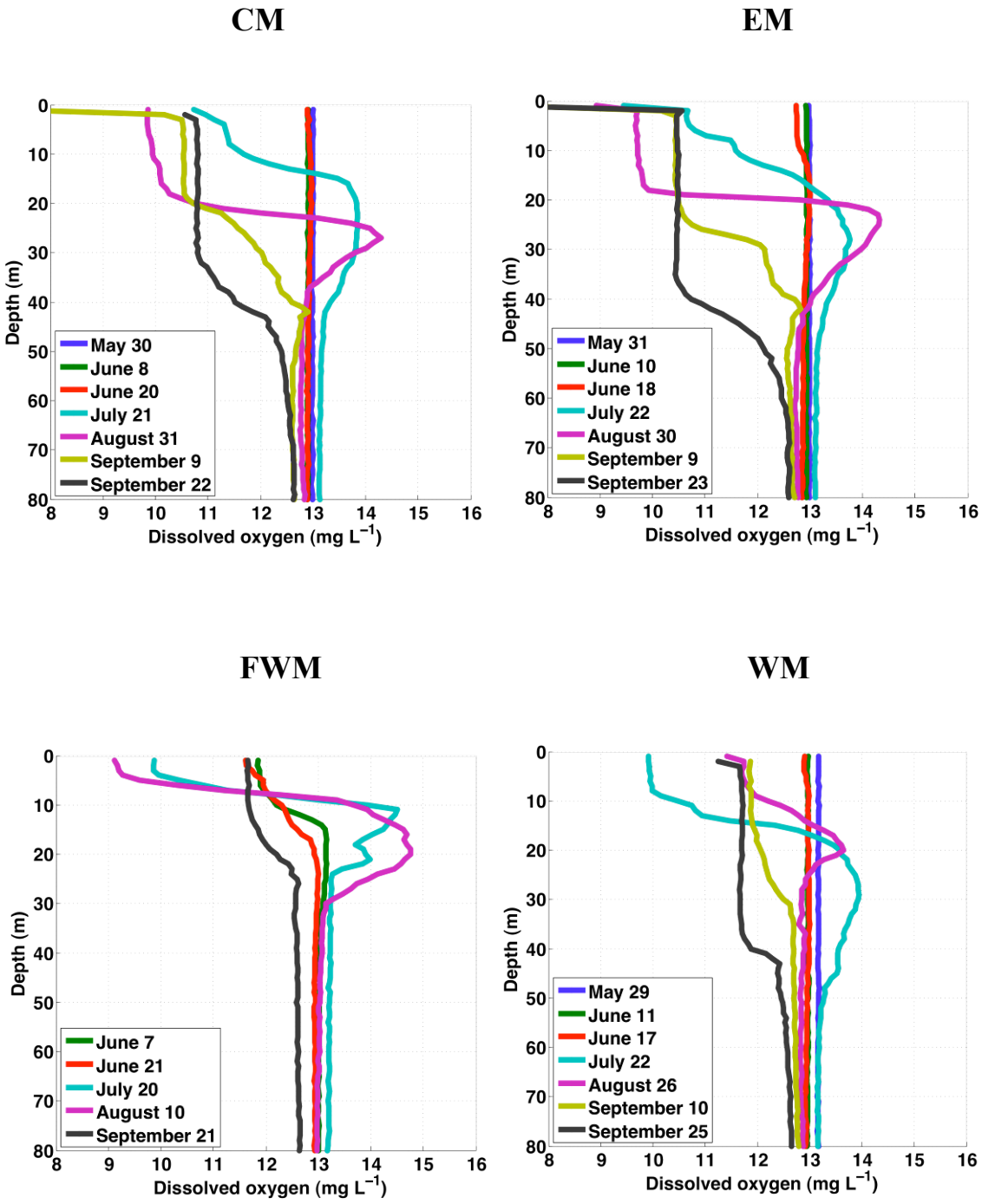

Figure 9: Profiles of dissolved oxygen as a percentage of saturation from west to east across the lake (clockwise from upper left: FWM, WM, CM, EM) through the summer of 2010. Note the different August sampling date for FWM compared to the other three stations. All profiles collected using the Blue Heron CTD. All calculations for determining dissolved oxygen saturation concentrations were made following Benson and Krause (1980).

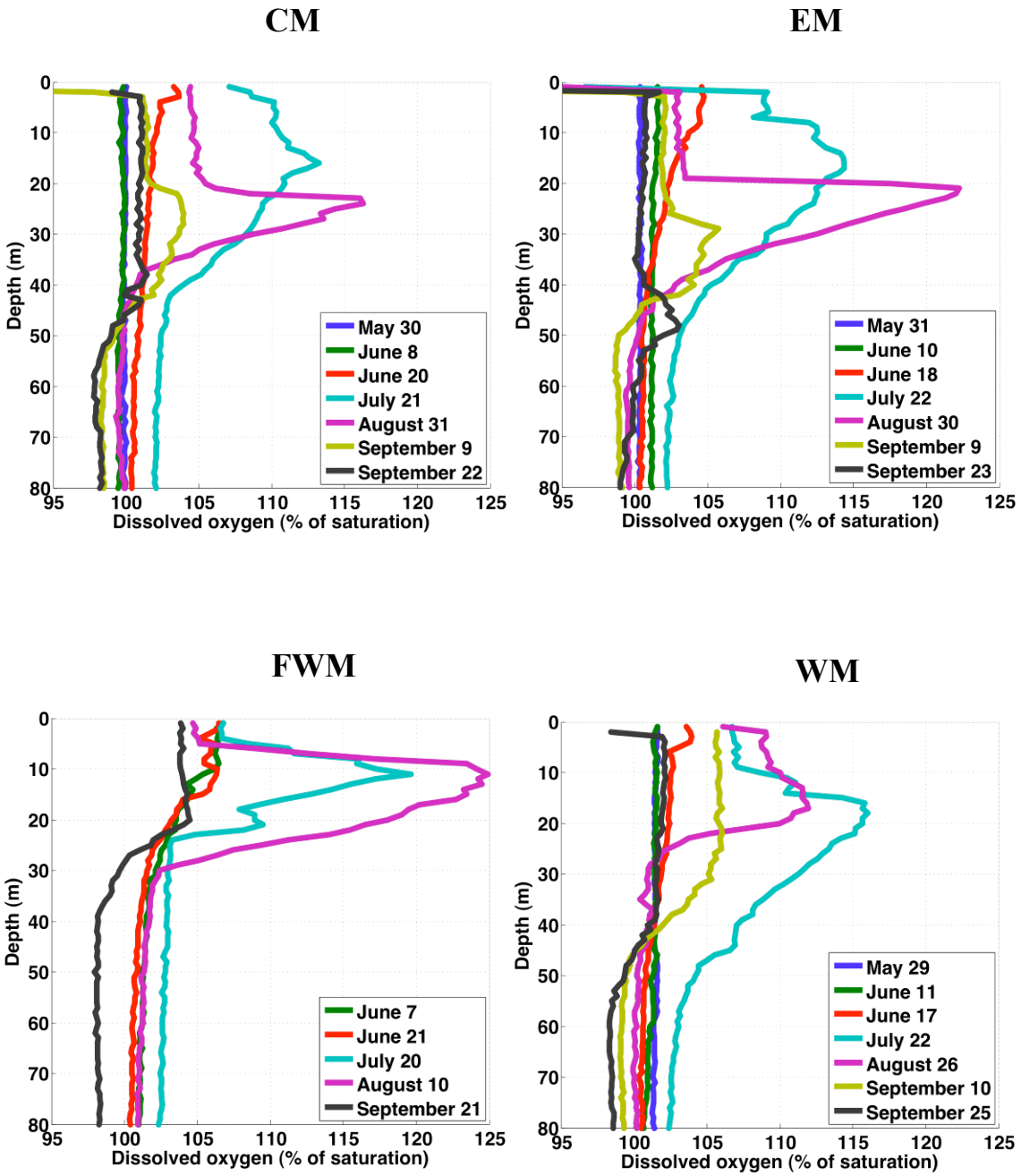

Figure 10: Trends in monthly mean light extinction coefficient (k_d) as measured by the Blue Heron CTD and mean percentage of surface PAR reaching the deep chlorophyll maximum (DCM) in Lake Superior from June to September 2010. The dashed line indicates the boundary of the euphotic zone, represented by 1% of surface PAR.

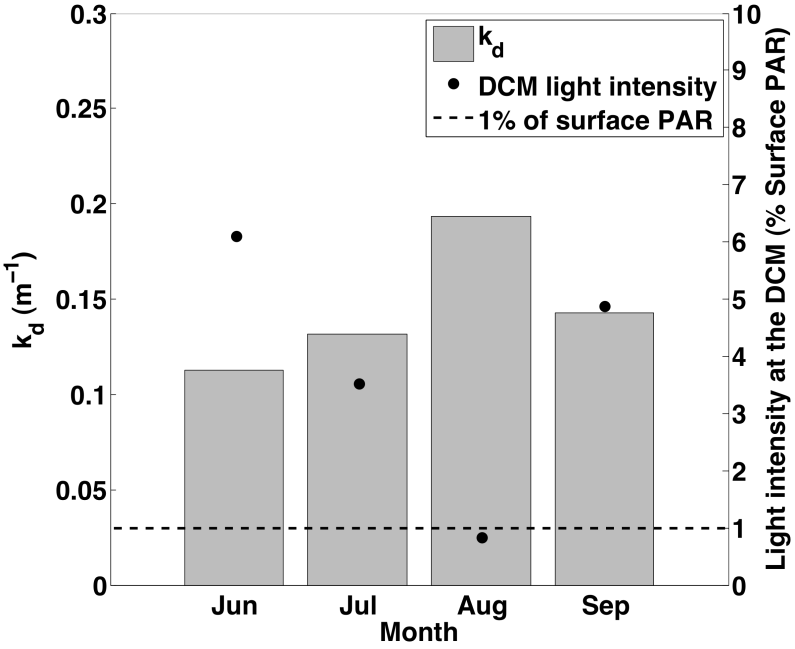

Figure 11: Seasonal trends in DCM depth and DCM water temperature at four stations across the lake from early June until early September 2010. A DCM was not present at all stations for each sampling date.

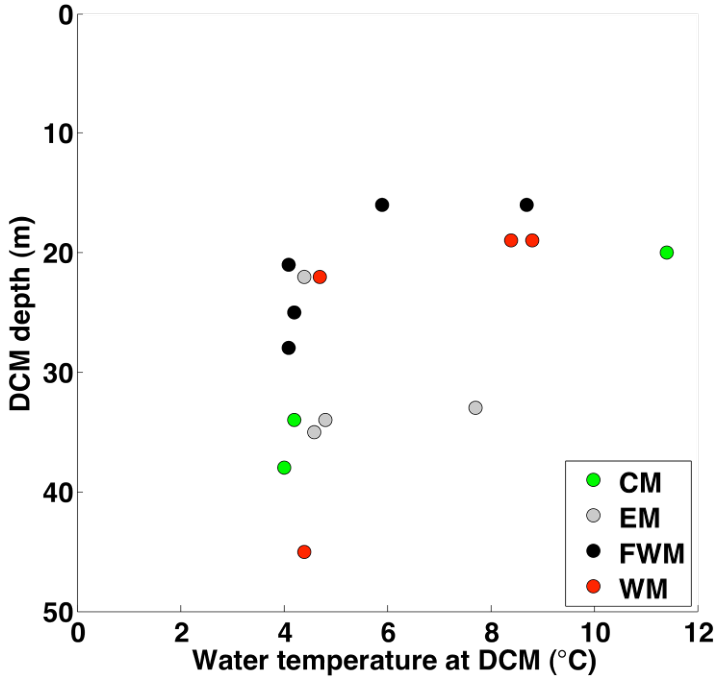

Figure 12: Spectral fluorometer (FluoroProbe) profiles from west to east across the lake (clockwise from upper left: FWM, WM, CM, EM) in late June 2010. The plotted lines denote phytoplankton pigment groups (phycocyanin (PC)-rich, phycoerythrin(PE)-rich, browns including diatoms, chrysophytes, and dinoflagellates) and total chl *a* as determined by the FluoroProbe.

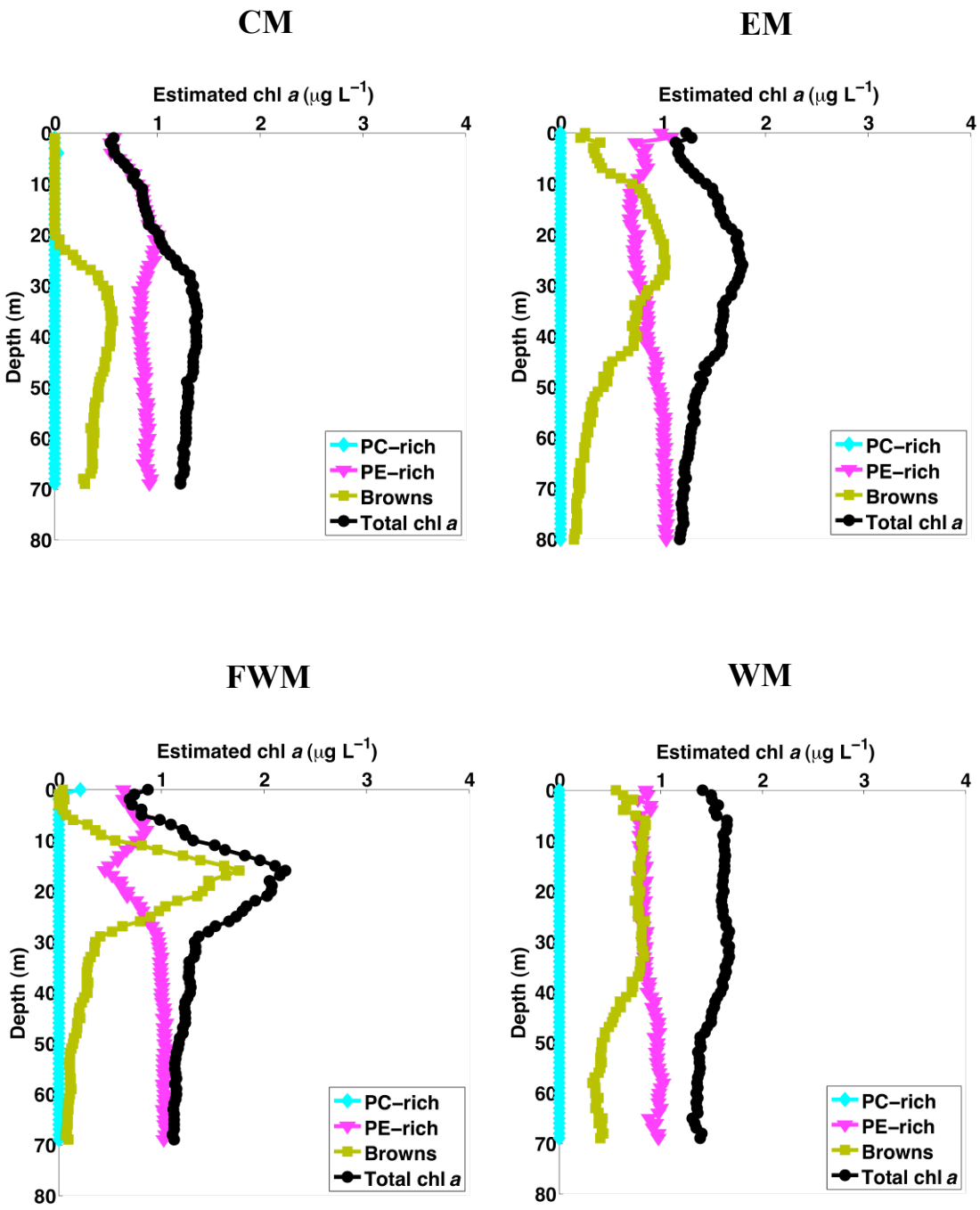

Figure 13: Spectral fluorometer (FluoroProbe) profiles from west to east across the lake (clockwise from upper left: FWM, WM, CM, EM) in late July 2010. The plotted lines denote phytoplankton pigment groups (phycocyanin (PC)-rich, phycoerythrin(PE)-rich, browns including diatoms, chrysophytes, and dinoflagellates) and total chl *a* as determined by the FluoroProbe.

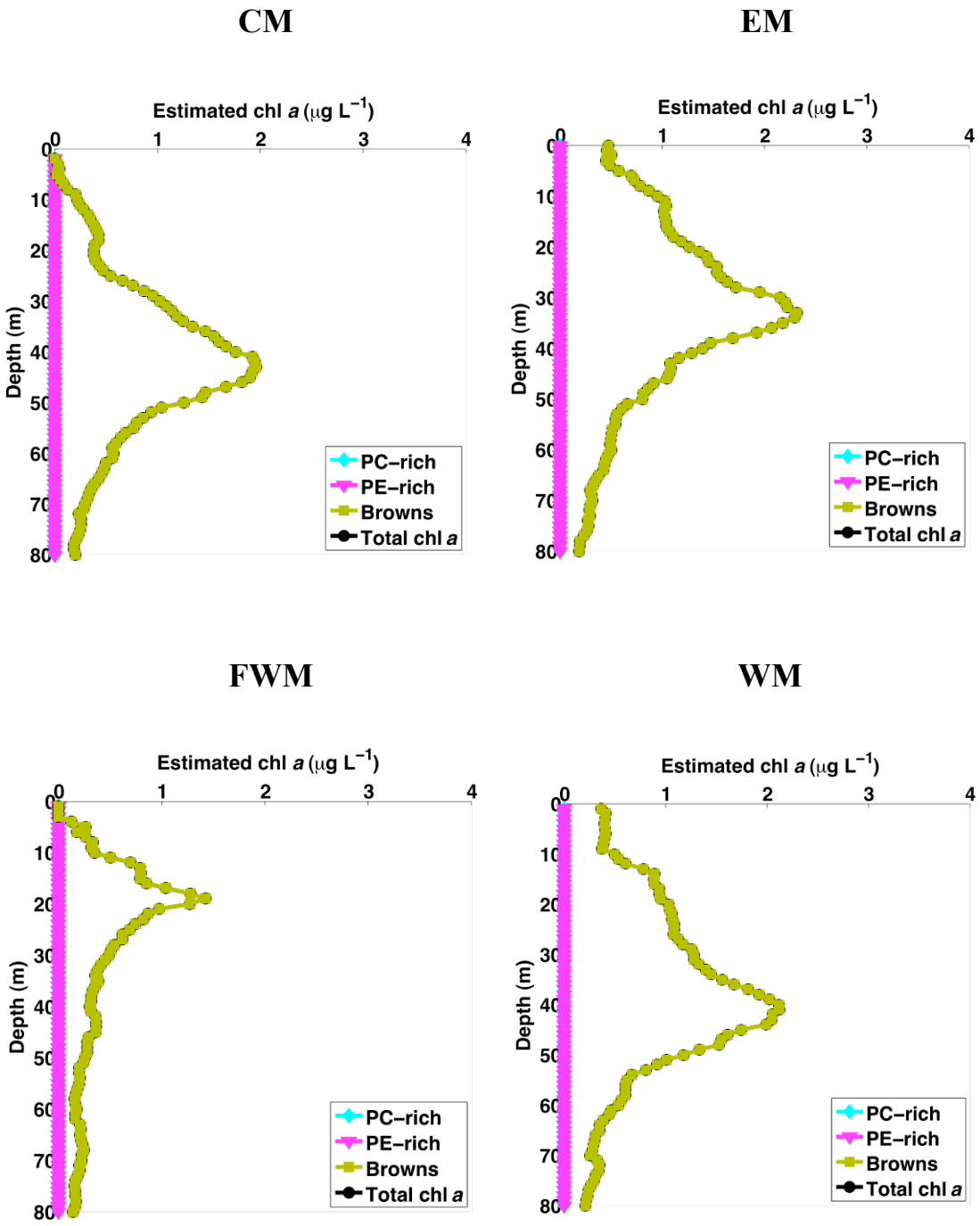

Figure 14: Spectral fluorometer (FluoroProbe) profiles from west to east across the lake (clockwise from upper left: FWM, WM, CM, EM) in late August 2010 (early August for FWM). The plotted lines denote phytoplankton pigment groups (phycocyanin (PC)-rich, phycoerythrin(PE)-rich, browns including diatoms, chrysophytes, and dinoflagellates) and total chl *a* as determined by the FluoroProbe

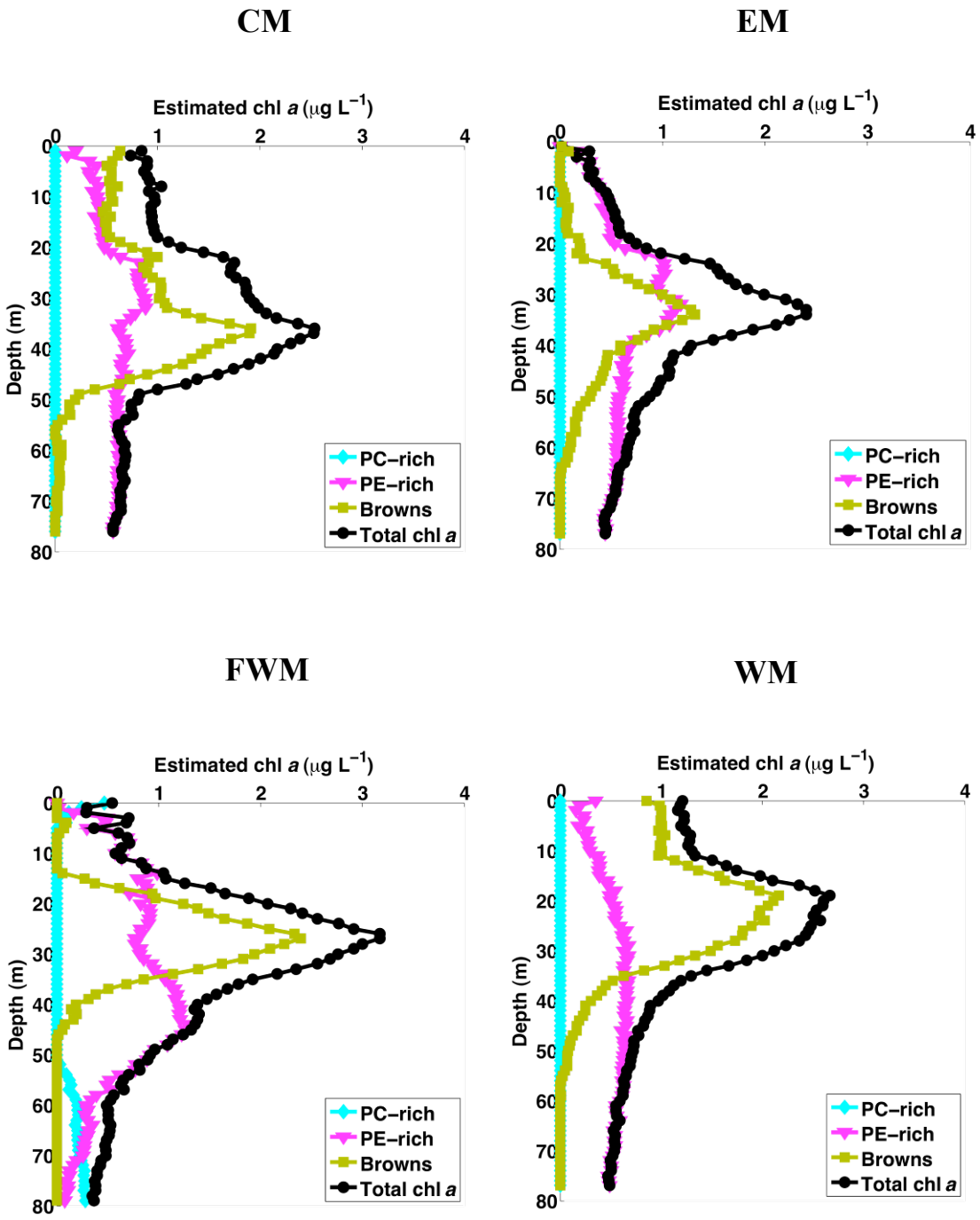

Figure 15: Changes in three chl *a*-normalized pigment absorption spectra (a^*_{PSII}) relative to maximum value of each spectrum at 440 nm for samples taken at EM between 30-35 m during the summer of 2010. The topmost panel is from early June, the middle panel is from late July, and the bottom panel is from late August. The grey boxes from 470-510 nm and 525-560 nm denote approximate absorption bands due to carotenoids and phycoerythrin (PE) respectively. The ratio of a^*_{PSII} to *a*chl*a* values numerically integrated across the wavelengths of the two absorption bands are given at the top of each box.

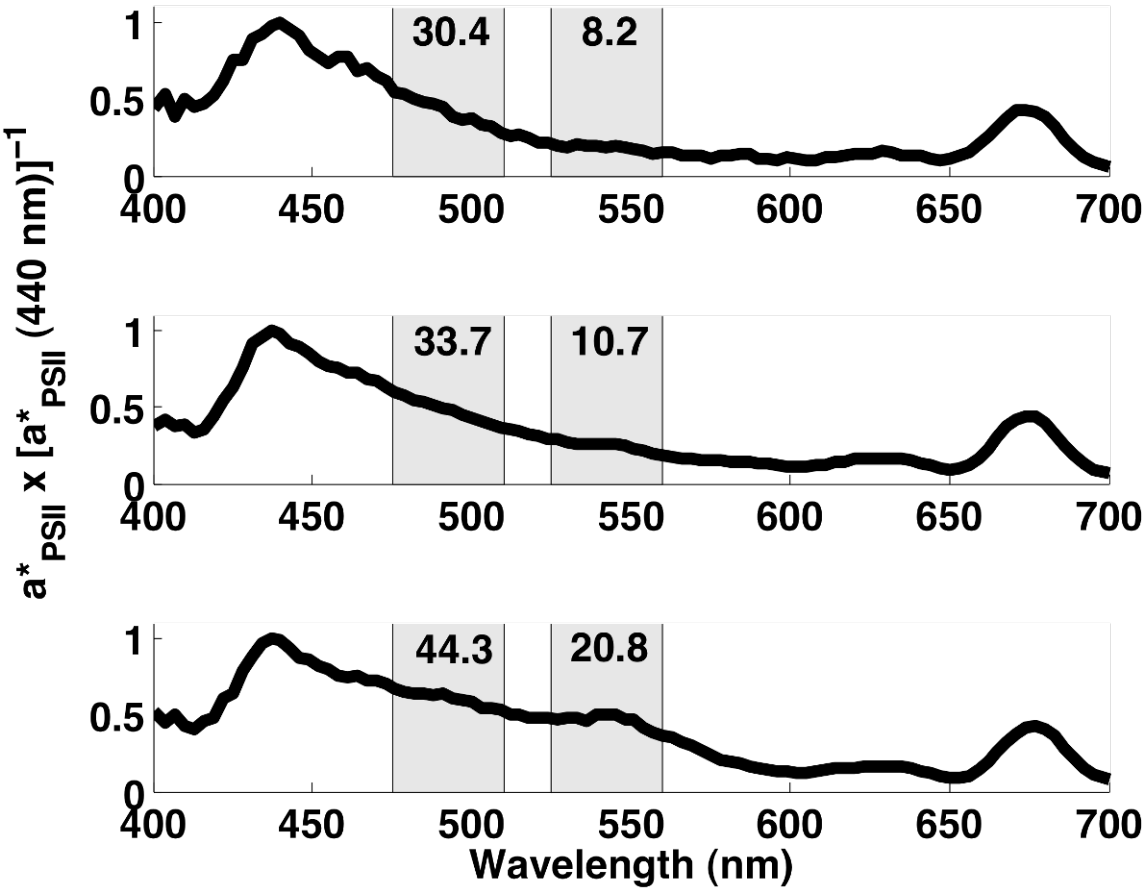

Figure 16: Depth changes in three chl *a*-normalized pigment absorption spectra (a^*_{PSII}) relative to the maximum value of each spectrum at 440 nm for samples taken at FWM in early August 2010. The topmost panel is from 10 m, the middle panel is from 20 m, and the bottom panel is from 30 m. The grey boxes from 470-510 nm and 525-560 nm denote approximate absorption bands due to carotenoids and phycoerythrin (PE) respectively. The ratio of a^*_{PSII} to *a*chl*a* values numerically integrated across the wavelengths of the two absorption bands are given at the top of each box

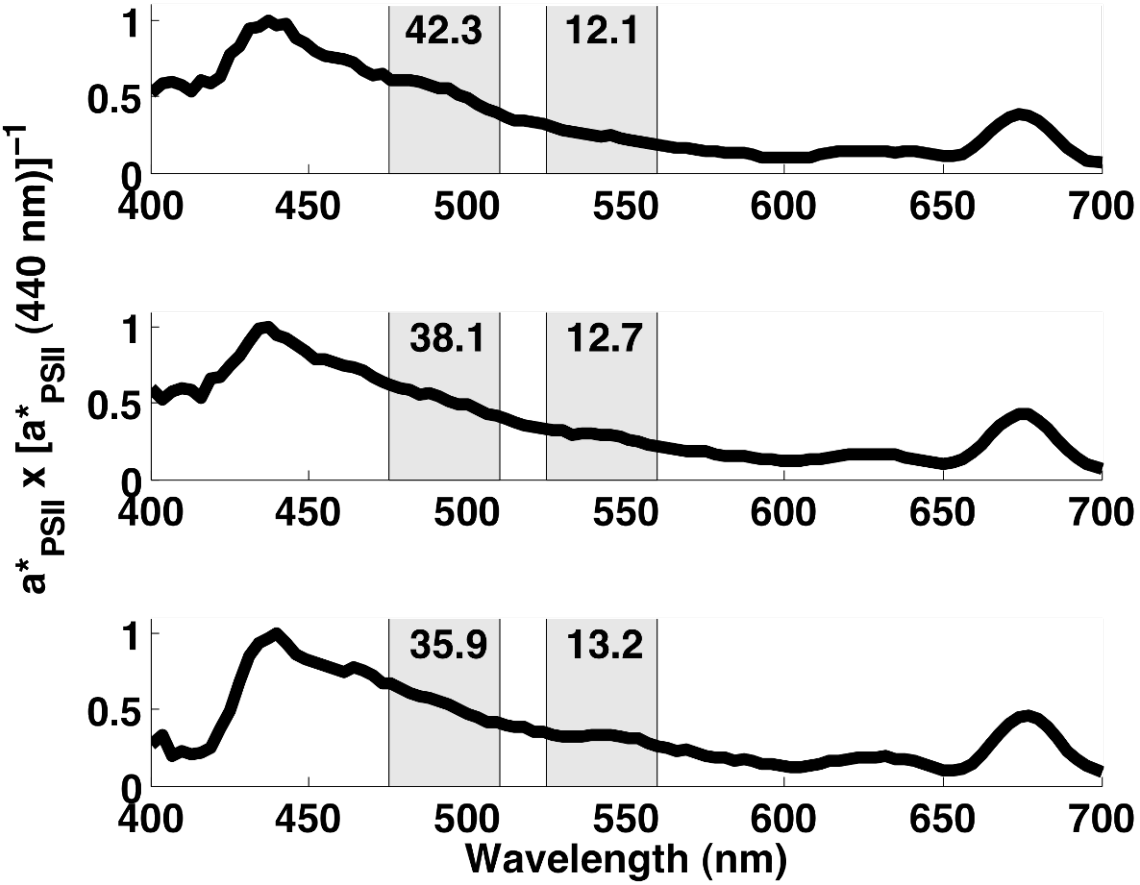

Figure 17: Ratio of photoprotectant carotenoids to photosynthetic carotenoids (PPC:PSC) for each PAS sample depth (n = 68). PPC:PSC ratios were calculated as described in the text.

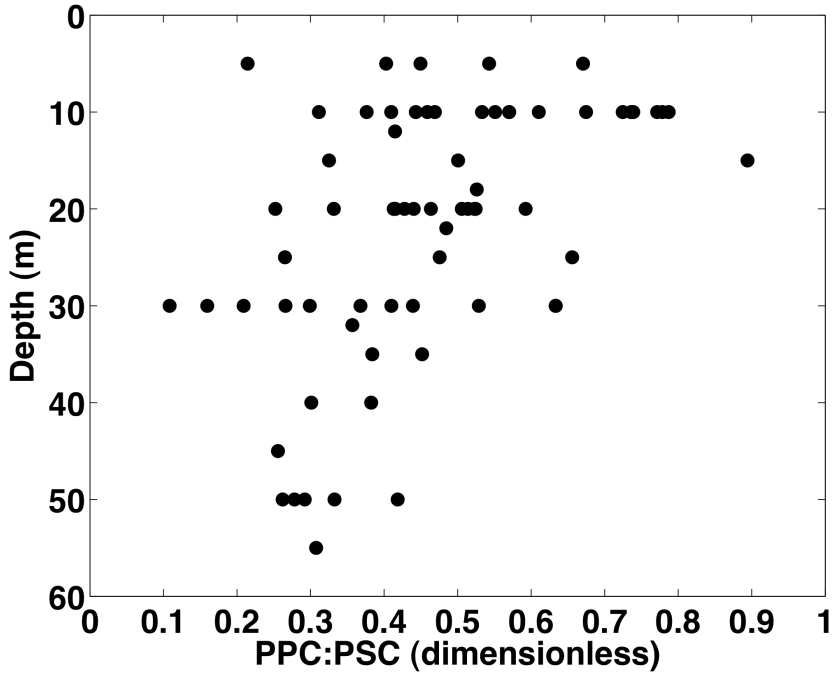

Figure 18: Spectral correction factors (SCFs) for FRRF σ_{PSII} measurements at each PAS sample depth where a FRRF profile was also taken (n = 61). SCFs were calculated as described in the text.

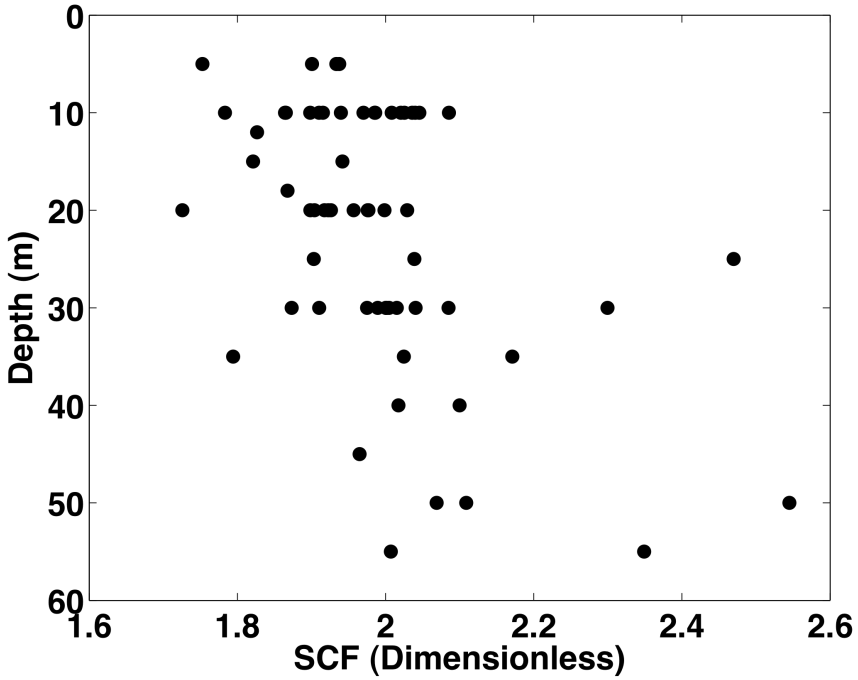

Figure 19: Profiles of the maximum quantum efficiency of PS II (F_v/F_m) normalized to 0.65 from west to east across the lake (clockwise from upper left: FWM, WM, CM, EM) through the summer of 2010. Note the different August sampling date for FWM compared to the other three stations. All profiles were collected using the dark chamber of the FRRF and corrected for pheophytin *a* fluorescence following the method of Fuchs et al (2002).

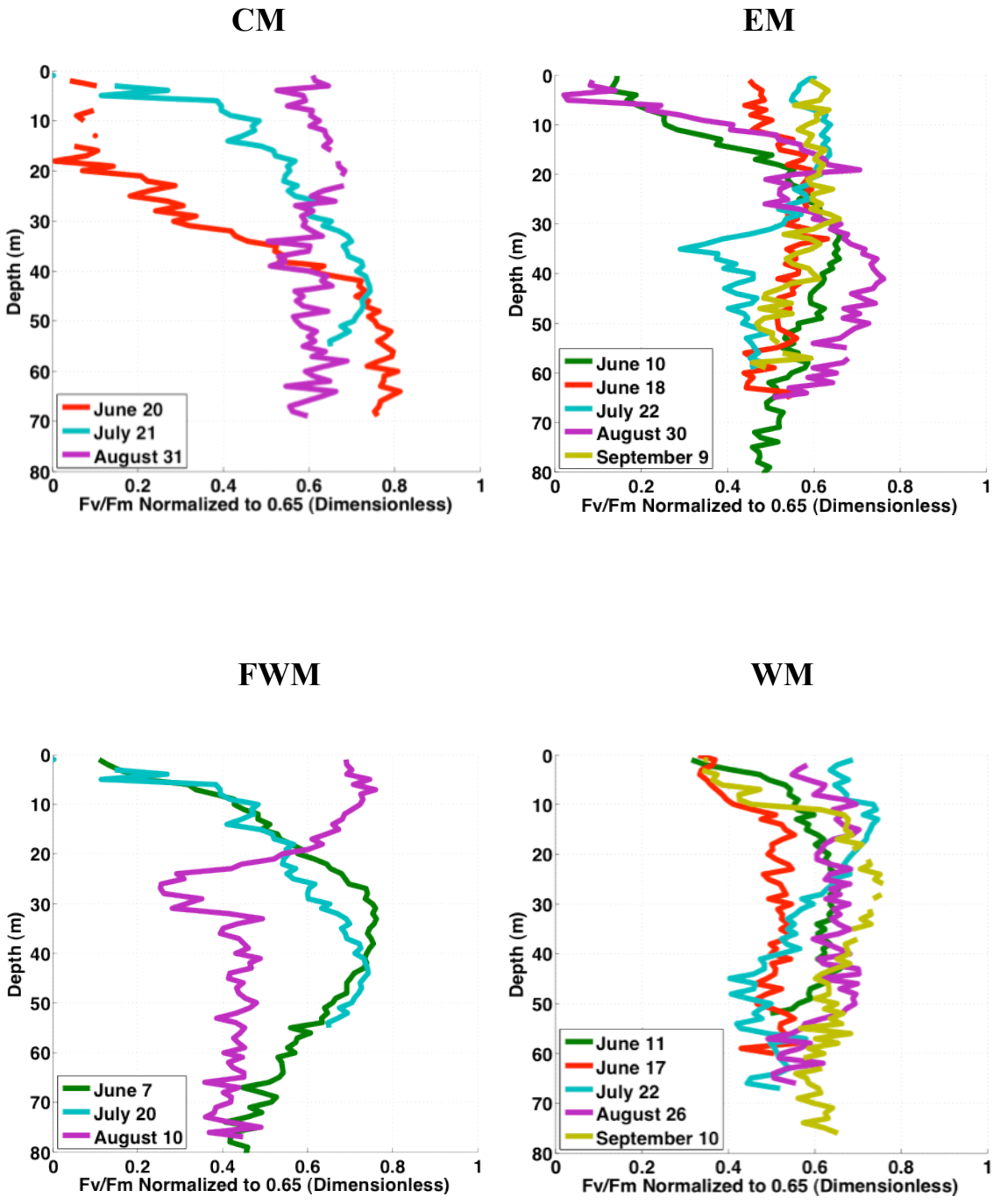

Figure 20: Profiles of the effective absorption cross section of PSII (σ_{PSII}) from west to east across the lake (clockwise from upper left: FWM, WM, CM, EM) through the summer of 2010. Note the different August sampling date for FWM compared to the other three stations. All profiles were collected using the dark chamber of the FRRF and spectrally corrected using the mean SCF values from PAS samples at 10 m, 20 m, and 30 m and linearly extrapolating those values through the water column.

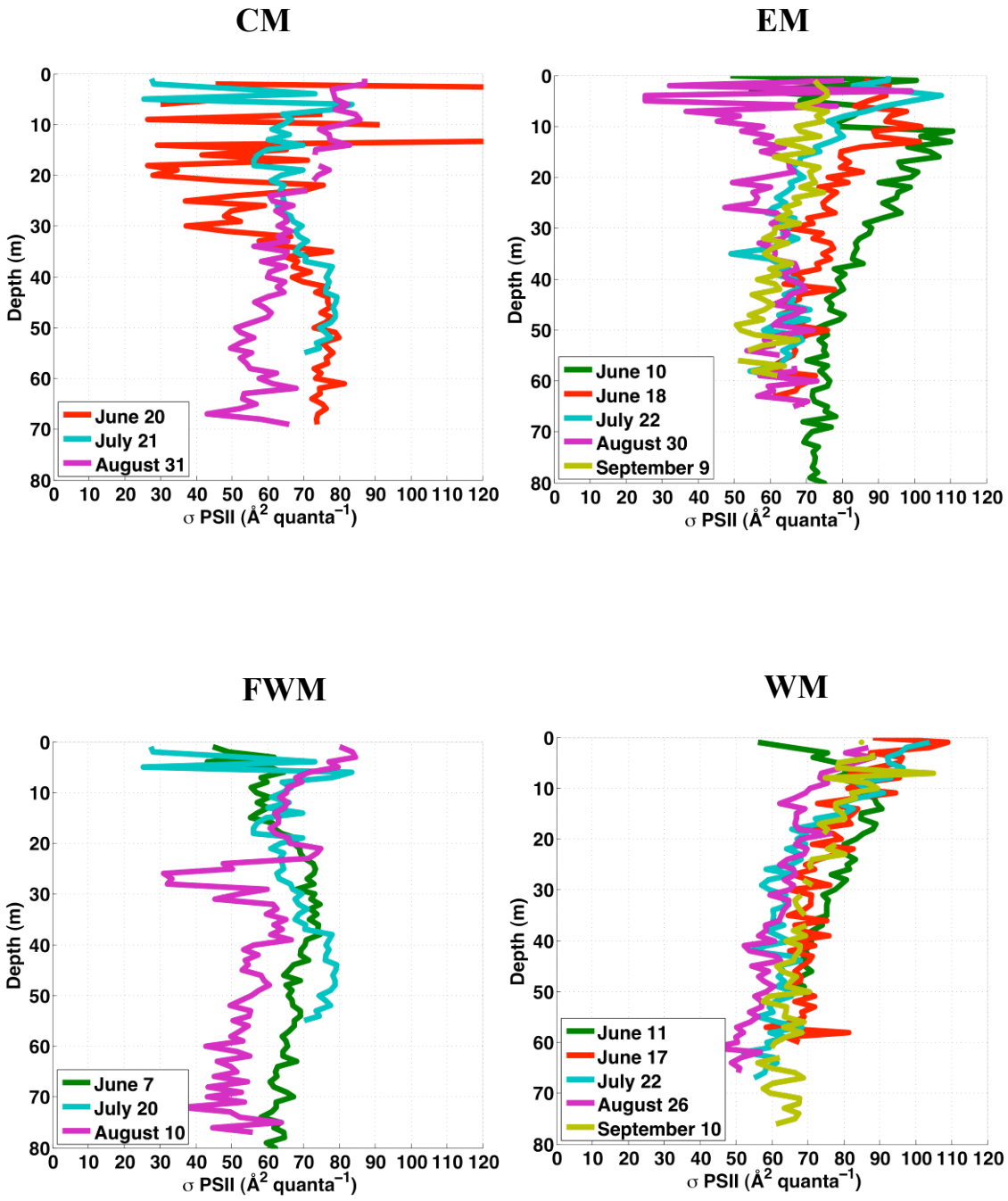

Figure 21: Linear regression between log10-transformed five-wavelength average *a*PS x 0.5 values and log 10-transformed mean FluoroProbe fluorescence for each PAS sample from Lake Superior (black points) and Lake Erie (gray points). The two points in the dashed oval at the upper right hand corner of the graph were surface samples taken from Sandusky Bay on Lake Erie during a cyanobacterial bloom and were not representative of open lake sampling conditions in Lake Superior. The three points in the dashed oval at the lower left hand corner of the graph and had mean fluorescence less than 1, considered to be too low to represent a phytoplankton pigment fluorescence signal above background instrument noise. The five circled points are included here for comparison only; they were not used in determining the linear regression.

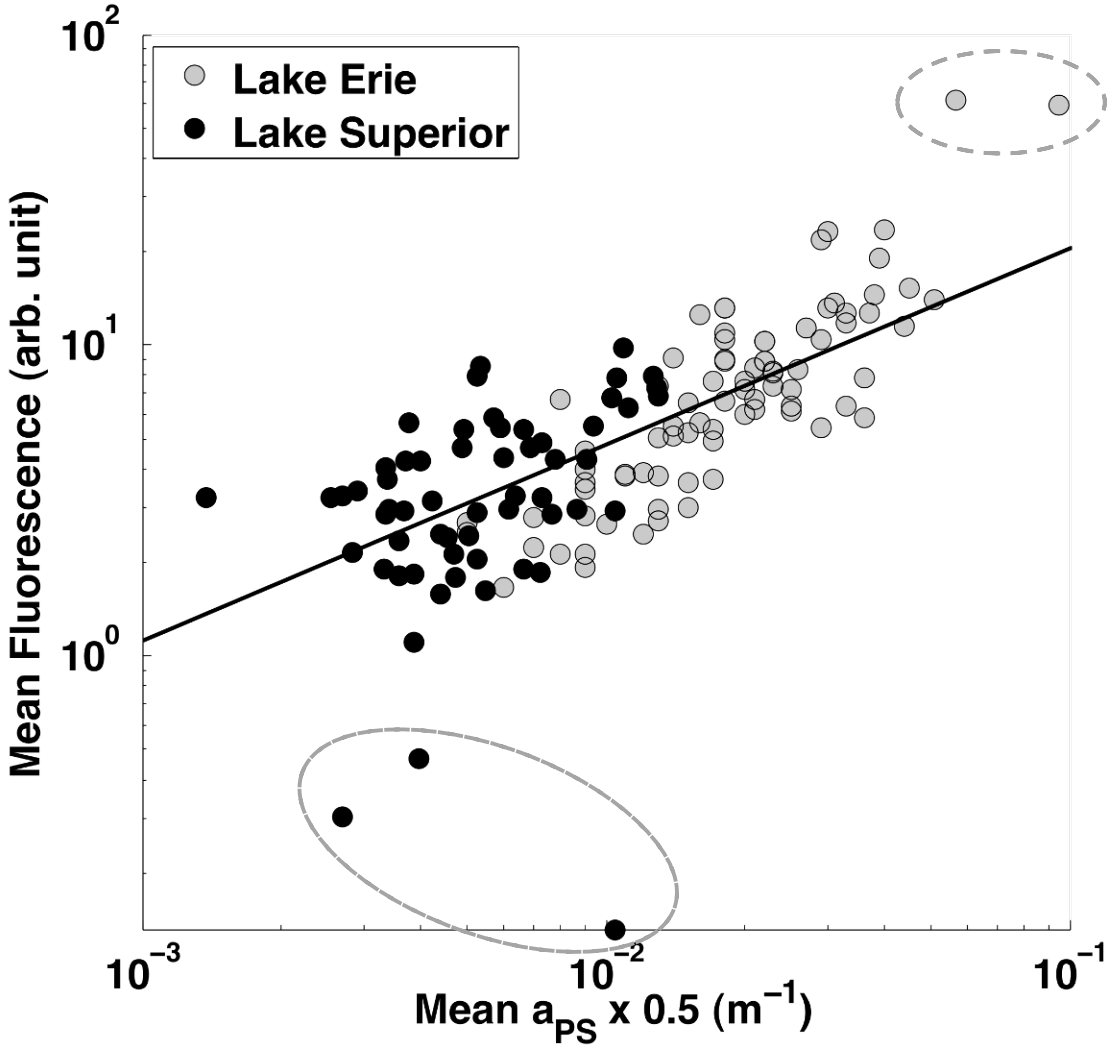

Figure 22: Comparison of chl *a*-normalized a_{PSII} values (a^*_{PSII}) calculated for PAS samples (n=56) using three different methods. From left to right: a_{PSII} method 1; a_{PSII} method 2; *a*PSII method 3 with the measured *a*PS value substituted for the calculated *a*PSII value for samples with $P > 1$ (n=15).

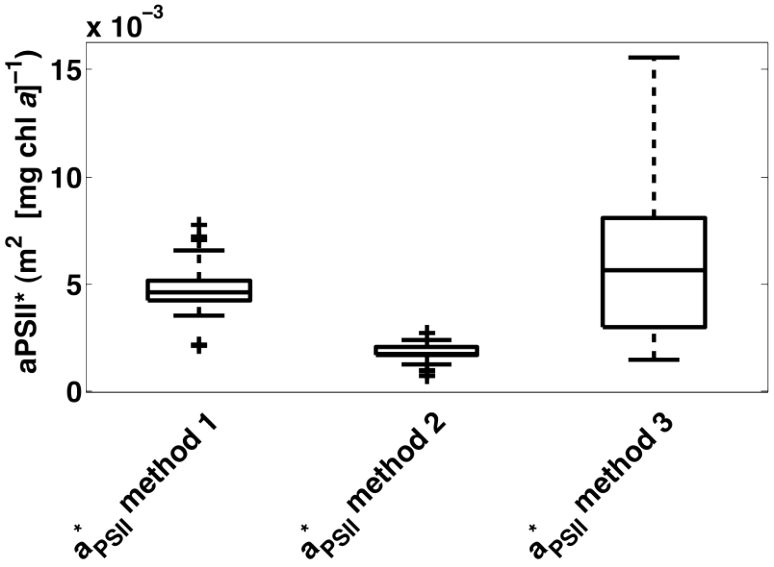

Figure 23: Comparison of the ratio of *a*PSII to *a*PS (*P*) for PAS samples (n=56) using two different *a*PSII calculation methods. The left bar represents *P* using *a*PSII method 2; The right bar represents *P* values calculated using *a*PSII method 3 with *P* set to one for any samples (n=15) where *a*PSII exceeded aPS ($P > 1$). *a*PSII method 1 assumes a constant *P* value of 0.5 and is not shown.

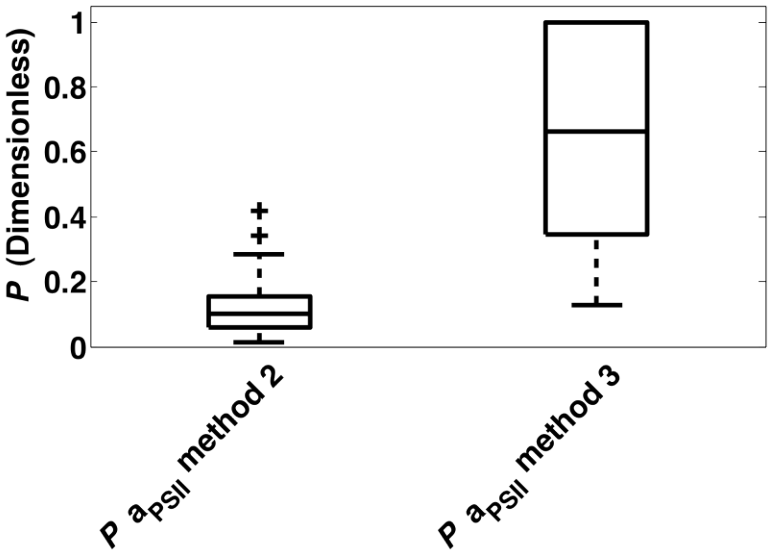

Figure 24: Calculated O_2 production rates for PAS samples using three different *a*PSII estimation techniques. The PAR profile used to calculate the O_2 production rates in each panel was derived from surface PAR measured on the summer solstice (1275 μmol quanta x $[m^2 \times s]^{-1}$) and the 2010 average light extinction coefficient measured with the FRRF ($k_d = 0.1511\ m^{-1}$). (A) O_2 production rates calculated using *a*PSII method 1. (B) O_2 production rates calculated using *a*PSII method 2. Note the different O_2 production scale for this plot. (C) O_2 production rates calculated using *a*PSII method 3 with *P* capped at one.

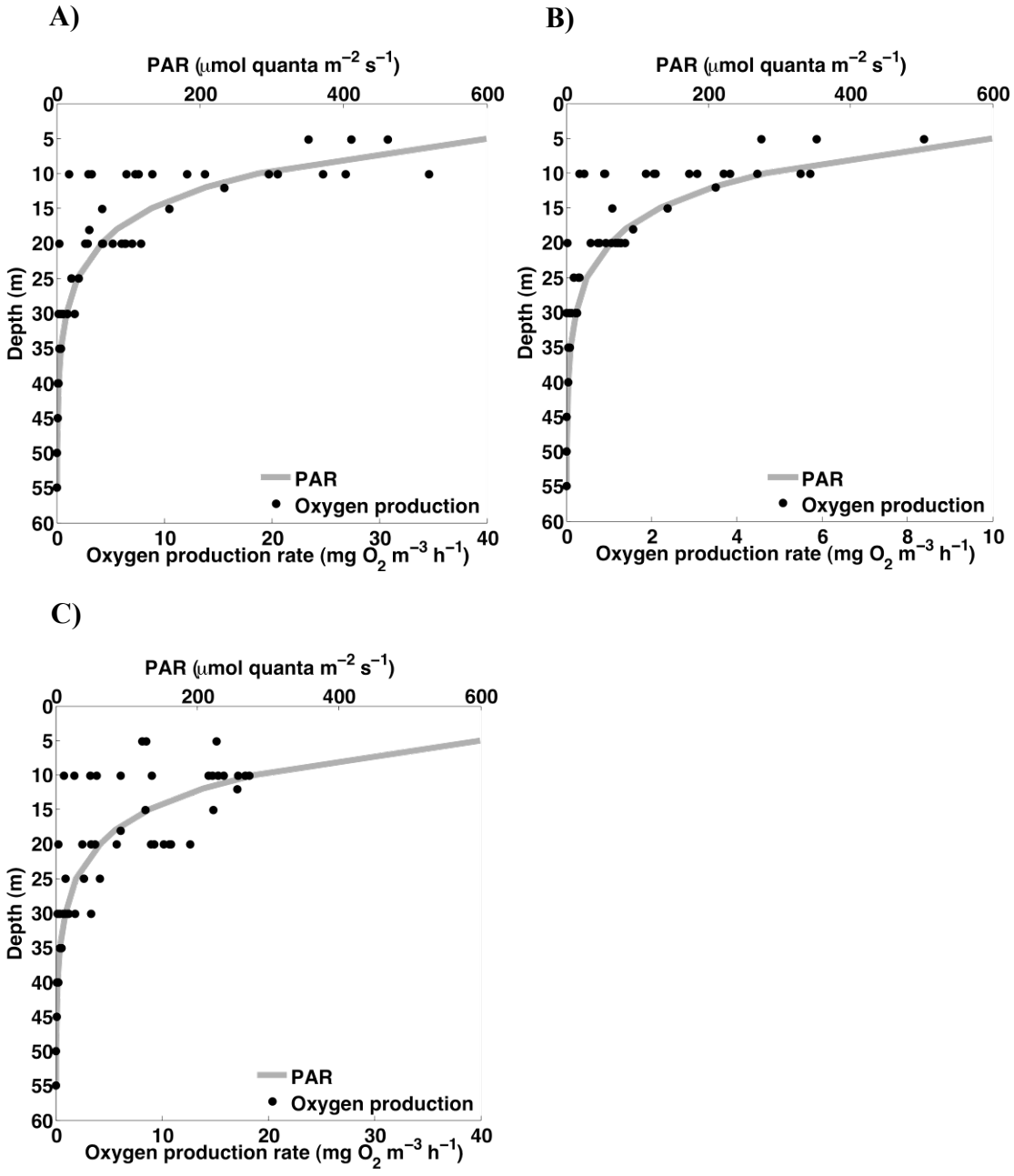

Figure 25: O_2 production rates from 10 to 40 m through one day using values of *a*PSII calculated with *a*PSII method 2 (top) and *a*PSII method 3 (bottom) for 11 August 2010 (left) and 12 August 2010 (right). PAR is standardized for all estimates following the method described in the text. Values from sunrise until 11:00 h (approximately 10:00 h solar time) are derived from mid morning FluoroProbe and FRRF profiles. Values from 11:00 h until sunset are derived from mid afternoon FluoroProbe and FRRF profiles. There is no interpolation between the estimates across their intersection. Colored contours denote times and depths of equal O_2 production rates (mg O_2 x [m^3 x h]$^{-1}$). Note the different O_2 production scales for the two *a*PSII estimation methods.

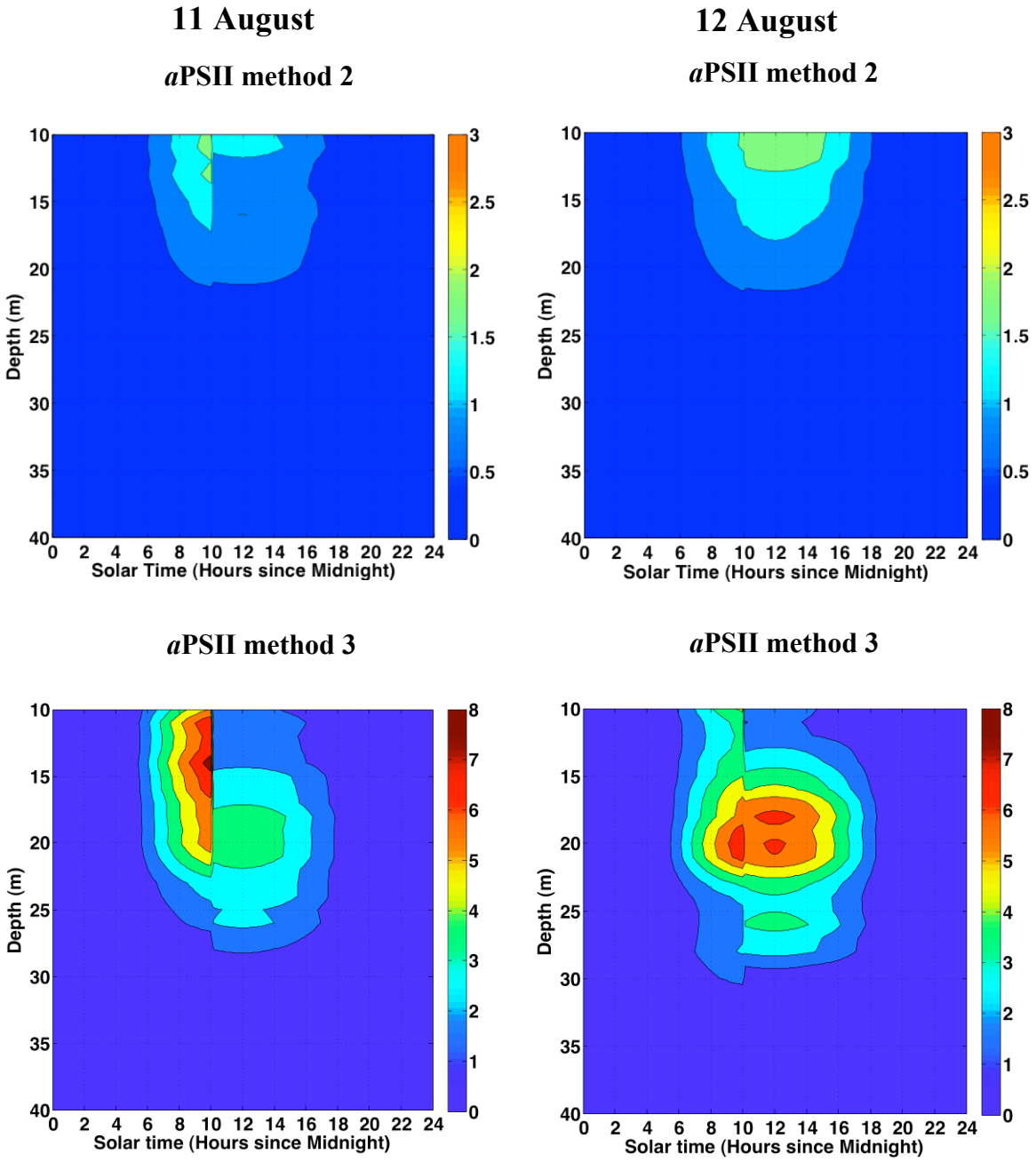

Figure 26: Potential O_2 production rates from 10 to 40 m through one day using FluoroProbe-derived *a*PSII method 3 values and FRRF-derived F_q'/F_m' values collected at four different times of day on 11 August 2010. PAR is standardized for all estimates following the method described in the text. Colored contours denote times and depths of equal O_2 production rates (mg O_2 x [m^3 x h]$^{-1}$).

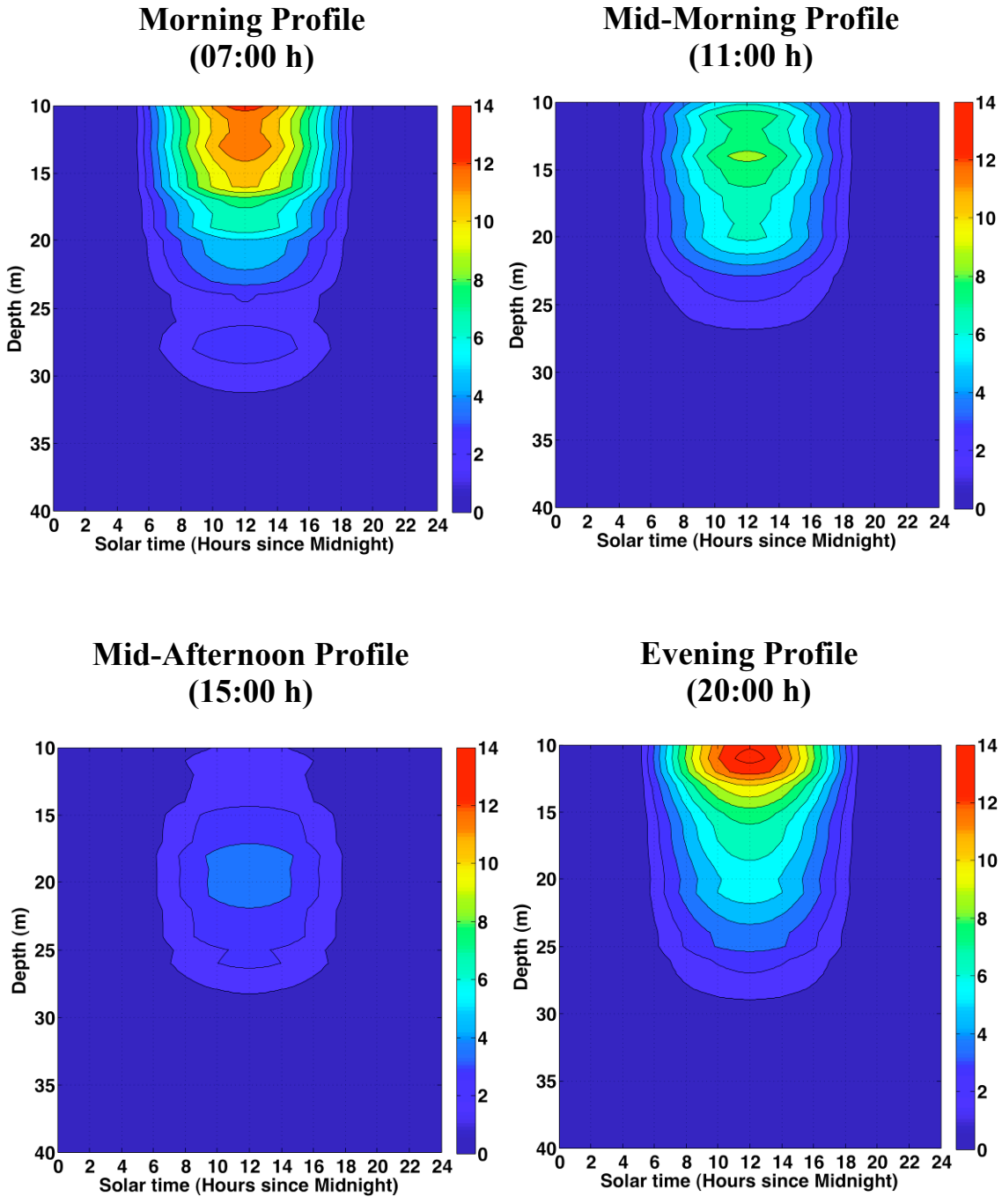

Figure 27: Potential O_2 production rates from 10 to 40 m through one day using FluoroProbe-derived *a*PSII method 3 values and FRRF-derived F_q'/F_m' values collected at four different times of day on 12 August 2010. PAR is standardized for all estimates following the method described in the text. Colored contours denote times and depths of equal O_2 production rates (mg O_2 x [m^3 x h]$^{-1}$).

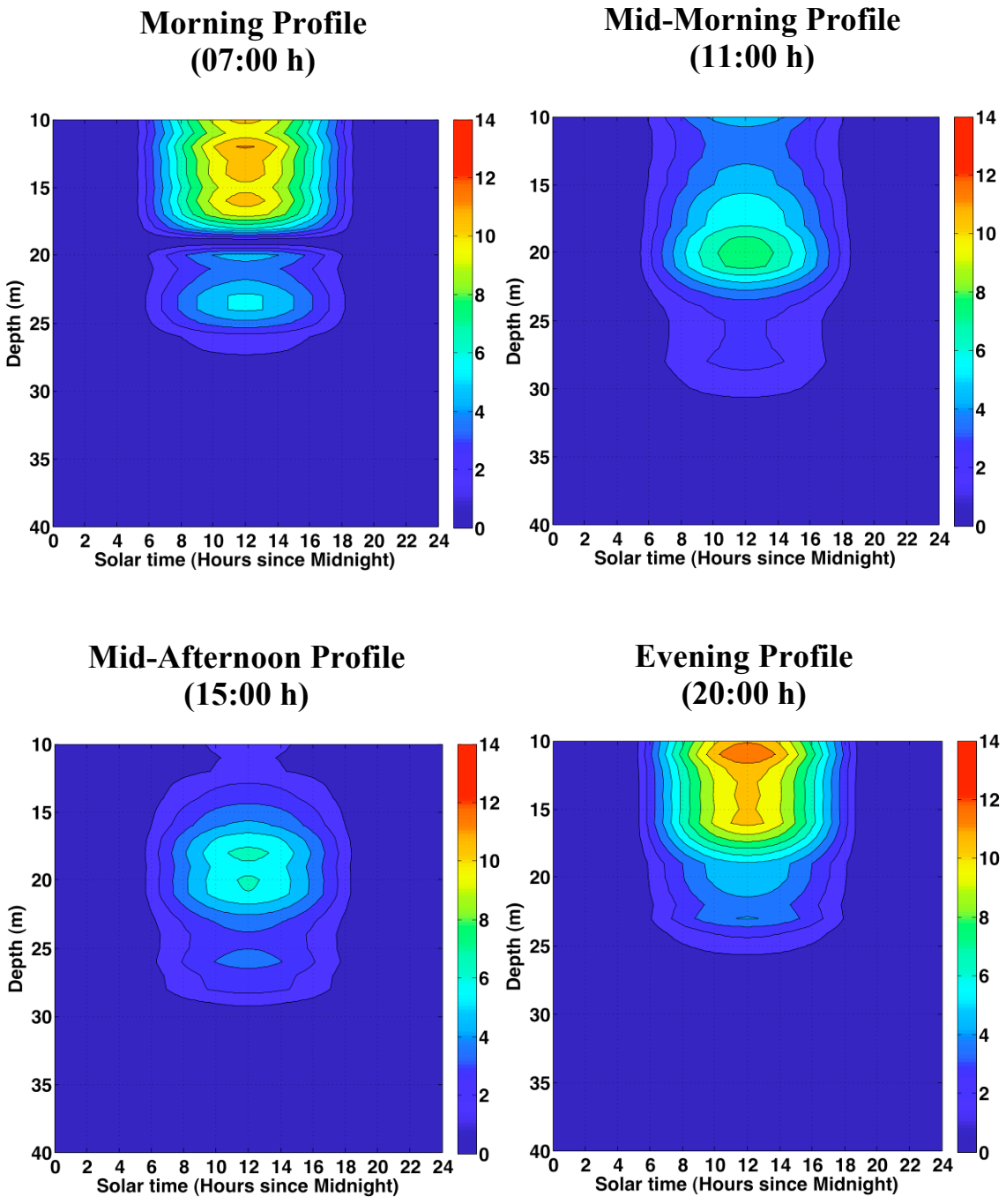

Figure 28: Spatial and seasonal variability in potential O_2 production rates from 10 to 40 m through one day using FluroProbe-derived *a*PSII values and FRRF-derived F_q'/F_m' values measured during mid afternoon. The daily PAR values used for O_2 production estimates from each sampling cruise were calculated using measured surface PAR and the mean FRRF-derived k_d value for each cruise. Colored contours denote times and depths of equal O_2 production rates (mg O_2 x [m^3 x h]$^{-1}$). Note the changes in scales and contour intervals between O_2 production estimates. This figure is continued on the following page.

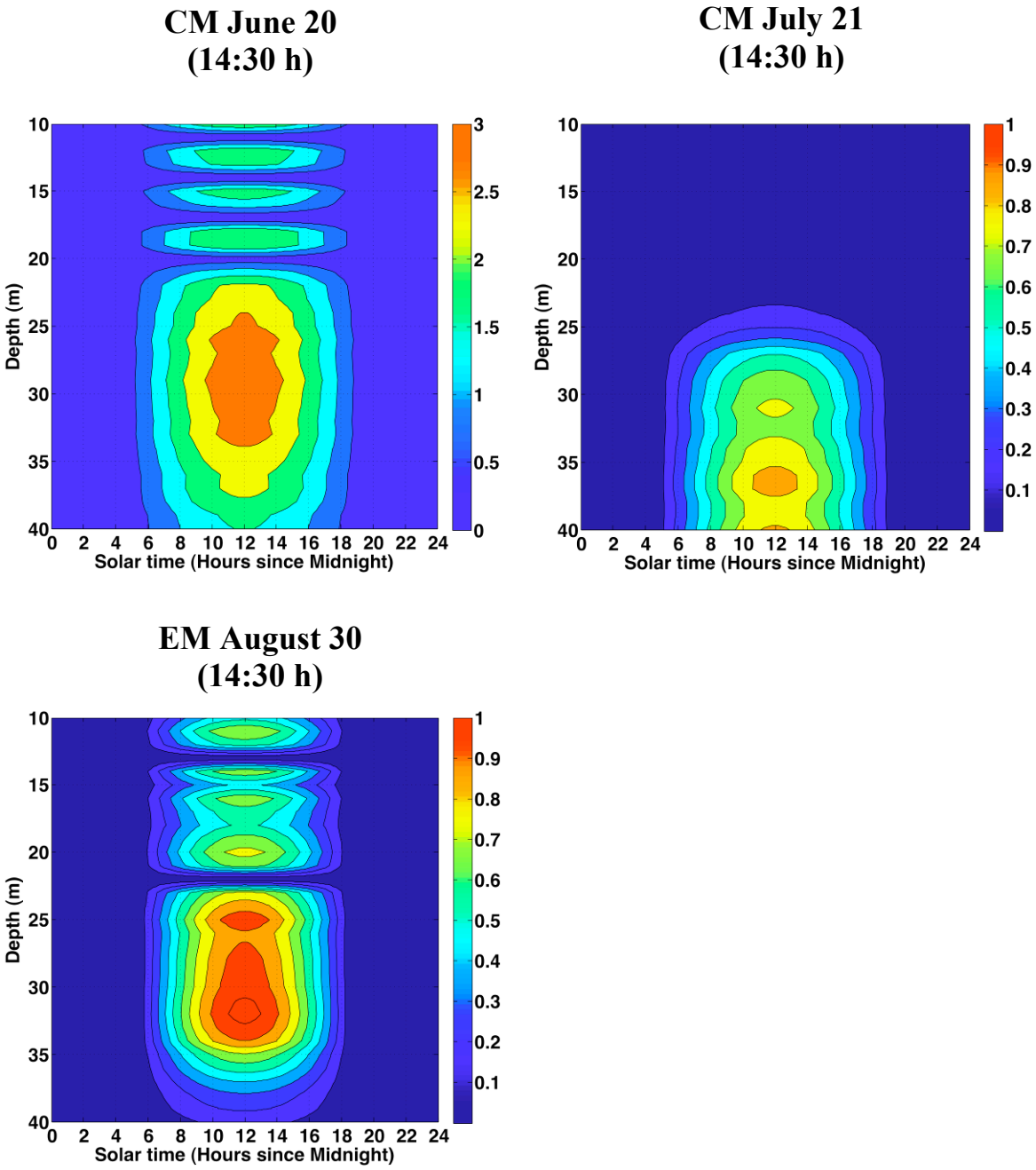

Figure 28 continued: Spatial and seasonal variability in potential O_2 production rates from 10 to 40 m through one day using FluroProbe-derived *a*PSII values and FRRF-derived F_q'/F_m' values measured during mid afternoon. The daily PAR values used for O_2 production estimates from each sampling cruise were calculated using measured surface PAR and the mean FRRF-derived k_d value for each cruise. Colored contours denote times and depths of equal O_2 production rates (mg O_2 x [m^3 x h]$^{-1}$).

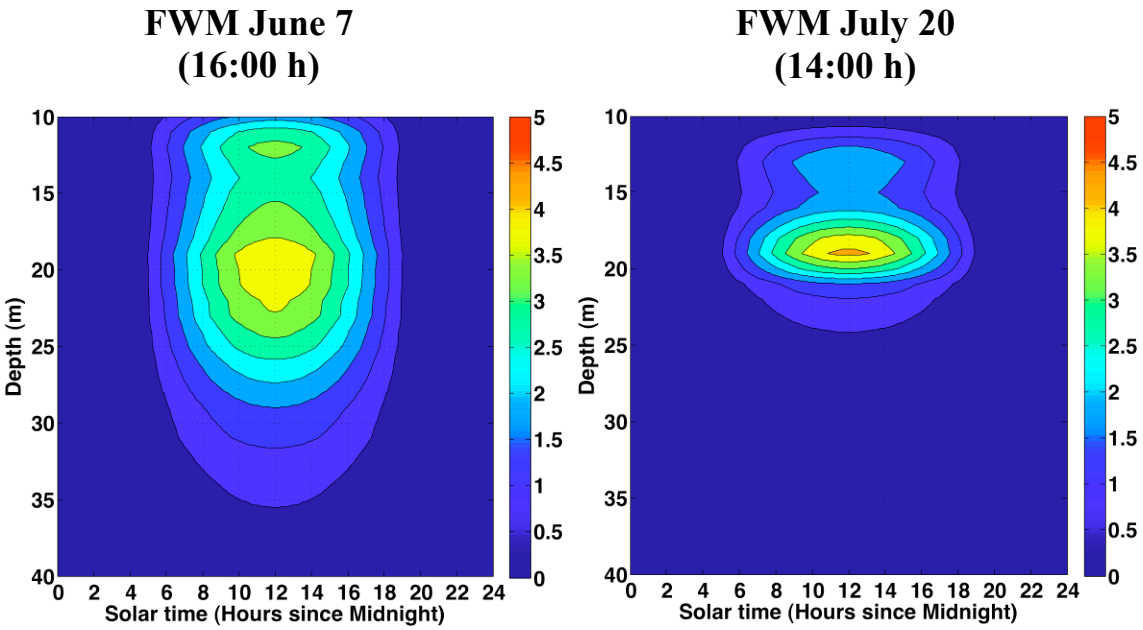

Table 1: Mean and standard deviation of extracted chl *a* concentrations from autotrophic picoplankton expressed as a percentage of total extracted chl *a* for depth bands above the DCM (n=13), within the DCM (n=13), and below the DCM (n=10) as identified using CTD chl *a* fluorescence profiles. Depth bands that have significantly different ($P < 0.05$) picoplankton abundances relative to total chl *a* are denoted with an asterisk.

Depth band	Mean	Standard deviation
Above DCM *	35.3	10.1
Within DCM	41.3	12.5
Below DCM *	43.1	4.5

Table 2: Comparison of whole-day O_2 production and C assimilation rates from 10-40 m at FWM calculated for two consecutive days using O_2 method 1 with *a*PSII method 2 and *a*PSII method 3. The estimates were derived using mid-morning FRRF and FluoroProbe profiles from sunrise until 11:00 h, and mid-afternoon FRRF and FluoroProbe profiles from 11:00 h until sunset. PAR through the water column was calculated as described in the text. Conversion between O_2 production and C assimilation was made using a PQ value of 1.29 (Depew et al 2006).

	August 11, 2010		**August 12, 2010**	
*a*PSII estimation method	***a*PSII method 2**	***a*PSII method 3**	***a*PSII method 2**	***a*PSII method 3**
O_2 production (mg O_2 x $[m^2$ x $d]^{-1}$)	121	556	151	670
C assimilation (mg C x $[m^2$ x $d]^{-1}$)	35	162	44	195

Table 3: Comparison of whole-day O_2 production and C assimilation rates from 10-40 m calculated using *a*PSII method 3 and O_2 method 2 for profiles that were taken at four different times each day for two consecutive days. Conversion between O_2 production and C assimilation was made using a PQ value of 1.29 (Depew et al 2006).

	August 11, 2010				**August 12, 2010**			
	Morning	**Mid-Morning**	**Mid-Afternoon**	**Evening**	**Morning**	**Mid-morning**	**Mid-afternoon**	**Evening**
O_2 production (mg O_2 x $[m^2$ x $d]^{-1}$)	1144	857	431	1078	1007	773	628	997
C assimilation (mg C x $[m^2$ x $d]^{-1}$)	333	249	125	313	293	225	183	290

Table 4: Whole-day O_2 production and C assimilation rates from 10-40 m calculated using three time intervals from morning until evening using O_2 method 3 and *a*PSII method 3. For each time interval the F_q'/F_m' and *a*PSII profiles used were the mean values of the two profiles taken at the endpoints of that time interval. Conversion between O_2 production and C assimilation was made using a PQ value of 1.29 (Depew et al 2006).

	August 11, 2010	**August 12, 2010**
O_2 production (mg O_2 x $[m^2$ x $d]^{-1}$)	741	793
C assimilation (mg C x $[m^2$ x $d]^{-1}$)	215	231

Table 5: ^{14}C incubation estimates of daily C assimilation rates from 10-40 m in Lake Superior for three consecutive years calculated from results in Table 3 of Sterner (2010).

	August 7, 2006	**July 31, 2007**	**July 31, 2008**
	EM	**WM**	**WM**
C assimilation (mg C x $[m^2$ x $d]^{-1}$)	219	227	181

Table 4: Whole-day O_2 production and C assimilation rates from 10-40 m calculated using three time intervals from morning until evening using O_2 method 3 and *a*PSII method 3. For each time interval the F_q'/F_m' and *a*PSII profiles used were the mean values of the two profiles taken at the endpoints of that time interval. Conversion between O_2 production and C assimilation was made using a PQ value of 1.29 (Depew et al 2006).

	August 11, 2010	**August 12, 2010**
O_2 production (mg O_2 x $[m^2$ x $d]^{-1}$)	741	793
C assimilation (mg C x $[m^2$ x $d]^{-1}$)	215	231

Table 5: ^{14}C incubation estimates of daily C assimilation rates from 10-40 m in Lake Superior for three consecutive years calculated from results in Table 3 of Sterner (2010).

	August 7, 2006	**July 31, 2007**	**July 31, 2008**
	EM	**WM**	**WM**
C assimilation (mg C x $[m^2$ x $d]^{-1}$)	219	227	181

Table 6: Spatial and seasonal variability in calculated daily O_2 production and C assimilation from 10-40 m derived from single profiles all taken during mid afternoon and using *a*PSII method 3. Conversion between O_2 production and C assimilation made using PQ value 1.29 (Depew et al 2006).

Profile date	**7 June**	**20 June**	**20 July**	**21 July**	**30 August**
Station	**FWM**	**CM**	**FWM**	**CM**	**EM**
Profile time	16:00 h	14:30 h	14:00 h	14:30 h	14:30 h
O_2 production (mg O_2 x [m^2 x d]$^{-1}$)	615	555	260	103	165
C assimilation (mg C x [m^2 x d]$^{-1}$)	179	161	76	30	48

Cited Literature

Austin, J. & Coleman, S. 2008. A century of temperature variability in Lake Superior. *Limnology and Oceanography* **53**:2724-30.

Barbiero, R. P. & Tuchman, M. L. 2001a. Results from the US EPA's biological open water surveillance program of the Laurentian Great Lakes: I. Introduction and phytoplankton results. *J. Gt. Lakes Res.* **27**:134-54.

Barbiero, R. P. & Tuchman, M. L. 2001b. Results from the US EPA's biological open water surveillance program of the Laurentian Great Lakes: II. Deep chlorophyll maxima. *J. Gt. Lakes Res.* **27**:155-66.

Barbiero, R. P. & Tuchman, M. L. 2004. The deep chlorophyll maximum in Lake Superior. *J. Gt. Lakes Res.* **30**:256-68.

Behrenfeld, M. J., Prasil, O., Babin, M. & Bruyant, F. 2004. In search of a physiological basis for covariations in light limited and light saturated photosynthesis. *Journal of Phycology* **40**:4-25.

Bennett, E. B. 1978. Characteristics of the thermal regime of Lake Superior. *J. Gt. Lakes Res.* **4**:310-19.

Benson, B. B. & Krause, J., D. 1980. The concentration and isotopic fractionation of gases dissolved in freshwater in equilibrium with the atmosphere. 1. Oxygen. *Limnology and Oceanography* **25**:662-71.

Berges, J. A., Charlebois, D. O., Mauzerall, D. C. & Falkowski, P. G. 1996. Differential effects of nitrogen limitation on photosynthetic efficiency of photosystems I and II in microalgae. *Plant Physiology* **110**:689-96.

Beutler, M., Wiltshire, K. H., Meyer, B., Moldaenke, C., Luring, C., Meyerhofer, M., Hansen, U. P. & Dau, H. 2002. A fluorometric method for the differentiation of algal populations in vivo and in situ. *Photosynthesis Research* **72**:39-53.

Binding, C. E., Jerome, J. H., Bukata, R. P. & Booty, W. G. 2008. Spectral absorption properties of dissolved and particulate matter in Lake Erie. *Remote Sens. Environ.* **112**:1702-11.

Bowers, J. A. 1988. Diel vertical migration of the Opossum Shrimp Mysis relicta in Lake Superior: Observations and sampling from the Johnson-Sea-Link II submersible. *Bulletin of Marine Science* **43**:730-38.

Callieri, C. 2007. Picophytoplankton in freshwater ecosystems: the importance of small-sized phototrophs. *Freshwater Reviews* **1**:1-28.

Campbell, D., Hurry, V., Clarke, A. K., Gustafsson, P. & Oquist, G. 1998. Chlorophyll fluorescence analysis of cyanobacterial photosynthesis and acclimation. *Microbiology and Molecular Biology Reviews* **62**:667-83.

Conway, J. B. 1977. Seasonal and depth distribution of Limnocalanus macrurus at a site on Western Lake Superior. *J. Gt. Lakes Res.* **3**:15-19.

Corno, G., Letelier, R. M., Abbott, M. R. & Karl, D. M. 2006. Assessing primary production variability in the North Pacific Subtropical Gyre: A comparison of Fast Repetition Rate Fluorometry and ^{14}C Measurements. *Journal of Phycology* **42**:51-60.

Cotner, J. B., Biddanda, B. A., Makino, W. & Stets, E. 2004. Organic carbon biogeochemistry of Lake Superior. *Aquatic Ecosystem Health & Management* **7**:451-64.

Cullen, J. J. 1982. The deep chlorophyll maximum: Comparing vertical profiles of chlorophyll *a*. *Canadian Journal of Fisheries and Aquatic Sciences* **39**:791-803.

Culver, M. E. & Perry, M. J. 1999. The response of photosynthetic absorption coefficients to irradiance in culture and in tidally mixed estuarine waters. *Limnology and Oceanography* **44**:24-36.

Depew, D. C., Smith, R. E. H. & Guildford, S. J. 2006. Production and respiration in Lake Erie plankton communities. *J. Gt. Lakes Res.* **32**:817-31.

Derenbach, J. B., Astheimer, H., Hansen, H. P. & Leach, H. 1979. Vertical microscale distribution of phytoplankton in relation to the thermocline. *Marine Ecology-Progress Series* **1**:187-93.

Eisner, L. B., Twardowski, M., S., Cowles, T., J. & Perry, M. J. 2003. Resolving phytoplankton photoprotective:photosynthetic carotenoid ratios on fine scales using in situ spectral absorption measurements. *Limnology and Oceanography* **48**:632-46.

Fahnenstiel, G. L. & Glime, J. M. 1983. Subsurface chlorophyll maximum and associated *Cyclotella* pulse in Lake Superior. *Internationale Revue der gesamten Hydrobiologie und Hydrographie* **68**:605-16.

Fahnenstiel, G. L., Sicko-Goad, L., Scavia, D. & Stoermer, E. F. 1986. Importance of picoplankton in Lake Superior. *Canadian Journal of Fisheries and Aquatic Sciences* **43**.

Falkowski, P. G. & Kolber, Z. 1995. Variations in chlorophyll fluorescence yields in phytoplankton in the world oceans. *Aust. J. Plant Physiol.* **22**:341-55.

Falkowski, P. G. & Raven, J. A. 2007. *Aquatic Photosynthesis.* Princeton University Press, Princeton, NJ,

Fee, E. J. 1976. The vertical and seasonal distribution of chlorophyll in lakes of the Experimental Lakes Area, northwestern Ontario: Implications for primary production estimates. *Limnology and Oceanography* **21**:767-83.

Fuchs, E., Zimmerman, R. C. & Jaffe, J. S. 2002. The effect of elevated levels of phaeophytin in natural water on variable fluorescence measured from phytoplankton. *J. Plankton Res.* **24**:1221-29.

Genty, B., Briantais, J.-M. & Baker, N. R. 1989. The relationship between the quantum yield of photosynthetic electron transport and quenching of chlorophyll fluorescence. *Biochimica et Biophysica Acta (BBA)* **990**.

Guildford, S. J., Bootsma, H. A., Fee, E. J., Hecky, R. E. & Patterson, G. 2000. Phytoplankton nutrient status and mean water column irradiance in Lakes Malawi and Superior. *Aquatic Ecosystem Health and Management* **3**:35-45.

Guildford, S. J. & Hecky, R. E. 2000. Total nitrogen, total phosphorus, and nutrient limitation in lakes and oceans: Is there a common relationship? *Limnology and Oceanography* **45**:1213-23.

Healey, P. F. 1985. Interacting effects of light and nutrient limitation on the growth rate of *Synechococcus linearis* (Cyanophyceae). *Journal of Phycology* **21**:134-46.

Ivanikova, N. V., Matteson, A. R., Gobler, C. J., Popels, L. C., McKay, M. L., Wilhelm, S. W. & Bullerjahn, G. S. 2008. Picoplanktonic cyanobacteria in Lakes Superior and Erie: phylogenies of endemic populations and cultured isolates. *Verhandlungen des Internationalen Verein Limnologie* **30**:459-65.

Ivanikova, N. V., Popels, L. C., McKay, R. M. L. & Bullerjahn, G. S. 2007. Lake superior supports novel clusters of cyanobacterial picoplankton. *Applied and Environmental Microbiology* **73**:4055-65.

Jerome, J. H., Bukata, R. P. & Bruton, J. E. 1983. Spectral attenuation and irradiance in the laurentian great lakes. *J. Gt. Lakes Res.* **9**:60-68.

Kaiblinger, C. & Dokulil, M. 2006. Application of fast repetition rate fluorometry to phytoplankton photosynthetic parameters in freshwaters. *Photosynthesis Research* **88**:19-30.

Kiefer, D. A., Holm-Hansen, O., Goldman, C. R., Richards, R. & Berman, T. 1972. Phytoplankton in Lake Tahoe: Deep-living populations. *Limnology and Oceanography* **17**:418-22.

Kirk, J. T. O. 1994. *Light and Photosynthesis in Aquatic Ecosystems.* Cambridge University Press, Cambridge,

Kolber, Z. S. & Falkowski, P. G. 1992. Fast repetition rate (FRR) fluorometer for making in situ measurements of primary productivity. *Proceedings of Oceans '92 Conference.* Brookhaven National Lab., Upton, NY (United States), pp. 637-41.

Kolber, Z. S., Prasil, O. & Falkowski, P. G. 1998. Measurements of variable chlorophyll fluorescence using fast repetition rate techniques: defining methodology and experimental protocols. *Biochimica et Biophysica Acta (BBA) - Bioenergetics* **1367**:88-106.

Kromkamp, J. C., Dijkman, N. A., Peene, J., Simis, S. G. H. & Gons, H. J. 2008. Estimating phytoplankton primary production in Lake IJsselmeer (The Netherlands) using variable fluorescence (PAM-FRRF) and C-uptake techniques. *European Journal of Phycology* **43**:327-44.

Markager, S. & Vincent, W. F. 2001. Light absorption by phytoplankton: development of a matching parameter for algal photosynthesis under different spectral regimes. *J. Plankton Res.* **23**:1373-84.

Maxwell, K. & Johnson, G. N. 2000. Chlorophyll fluorescence - a practical guide. *Journal of Experimental Botany* **51**:659-68.

McManus, J., Heinen, E. A. & Baehr, M. M. 2003. Hypolimnetic oxidation rates in Lake Superior: Role of dissolved organic material on the lake's carbon budget. *Limnology and Oceanography* **48**:1624-32.

Mitchell, B. G., Kahru, M., Wieland, J. & Stramska, M. 2003. Determination of spectral absorption coefficients of particles, dissolved material and phytoplankton for discrete water samples. . *In*: Mueller, J. L., Fargion, G. S. & McClain, C. R. [Eds.] *Ocean optics protocols for satellite ocean colour sensor validation, Revision 4, Volume IV: Inherent optical properties: Instruments, characterizations, field measurements and data analysis protocols.* National Aeronautical and Space Administration: Goddard Space Flight Center, Greenbelt, Maryland.

Munawar, M. & Munawar, I. F. 1978. Phytoplankton of Lake Superior 1973. *J. Gt. Lakes Res.* **4**:415-42.

Pemberton, K. L., Clarke, K. R. & Joint, I. 2006. Quantifying uncertainties associated with the measurement of primary production. *Marine Ecology-Progress Series* **322**:51-59.

Pemberton, K. L., Smith, R. E. H., Silsbe, G. M., Howell, T. & Watson, S. B. 2007. Controls on phytoplankton physiology in Lake Ontario during the late summer: Evidence from new fluorescence methods. *Canadian Journal of Fisheries and Aquatic Sciences* **64**:58-73.

Peterson, B. J. 1980. Aquatic primary productivity and the ^{14}C-CO_2 method: a history of the productivity problem. *Annual Review of Ecology and Systematics* **11**:359-85.

Quigg, A., Kevekordes, K., Raven, J. & Beardall, J. 2006. Limitations on microalgal growth at very low photon fluence rates: the role of energy slippage. *Photosynthesis Research* **88**:299-310.

Raateoja, M. P., Seppala, J. & Kuosa, H. 2004. Bio-optical modelling of primary production in the SW Finnish coastal zone, Baltic Sea: fast repetition rate fluorometry in Case 2 waters. *Marine Ecology-Progress Series* **267**:9-26.

Roesler, C. S. 1998. Theoretical and experimental approaches to improve the accuracy of particulate absorption coefficients derived from the quantitative filter technique. *Limnology and Oceanography* **43**:1649-60.

Silsbe, G. M. 2010. *Bio-optical Modeling of Aquatic Photosynthesis in the Laurentian Great Lakes.* PhD, University of Waterloo, 197 pp.

Sterner, R. W. 2010. *In situ*-measured primary production in Lake Superior. *J. Gt. Lakes Res.* **36**:139-49.

Sterner, R. W., Smutka, T. M., McKay, R. M. L., Qin, X. M., Brown, E. T. & Sherrell, R. M. 2004. Phosphorus and trace metal limitation of algae and bacteria in Lake Superior. *Limnology and Oceanography* **49**:495-507.

Stomp, M., Huisman, J., Voros, L., Pick, F. R., Laamanen, M., Haverkamp, T. & Stal, L. J. 2007. Colourful coexistence of red and green picocyanobacteria in lakes and seas. *Ecology Letters* **10**:290-98.

Suggett, D. J., Kraay, G. W., Holligan, P. M., Davey, M., Aiken, J. & Geider, R. J. 2001. Assessment of photosynthesis in a spring cyanobacterial bloom by use of a fast repetition rate fluorometer. *Limnology and Oceanography* **46**:802-10.

Suggett, D. J., MacIntyre, H. L. & Geider, R. J. 2004. Evaluation of biophysical and optical determinations of light absorption by photosystem II in phytoplankton. *Limnology and Oceanography: Methods* **2**:316-32.

Suggett, D. J., MacIntyre, H. L., Kana, T. M. & Geider, R. J. 2009a. Comparing electron transport with gas exchange: parameterising exchange rates between alternative photosynthetic currencies for eukaryotic phytoplankton. *Aquat. Microb. Ecol.* **56**:147-62.

Suggett, D. J., Moore, C. M., Hickman, A. E. & Geider, R. J. 2009b. Interpretation of fast repetition rate (FRR) fluorescence: signatures of phytoplankton community structure versus physiological state. *Marine Ecology-Progress Series* **376**:1-19.

Suggett, D. J., Prášil, O., Borowitzka, M. A., Moore, C. M. & Geider, R. J. 2010. Estimating aquatic productivity from active fluorescence measurements. *Chlorophyll a Fluorescence in Aquatic Sciences: Methods and Applications.* Springer Netherlands, pp. 103-27.

Tassan, S. & Ferrari, G. M. 1995. An alternative approach to absorption measurements of aquatic particles retained on filters. *Limnology and Oceanography* **40**:1358-68.

Titman, D. & Kilham, P. 1976. Sinking in freshwater phytoplankton: Some ecological implications of cell nutrient status and physical mixing processes. *Limnology and Oceanography* **21**:409-17.

Twiss, M. R. 2011. Variations in chromophoric dissolved organic matter and its influence on the use of pigment-specific fluorimeters in the Great Lakes. *J. Gt. Lakes Res.* **37**:124-31.

Urban, N. R., Auer, M. T., Green, S. A., Lu, X., Apul, D. S., Powell, K. D. & Bub, L. 2005. Carbon cycling in Lake Superior. *J. Geophys. Res.-Oceans* **110**.

Vassiliev, I. R., Prasil, O., Wyman, K. D., Kolber, Z., Hanson Jr, A. K., Prentice, J. E. & Falkowski, P. G. 1994. Inhibition of PS II photochemistry by PAR and UV radiation in natural phytoplankton communities. *Photosynthesis Research* **42**:51-64.

Appendix

Figure A1: Schematic representation of the three different O_2 production calculation methods used in this project, each of which uses different combinations of profiles taken at four times during the day (morning, mid morning, mid afternoon, evening) to calculate daily O_2 production. Of the three methods, O_2 method 2 is the simplest and O_2 method 3 is the most complicated